SINR DISTRIBUTIONS IN CELLULAR NETWORKS: SPATIAL STOCHASTIC MODEL FITTING AND ANALYSES

A Dissertation

Submitted to the Graduate School
of the University of Notre Dame
in Partial Fulfillment of the Requirements
for the Degree of

Doctor of Philosophy

by

Anjin Guo

Martin Haenggi, Director

Graduate Program in Electrical Engineering
Notre Dame, Indiana

July 2016

SINR DISTRIBUTIONS IN CELLULAR NETWORKS:
SPATIAL STOCHASTIC MODEL FITTING AND ANALYSES

Abstract

by

Anjin Guo

In recent years, stochastic geometry theory has become a very promising tool to analyze the performance of wireless networks. By taking into account the spatial structure of the base stations (BSs) in homogeneous cellular networks, which plays a key role in evaluating the downlink performance, the theory gives direct insights about how the geometry of the BSs affect the network performance and enables tractable analyses on the signal-to-interference-plus-noise-ratio (SINR) distributions. In this dissertation, we mainly study the SINR distributions and their properties in cellular networks.

The BSs are usually assumed to form a lattice or a Poisson point process (PPP). In reality, however, they are deployed neither fully regularly nor completely randomly. For the first step of our analyses, we use different spatial stochastic models, including the PPP, the Poisson hard-core process (PHCP), the Strauss process (SP), and the perturbed triangular lattice, to model the spatial structure by fitting them to the locations of BSs in real cellular networks obtained from a public database. We provide two general approaches for fitting and find that fitted models can be obtained whose coverage performance matches that of the given data set very accurately.

For the second step, through observations of the model fittings, we discover that the shape of the complementary cumulative distribution function (CCDF) of the SINR for essentially all motion-invariant and ergodic point processes is the same, which means the

SINR distribution for general point processes (i.e., general BS distributions) can be approximated by applying a horizontal shift to the corresponding (simple or maybe tractable) result of the PPP model. We demonstrate this finding by studying the lower tail of the CCDF of the SINR, or equivalently, its high-reliability regime.

For the third step, we extend our theoretical asymptotic analyses to the upper tail of the SINR and non-simple point processes (where points can be colocated).

For the fourth step, since the independent randomness in the positions of the base stations (BSs) and the propagation conditions we usually assume does not comply with the real procedure of BS deployments, we propose a new class of cellular model, where BSs are deployed to make all users at cell edges achieve a minimum required signal power level from the serving BS. The equalized received signal power at cell edges is the outcome of both the spatial structure of the BSs and the propagation model of the signals. We call such system models *joint spatial and propagation* (JSP) models and provide two approaches to formulating the models. The SINR distribution is evaluated. Our results show that networks with Poisson distributed BSs appear to the user like lattice networks if the dependence between BS placement and propagation is accounted for.

DEDICATION

This dissertation is gratefully dedicated to my father and mother. Their encouragement and love are always impetuses to me for exploring new things.

CONTENTS

FIGURES

ACKNOWLEDGMENTS

I would like to acknowledge my advisor Prof. Martin Haenggi. He has given me so much inspiration and help. Without him, this work would not have been possible.

Finally, I would like to thank the NSF, for their generous grants, CNS 1016742 and CCF 1216407, which allowed me to pursue my work.

SYMBOLS

Φ	a point process
λ	intensity of a point process
λ_{p}	intensity of the parent point process
λ_{b}	intensity of the basic point process
P_{o}	outage probability
P_{c}	coverage probability
$P_{\mathrm{c}}^{\mathrm{PPP}}$	coverage probability of the PPP
$P_{\mathrm{o}}^{\mathrm{PPP}}$	outage probability of the PPP
$P_{\mathrm{c}}^{\mathrm{TL}}$	coverage probability of the triangular lattice
$P_{\mathrm{o}}^{\mathrm{TL}}$	outage probability of the triangular lattice
$\mathcal{N}$	the set of counting measures on $\mathbb{R}^2$
$\mathfrak{N}$	the σ-algebra of counting measures
$\Phi(B)$	the number of points in set $B \subset \mathbb{R}^2$ for a point process Φ
φ	a concrete realization of Φ
$\varphi(B)$	deterministic counting measure that denotes the number of points in B
$\tilde{R}$	the interaction radius of the Strauss process
$G(\cdot)$	the nearest-neighbor distance distribution function
$F(\cdot)$	the empty space function
$K(\cdot)$	Ripley's K function
α	the path loss exponent
$\ell(\cdot)$	the path loss function
$\bar{\gamma}$	the average ergodic rate

$G(p_t)$	the deployment gain at p_t
$\hat{S}_g$	the average deployment gain
$\alpha^{(n)}$	the nth-order factorial moment measure
$\rho^{(n)}$	the nth moment density
NP_φ	the nearest-point operator for a point pattern $\varphi \subset \mathbb{R}^2$
$I(\Phi)$	the total interference in Φ
$b(x, r)$	the open disk centered at x with radius r
$\hat{G}$	the asymptotic deployment gain
ξ	the contact distance
ξ_max	the supremum of the contact distance
o	the origin
Φ_o^ζ	$(\Phi \mid \mathrm{NP}_\Phi(o) = \zeta)$
Φ^ζ	$(\Phi \mid \zeta \in \Phi)$
$\hat{I}(\Phi^\zeta)$	the interference of Φ^ζ outside a disk of radius $\|\zeta\|/2$ around the origin
$B_{\zeta/2}$	$\mathbb{R}^2 \setminus b(o, \|\zeta\|/2)$
$\nu(\cdot)$	the Lebesgue measure
W	the thermal noise power
δ	$2/\alpha$
M_Φ	the mean SINR for Φ
M_PPP	the mean SINR for the PPP

CHAPTER 1

INTRODUCTION

1.1 Motivation

In cellular networks, as the power of received signals and interferences depends on the distances between the receiver and base stations (BSs), the downlink performance is affected by the spatial structure. System engineers and researchers often use a regular triangular lattice or a square lattice [1–3] to model the structure deterministically. But in reality, the topology of the BSs is not so ideal but depends on many natural or man-made factors, such as the landscape, topography, bodies of water, population densities, and traffic demands. As a consequence, the BSs are more suitably modeled as deployed randomly instead of deterministically, and stochastic geometry is an efficient tool to analyze this kind of geometrical configurations and provide theoretical insights [4, 5]. Recently, it was shown in [8] that a completely irregular point process, the Poisson point process (PPP) [4, 5], may be used without loss in accuracy (compared to the lattice) but significant gain in analytical tractability. Observations of real BS locations in UK, however, show that real deployments fall somewhere in between the two extremes of full regularity (the triangular lattice) and complete randomness (the PPP). They exhibit some degree of repulsion between the BSs, as expected, since the operators do not place the BSs closely together.

A natural question is whether there is a point process model that is better in modeling the BS topology than the PPP. The critical first step to answer the question is to collect data of real BS locations, investigate some regular (or repulsive) point processes and the PPP by fitting them to the data, and then evaluate the goodness-of-fit. Those works will

be discussed in Chapter 2. The answer to the question is positive. The Poisson hard-core process (PHCP), the Strauss process (SP), and the perturbed triangular lattice can provide better fitting results than the PPP, in term of the *coverage probability*, which is defined as the complementary cumulative distribution function of the signal-to-interference-plus-noise ratio (SINR), i.e., $P_{\mathrm{c}}(\theta) \triangleq \mathbb{P}(\mathrm{SINR} > \theta)$.

The next question is how we can deal with those non-Poisson point processes, i.e., whether we can obtain good analytical results from them by applying them to wireless networks. Generally speaking, the analysis of non-Poisson point processes is significantly more difficult than the analysis of the PPP, since dependencies exist between the locations of the BSs. We are not aware of any tractable analytical methods that are applicable in general. In Chapter 3, we will provide an indirect approach to evaluate the coverage probability of cellular networks, where BSs follow a general class of point process models, using the *asymptotic deployment gain* (ADG). The ADG characterizes the horizontal gap between the coverage probability of the PPP and another point process in the high-reliability regime.

We are not limiting ourselves to the high-reliability regime, and extend our findings of the horizontal gap to the upper tail of the SIR distribution in Chapter 4. Nevertheless, it remains unknown whether the observation and the property still hold for other scenarios, such as ad hoc networks. In order to obtain good approximations of the SIR distribution for those scenarios, we analyze the asymptotic properties of the CCDF of the SIR distribution for a variety of network models. Therefore, Chapter 4 summarizes the known asymptotic properties, derives results for scenarios that have not been previously studied, and gives insight about the factors that mainly determine the behavior of the SIR. We also assess the impact of the nearest-interferer on the asymptotics.

The reasons that we focus on the asymptotic analysis are as follows.

- It captures succinctly the performance of the various network models (especially for the high-reliability regime).

- It permits the isolation of the key network properties that affect the SIR distribution.
- It gives insight into when it is safe to use the singular path loss model instead of a bounded one.
- It shows when a nearest-interferer approximation is accurate.

After the analyses of the asymptotics of the SINR distributions for the conventional cellular networks, in Chapter 5, we propose a new class of cellular models – joint spatial and propagation (JSP) models, where BSs are deployed to make all users at cell edges achieve a minimum required signal power level from the serving BS.

In all current models for cellular networks, independent randomness in the positions of the base stations (BSs) and the propagation models (path loss and fading) is assumed, e.g., [8, 48, 60, 66]. In [8], the authors assumed a homogeneous Poisson distributed network and the power-law path loss model $\ell(x) = \|x\|^{-\alpha}$, where $x \in \mathbb{R}^2$ and calculated the coverage probability, defined as the complementary cumulative distribution function (CCDF) of the SINR, i.e., $P_{\mathrm{c}}(\theta) = \mathbb{P}(\mathrm{SINR} > \theta)$. Under the assumptions of Rayleigh fading, no noise and $\alpha = 4$, $P_{\mathrm{c}}(1) = 0.56$ and $P_{\mathrm{c}}(10) = 0.20$. The main reason why the result is so pessimistic is that mobile users near the edge suffer from low signal strength in large cells. In [48], the authors used the β-Ginibre point process, where points exhibit repulsion, to model the spatial distribution of the BSs and considered the bounded power-law path loss model $\ell(r) = (\max\{r_0, r\})^{-\alpha}$, where r_0 is a positive constant and $r \in \mathbb{R}^+$. The coverage probability is better than that of the Poisson network, since in the β-Ginibre network ($\beta > 0$), BSs are less likely to be close to each other and thus severe interference from nearby BSs is avoided. Moreover, the variance of the cell size is reduced.

In practice, when the goal of the BS deployment is to achieve good baseline coverage, cellular operators place the BSs further apart if propagation is favorable, and vice versa. Thus, a large cell implies smaller path loss or less severe shadowing, and vice versa. This dependence between cell sizes and propagation has been completely ignored, despite (as we shall see) having a significant impact on the performance. In large cells, users near

cell edges usually suffer from unsatisfactory communication conditions with low received signal power, in addition to being subject to relatively high interference. In reality, to avoid those bad situations, cellular operators would place another BS to reduce the cell size and improve the signal strength of edge users. The optimal situation would be that the received signal strengths along all cell edges are equal and meet the minimum requirement.

1.2 Spatial Stochastic Model Fitting (Chapter 2)

1.2.1 Contributions

Our work on spatial stochastic model fitting is based on the real deployment of BSs; we have several point sets that denote the actual locations of BSs collected from the Ofcom[1] - the independent regulator and competition authority for the UK communications industries, where the data are open to the public. Table 1.1 gives the details of the three point sets used in this thesis, and Figs. 1.1-1.3 visualize these point sets. Note that these point sets all represent the BSs of the operator Vodafone with frequency band 900 MHz (GSM). Although the data sets of certain operators in the Ofcom database are almost 10 years old, the data set of the operator Vodafone, is quite up-to-date, since its last update in the Ofcom database occurred in October 2011.

The main objective of the model fitting is to find an accurate point process to model the real deployment of BSs. To accomplish it, we have to first define the metrics to evaluate the goodness of different models. Some classical statistics in stochastic geometry, such as the J function and the L function [5], can be used. Nevertheless, simulations show they are not sufficient to discriminate between different models. Since we study the point processes in the context of wireless networks, it is natural to instead use a key performance metric of cellular systems, namely the coverage probability [5, Ch. 13], [8, 9].

As [8] indicates, the PPP model and the lattice provide a lower bound and an upper

[1]Ofcom website: `http://sitefinder.ofcom.org.uk/search`

TABLE 1.1

DETAILS OF THE THREE POINT SETS

	Operator	Area ($m \times m$)	Center Location	Number of BSs
Urban region	Vodafone	1500×1050	(51.515° N, -0.132° W)	64
Rural region 1	Vodafone	78200×48200	(52.064° N, -1.381° W)	62
Rural region 2	Vodafone	66700×50000	(52.489° N, 0.704° W)	69

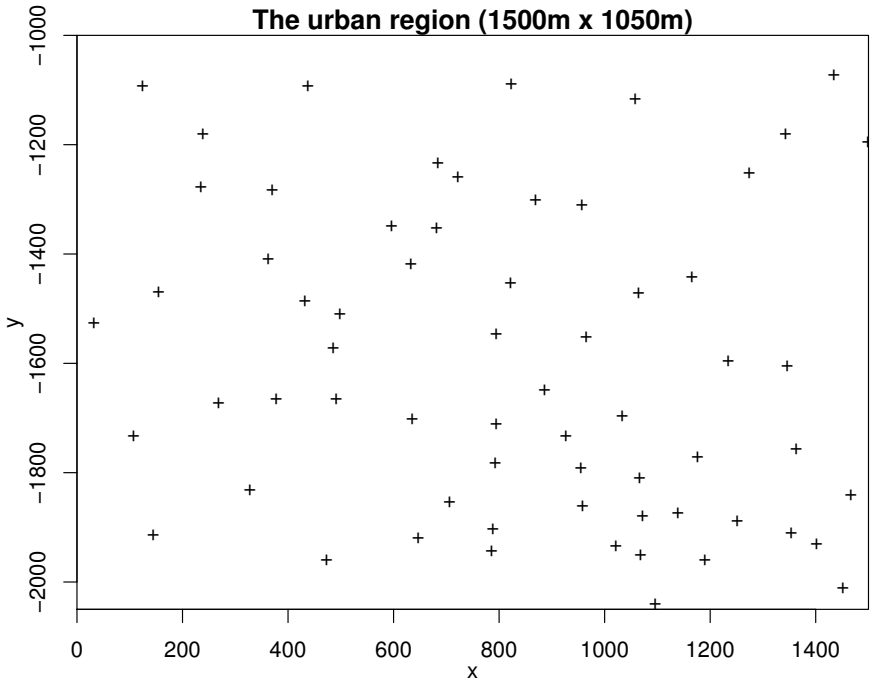

Figure 1.1. The locations of the BSs (the urban region).

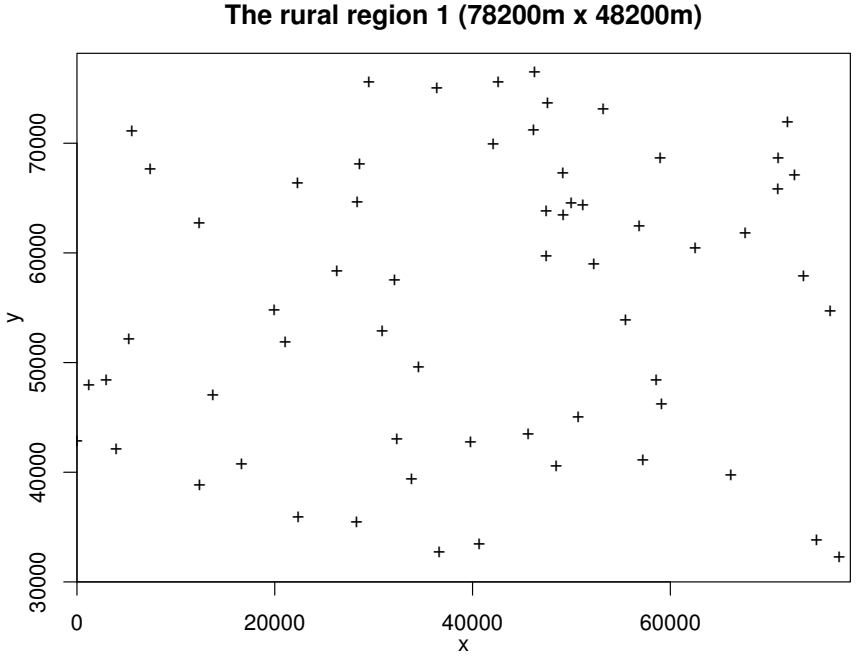

Figure 1.2. The locations of the BSs (the rural region 1).

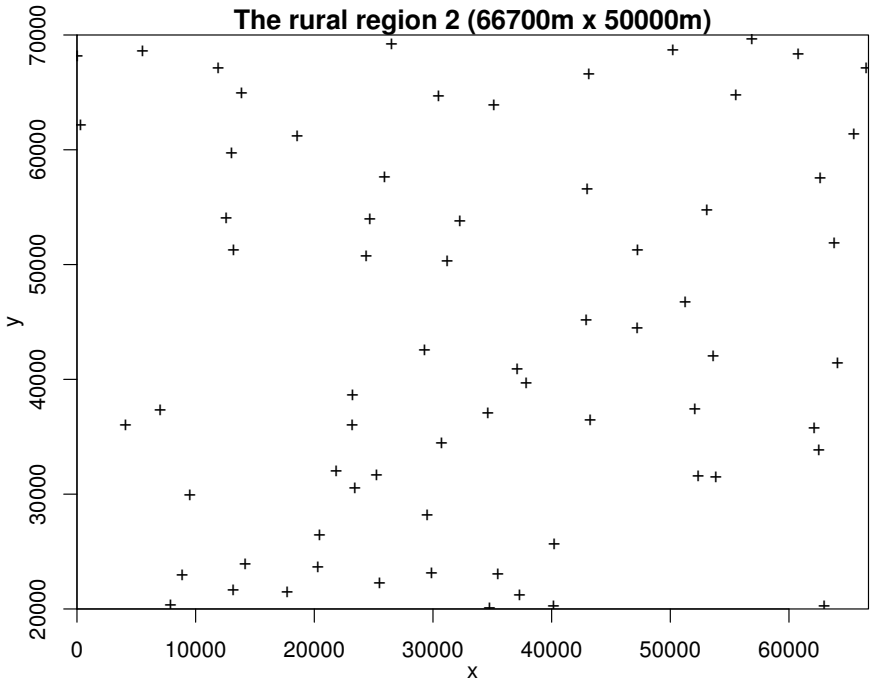

Figure 1.3. The locations of the BSs (the rural region 2).

bound on the coverage probability, respectively. Since the point sets appear to be regular and their coverage probabilities lie between the PPP's and the lattice's, we are interested in point process models that lie in between the two in terms of regularity, such as the Poisson hard-core process (PHCP), the Strauss process (SP), and the perturbed triangular lattice. In order to find the desired point process, we use two different fitting methods. The first one is the method of maximum pseudolikelihood [22], which is the usual method for model fitting in stochastic geometry. The second one is the method of minimum contrast [23], which is used to find the fitted model that minimizes the average squared error of the coverage probability.

Using the first method, we fit the PPP, the PHCP, and the SP to the point sets and determine the best fitted model. Simulations indicate that the SP is the best, followed by the PHCP and then the PPP. But there is still a gap between the coverage probabilities of the SP and the corresponding point set. The perturbed triangular lattice is not considered, since its likelihood and pseudolikelihood are generally unknown.

In the second method, the intensity is assumed to be fixed to the density of the given point sets. The PPP is not considered, since it would result in the same model as with the first method. The fitted models of the SP, the PHCP, and the perturbed triangular lattice for the point sets are obtained. They exhibit quite exactly the same coverage performance as the given point sets. Note that this method is not limited to the average squared error minimization of the coverage probability; it can be applied to many other performance metrics in wireless networks and second-order statistics in stochastic geometry.

Using the two fitting methods, we can find a fitted model that describes the given point set accurately. Although the SP, the PHCP and the perturbed triangular lattice are not as tractable as the PPP, they still have many useful properties. By studying the fitted model, we can obtain properties for a class of point sets.

For some applications where the chief concern is the coverage evaluation of the point sets rather than their spatial structure, there is a simple way of the evaluation using a novel

metric we propose, which is called the *deployment gain*; it measures how close the coverage curve of a point set or a point process model is to that of the PPP. A larger deployment gain means the point set or the model provides better coverage. For example, the deployment gains of the three point sets are: urban region > rural region 1 > rural region 2, which is also the rank of their coverage curves from top to bottom. The deployment gain provides a simple yet highly accurate way of using the analytical results available for the PPP for the analysis of more realistic point process models.

The main contributions on the spatial stochastic model fitting are summarized as follows:

- We use the coverage probability as a metric to compare different point processes and publicly available point sets, which is shown to be more effective than the classical statistics in stochastic geometry for the data sets we used;
- Through fitting the PPP, the PHCP, and the SP to the given point set using the method of maximum pseudolikelihood, we discover that the SP has the best coverage performance, while the PPP has the worst;
- Through fitting the SP, the PHCP, and the perturbed triangular lattice by minimizing the average squared error of the coverage probability, we find that the fitted models have nearly the same coverage probability as the given point set, and thus, in terms of the coverage probability, they are accurate models of the real deployments of the BSs;
- We propose the deployment gain to analytically compare the coverage probability performances of different point sets or different models and to show how results for the PPP can be applied to more accurate point process models.

1.2.2 Related Work

Since the Poisson point process (PPP) [4–7] is highly tractable, it is frequently used to model a variety of networks, such as cellular networks [8–12], mobile ad hoc networks [4–6], cognitive radio networks [13] and wireless sensor networks [14]. For cellular networks, in [8], the authors assume the distribution of BSs follows a homogeneous PPP and derive theoretical expressions for the downlink signal-to-interference-plus-noise-ratio (SINR) complementary cumulative distribution function (CCDF) and the average ergodic

rate under some assumptions. [9] is an extension of [8], in which the authors model the infrastructure elements in heterogeneous cellular networks as multi-tier independent PPPs. In [10], the BSs locations are also modeled as a homogenous PPP, and the outage probability and the handover probability are evaluated. Although many useful theoretical results can be derived in closed form for the PPP, the PPP may not be a good model for real BSs' deployments in homogenous networks, as will be shown in Chapter 2.

Indeed, the BS locations appear to form a more regular point pattern than the PPP, which means there exists repulsion between points, hence the hard-core processes and the Strauss process might be better to describe them. Matérn hard-core processes [5–7] are often used to model concurrent transmitters in CSMA networks [15–17]. In [17], the author uses them to determine the mean interference in CSMA networks, observed at a node of the process. In [18], a modified Matérn hard-core process is proposed to model the access points in dense IEEE 802.11 networks. But to the best of our knowledge, no work prior to ours has modeled the BSs in cellular networks using hard-core processes.

The Strauss process has not been used in wireless networks, but its generalization, the Geyer saturation process [19], is fitted to the spatial structures of a variety of wireless network types using the method of maximum pseudolikelihood in [20]. The difference between the two processes is that the Strauss process is a regular (or soft-core) process, while the Geyer saturation process can be both clustered and regular depending on its parameters. To evaluate the goodness-of-fit in [20], the authors compare the statistics of the original data and the fitted model, such as the nearest-neighbor distance distribution function, the empty space function, the J function, the L function, and the residuals of the model. Though these statistics verify that the Geyer saturation process is suitable to model the data set, they may not be sufficient to discriminate between different point processes in terms of a metric specific to wireless networks. In Chapter 2, all the processes mentioned above are studied comprehensively, and we use different statistics to compare their suitability as models for cellular networks.

The perturbed lattice, which is another soft-core model and thus less regular than the lattice, can also be used to model the BS locations. In [21], the authors consider the BSs as a perturbed lattice network and analyze the fractional frequency reuse technique. The degree of the perturbation is assumed to be a constant. But this constant may not be consistent with real configurations of the BSs. In our work, perturbed lattice networks with different levels of the perturbation are investigated.

1.3 Asymptotic Deployment Gain (Chapter 3)

1.3.1 Contributions

In our work on the asymptotic deployment gain (ADG), we provide an indirect approach to the coverage probability analysis of an arbitrary motion-invariant (isotropic and stationary[2]) point process [5, Ch. 2] by comparing its coverage probability to the coverage probability of the PPP. To validate this approach, we establish that *the outage probability* $1 - P_{\mathrm{c}}(\theta)$ *of essentially all motion-invariant (m.i.) point processes, expressed in dB, as a function of the SINR threshold* θ*, also in dB, has the same slope as* $\theta \to 0$ (or $\theta \to -\infty$ dB). The slope depends on the fading statistics. This result shows that asymptotically the coverage probability curves $P_{\mathrm{c}}(\theta)$ of all m.i. models are just (horizontally) shifted versions of each other in a log-log plot, and the shift can be quantified in terms of the horizontal difference $\hat{G}$ along the θ (in dB) axis. Since the success probability of the PPP is known analytically, the PPP is a sensible choice as a reference model, which then allows to express the coverage probability of an arbitrary m.i. model as a gain relative to the PPP. This gain is called the *asymptotic deployment gain* (ADG).

As a result, the SINR distribution of real BS deployments is approximately a shifted version of that of the PPP. According to this result, we only need the coverage probability at one SINR threshold in real BS deployments to estimate the whole coverage probability

[2]Stationarity implies that the coverage probability does not depend on the location of the typical user.

curve using the commonly known results of the PPP. Similarly, given the mean SINR or the average ergodic rate, we can also estimate the whole coverage probability curve, as will be shown later. In other words, the analysis of the PPP can be carried out into the real BS deployments by doing some simple conversion. The finding may help mobile network providers to get some useful insights on the performance of the real BS deployments, without complicated simulations or measurements.

We introduced the concept of the *deployment gain* (DG) in Section 1.2.1. It measures how close a point process or a point set is to the PPP at a given target coverage probability. Here we extend the DG to include noise and then, to obtain a quantity that does not depend on a target coverage probability, formally define its asymptotic counterpart—the ADG.

Chapter 3 makes the following contributions:

- We introduce the asymptotic deployment gain.
- We formally prove its existence for a large class of m.i. point processes.
- We show how the asymptotic slope of the outage probability depends on the fading statistics.
- We demonstrate through simulations how the ADG can be used to quantify the coverage probability of several non-Poisson models, even if the SINR threshold θ is not small.

1.3.2 Related Work

The spatial configuration of the BSs (or transmitters) plays a critical role in the performance evaluation of cellular networks (or general wireless networks), since the SINR critically relies on the distances between BSs and users (or transmitters and receivers). Network performance analysis using stochastic geometry have drawn considerable attention [4, 8, 17, 20, 33–48]. Recent related works can be roughly divided into two categories. One is based on the assumption of modeling the BSs or access points as Poisson-based point processes (e.g., the PPP and the Poisson cluster process) in cellular networks, e.g. [8, 34–37]. The other one is dealing with general point processes in non-cellular networks, espe-

cially in wireless ad hoc networks, e.g. [42–46]. Of course, there are some other types of works, such as those using the Poisson-based point processes in non-cellular networks, e.g. [38–40], and using non-Poisson point processes in non-cellular networks, e.g. [17, 41], but they are not closely related to this chapter. Our focus is applying general point processes to cellular networks, which has seldom been studied.

Regarding the first category, in cellular networks, the PPP is advantageous for modeling the BSs configuration [8, 34–36] due to its analytical tractability. Poisson-based processes, especially Poisson cluster processes, e.g., in [37], have been used to model the small cell tier in heterogeneous cellular networks, where the BS tier is still modeled as the PPP. Non-Poisson processes, such as hard-core processes, are less studied in cellular networks, due to the absence of an analytical form for the probability generating functional and the Palm characterization of the point process distribution. Exceptions are the related works in [20, 47, 48]. In [47] and [48], the 1-Ginibre point process and the β-Ginibre point process, where points exhibit repulsion, are applied in cellular networks. In [20], the Geyer saturation process was used to model the real cellular service site locations.

As for the second category, general point processes have been used to model the transmitting nodes in non-cellular networks, see, e.g., [43–46]. In [43], the authors analyzed the coverage probability in an asymptotic regime where the density of interferers goes to 0 in wireless networks with general fading and node distribution. The paper [44] provides an in-depth study of the outage probability of general ad hoc networks, where the nodes form an arbitrary motion-invariant point process, under Rayleigh fading as the density of interferers goes to 0. In [45], the tail properties of interference for any motion-invariant spatial distribution of transmitting nodes were derived. In [46], dealing with a wide range of point processes, the authors provided accurate approximations of the transmission capacity in the low-outage regime based on the second-order product density of the node distribution in wireless ad hoc networks.

In Chapter 3, we consider a general class of point processes for modeling possible BS

configurations. In homogeneous cellular networks, each user is usually serviced by its nearest BS, though not necessarily. When general point processes are applied in such networks, one of the main emerging difficulties is that the point process distribution conditioned on an empty ball around the user is unknown. Moreover, the empty space function has to be considered, resulting in the growth of the complexity. Tackling those difficulties directly is seldom seen in the literature.

1.4 SIR Asymptotics in General Network Models (Chapter 4)

1.4.1 Contributions

In Chapter 4, we mainly derive the asymptotic properties of the success probability $P_{\mathrm{s}}(\theta)$, which is defined as the CCDF of the SIR, i.e. $P_{\mathrm{s}}(\theta) \triangleq \mathbb{P}(\mathrm{SIR} > \theta)$. Regarding the transmitter/base station (BS) distributions, we do not restrict ourselves to simple point processes (where there is only one point at one location as surely), which have always been used by the literature, but also consider the "duplicated-2-point" point processes. The duplicated-2-point point processes are defined as the point processes where there are 2 duplicated points at one location. The asymptotic properties of $P_{\mathrm{s}}(\theta)$ are summarized in Table 1.2 with respect to θ as $\theta \to 0$ and $\theta \to \infty$ for both singular and bounded path loss models, both ad hoc models and cellular models, and both simple point processes and duplicated-2-point point processes. Our results show that the asymptotic SIR behavior is determined by two factors — m and δ. m is the Nakagami fading parameter and $\delta \triangleq 2/\alpha$, where α is the path loss exponent.

Note that the shading indicate that the results have been derived in the literature marked with the corresponding reference; the entries marked with (*) indicate that the results are only proven for the Poisson case with Rayleigh fading and the entries marked with (**) indicate that the results are only proven for the case of Rayleigh fading and the duplicated-2-point point process where the distinct locations form a PPP.

Besides, we study the impact of the nearest interferer on the asymptotic properties of the SIR distribution, to see whether the nearest interferer plays a dominant role in determining the asymptotics.

TABLE 1.2

ASYMPTOTIC PROPERTIES ("SIMPLE": SIMPLE POINT PROCESSES; "DUPLICATED": DUPLICATED-2-POINT POINT PROCESSES)

Models	$\theta \to 0$	$\theta \to \infty$
Simple & Ad Hoc & Singular path loss	$1 - P_{\mathrm{s}}(\theta) = \Theta(\theta^{\delta})$	$P_{\mathrm{s}}(\theta) = e^{-\Theta(\theta^{\delta})}$ [5] (*)
Simple & Ad Hoc & Bounded path loss	$1 - P_{\mathrm{s}}(\theta) = \Theta(\theta^{m})$	$P_{\mathrm{s}}(\theta) = e^{-\Theta(\theta^{\delta})}$ (*)
Simple & Cellular & Singular path loss	$1 - P_{\mathrm{s}}(\theta) = \Theta(\theta^{m})$	$P_{\mathrm{s}}(\theta) = \Theta(\theta^{-\delta})$ [61]
Simple & Cellular & Bounded path loss	$1 - P_{\mathrm{s}}(\theta) = \Theta(\theta^{m})$	$P_{\mathrm{s}}(\theta) = e^{-\Theta(\theta^{\delta})}$ (*)
Duplicated & Ad Hoc & Singular path loss	$1 - P_{\mathrm{s}}(\theta) = \Theta(\theta^{\delta})$	$P_{\mathrm{s}}(\theta) = e^{-\Theta(\theta^{\delta})}$ (**)
Duplicated & Ad Hoc & Bounded path loss	$1 - P_{\mathrm{s}}(\theta) = \Theta(\theta^{m})$	$P_{\mathrm{s}}(\theta) = e^{-\Theta(\theta^{\delta})}$ (**)
Duplicated & Cellular & Singular path loss	$1 - P_{\mathrm{s}}(\theta) = \Theta(\theta^{m})$	$P_{\mathrm{s}}(\theta) = \Theta(\theta^{-\delta-m})$
Duplicated & Cellular & Bounded path loss	$1 - P_{\mathrm{s}}(\theta) = \Theta(\theta^{m})$	$P_{\mathrm{s}}(\theta) = e^{-\Theta(\theta^{\delta})}$ (**)

1.4.2 Related Work

In the downlink of cellular networks, some asymptotic properties of the SIR distribution have already been derived. In [60], a simple yet powerful and versatile analytical framework for approximating the SIR distribution in the downlink of cellular systems was proposed

using the mean interference-to-signal ratio. In [61], the authors considered general cellular networks with general fading and singular path loss, and studied the asymptotic behaviors of the SIR distribution both at 0 and at infinity.

In ad hoc networks, the corresponding asymptotic properties have only been derived for a few very specific models, and some interesting and useful properties of the interference and the SIR distribution have been studied. In [42], the interference in general ad hoc networks has been analyzed. Considering both singular and bounded path loss models, it provided several useful bounds on the CCDF of the interference and derived asymptotic behavior of the interference distribution. [64] provided a general framework for the analysis of outage probabilities in the high-reliability regime in general ad hoc networks with Rayleigh fading and both singular and bounded path loss models.

1.5 Joint Spatial and Propagation Models (Chapter 5)

In Chapter 5, we propose a new class of cellular models, where all users at the cell edges achieve a minimum target signal power level from their serving BSs. The spatial structure of the BSs is a result of the propagation environment and the target signal power. We call such models joint spatial and propagation (JSP) models. One special case of the JSP model is the triangular lattice (which has hexagonal cells) with the deterministic power-law path loss model, where the path loss exponent is constant and the received signal power at the cell edges is approximately the same.

In Chapter 5, we propose two approaches to formulating JSP models. In the first approach, we redefine the path loss model. We assume the path loss still follows the power law, but the path loss exponent is variable to satisfy the requirement of the target signal power at the cell edges, given a distribution of the BSs. In the second approach, we redefine the shadowing model. We assume that all cell shapes are disks with different sizes and the "shadowing" parameter in each cell is the power attenuation factor that makes the target signal power achieved at cell edges. We derive the coverage probability analytically

and obtain simulation results for both approaches. To our best knowledge, this is the first work that takes into account the dependence between cell sizes and shapes and signal propagation.

CHAPTER 2

SPATIAL STOCHASTIC MODEL FITTING

In this chapter, we discuss in detail how to find an accurate point process to model the real deployment of BSs, using the method of maximum pseudolikelihood and the method of minimum contrast. Moreover, we introduce the notion of the deployment gain.

This chapter is organized as follows. In Section 2.1, basic concepts of point processes are introduced. In Section 2.2, the PPP, the PHCP, and the SP are fitted to the point sets using the method of maximum pseudolikelihood, and some classical statistics, the coverage probability and the average ergodic rate are used to test the goodness of fitted models. In Section 2.3, the SP, the PHCP, and the perturbed triangular lattice are used to model the given point set by the method of minimum contrast. The deployment gain is introduced in Section 2.4. Conclusions are drawn in Section 2.5.

2.1 Spatial Point Process Models

2.1.1 Overview

The spatial point processes we consider lie in the Euclidean plane $\mathbb{R}^2$. Informally, a point process is a countable random collection of points in $\mathbb{R}^2$. If it is simple (there is only one point at each location a.s.), it can be represented as a countable random set $\Phi = \{x_1, x_2, \ldots\}$, where $x_i \in \mathbb{R}^2$ are the points. Usually, it is characterized by a random counting measure $N \in \mathcal{N}$, where $\mathcal{N}$ is the set of counting measures on $\mathbb{R}^2$. $(\mathcal{N}, \mathfrak{N})$ is the measurable space, where $\mathfrak{N}$ is the σ-algebra of counting measures. $N(B)$ is a random variable that denotes the number of points in set $B \subset \mathbb{R}^2$ for a point process Φ. Instead

of $N(B)$, the notation $\Phi(B)$ is frequently used, since it makes the connection of the point process to the counting measure explicit. A concrete realization of Φ is denoted as φ. Hence $\varphi(B)$ is a deterministic counting measure that denotes the number of points in B. See [5, Ch. 2] for details.

There are many kinds of point processes, such as the PPP, cluster processes, hard-core processes and Gibbs processes [5, Ch. 3]. They can be placed into three categories, the complete spatial randomness (i.e., the PPP), clustered processes, and regular processes. Clustering means there is attraction between points, while regularity means there is repulsion. So the probability of having a nearby neighbor in regular processes is smaller than in the PPP and clustered processes. Since regularity is good for interference minimization and coverage optimization in wireless networks and the deployment of BSs appears to be regular according to the point sets we collected, some regular point processes, including the PHCP, the SP and the perturbed triangular lattice, are considered. We focus on the motion-invariant case of the PPP, the PHCP, and the SP, and the stationary case of the perturbed triangular lattice. A point process is stationary if its distribution is translation-invariant and isotropic if its distribution is rotationally invariant with respect to rotations about the origin. If a point process is both stationary and isotropic, then it is motion-invariant. A stationary PPP is motion-invariant and also said to be homogeneous [5].

2.1.2 The Poisson Point Process

Definition 2.1 (Poisson point process)**.** *The PPP with intensity λ is a point process $\Phi \subset \mathbb{R}^2$ so that 1) for every bounded closed set B, $\Phi(B)$ follows a Poisson distribution with mean $\lambda|B|$ (where $|\cdot|$ is the Lebesgue measure in two dimensions and λ is the expected number of points per unit area), 2) $\Phi(B_1), \Phi(B_2), \ldots, \Phi(B_m)$ are independent if $B_1, B_2, \ldots, B_m$ are disjoint.*

2.1.3 The Strauss Process

The SP constitutes an important class of Gibbs processes. Loosely speaking, Gibbs processes can be obtained by shaping the distribution of a PPP using a density function $f(\varphi)$ on the space of counting measures $\mathcal{N}$. The density function is also called the *likelihood* function. Suppose $f(\varphi)$ is a function such that $f(\varphi) > 0$ implies $f(\varphi') > 0$ whenever $\varphi' \subseteq \varphi$, and Q is the distribution of a PPP with intensity $\lambda = 1$. Regarding φ as a counting measure, we have $\int_{\mathcal{N}} Q(d\varphi) = 1$. If $\int_{\mathcal{N}} f(\varphi)Q(d\varphi) = 1$, then the probability measure $P(Y)$ on the measurable space $(\mathcal{N}, \mathfrak{N})$ that satisfies $P(Y) = \int_Y f(\varphi)Q(d\varphi)$, $\forall Y \in \mathfrak{N}$, is the distribution of a Gibbs process.

Definition 2.2 (Strauss process)**.** *The SP is a Gibbs process with a density function* $f : \mathcal{N} \mapsto \mathbb{R}^+$ *with*

$$f(\varphi) = ca^{\varphi(\mathbb{R}^2)} \exp(-bt_{\tilde{R}}(\varphi)), \tag{2.1}$$

where $a, \tilde{R} > 0$, $b \in \mathbb{R}^+ \cup \infty$, *c is a normalizing constant, and* $t_{\tilde{R}}(\varphi)$ *is the number of point pairs* $\{x, y\}$ *of* φ *with* $\|x - y\| < \tilde{R}$.

$\tilde{R}$ is called the interaction radius. b determines the strength of repulsion between points, which makes the SP suitable for modeling regular point sets. In other words, the SP is a *soft-core process.*

2.1.4 The Poisson Hard-core Process

Just as the name implies, the distance between any two points of the PHCP is larger than a constant R, which is called the hard-core distance.

Definition 2.3 (Poisson hard-core process)**.** *The PHCP is a special case of the SP. Its density function is obtained by setting* $b = \infty$ *in (2.1), i.e.,*

$$f(\varphi) = \begin{cases} 0 & \text{if } t_R(\varphi) > 0 \\ ca^{\varphi(\mathbb{R}^2)} & \text{if } t_R(\varphi) = 0. \end{cases} \tag{2.2}$$

2.1.5 The Perturbed Triangular Lattice

Definition 2.4 (Triangular lattice)**.** *The triangular lattice $\mathbb{L} \subset \mathbb{R}^2$ is defined as*

$$\mathbb{L} = \{u \in \mathbb{Z}^2 : \mathbf{G}u\}, \tag{2.3}$$

where $\mathbf{G} = \eta \begin{bmatrix} 1 & 1/2 \\ 0 & \sqrt{3}/2 \end{bmatrix}$, $\eta \in \mathbb{R}^+$, *is the generator matrix.*

The area of each Voronoi cell is $V = |\det \mathbf{G}| = \eta^2\sqrt{3}/2$, and the density of the triangular lattice is $\lambda_{tri} = V^{-1}$.

The triangular lattice is obviously not stationary. However, we can make it stationary by translating the lattice by a random vector uniformly distributed over the Voronoi cell of the origin. In the rest of the chapter, the triangular lattices considered are all assumed to be stationary.

Definition 2.5 (Stationary triangular lattice)**.** *Let $V(o)$ be the Voronoi cell of the origin o in $\mathbb{L}$. The stationary triangular lattice is*

$$\Phi = \{u \in \mathbb{Z}^2 : \mathbf{G}u + Y\}, \tag{2.4}$$

where Y is uniformly distributed over $V(o)$.

The perturbed triangular lattice is based on the stationary triangular lattice and is also stationary.

Definition 2.6 (Perturbed triangular lattice)**.** *Let (X_u), $u \in \mathbb{Z}^2$, be a family of i.i.d. random variables, uniformly distributed on the disk $b(o, R)$. The perturbed triangular lattice, i.e., the triangular lattice with uniform perturbation on the disk $b(o, R)$, is defined as*

$$\Phi = \{u \in \mathbb{Z}^2 : \mathbf{G}u + Y + X_u\}. \tag{2.5}$$

2.2 Fitting by Pseudolikelihood Maximization

In this section, in order to find an accurate model, different point processes (the PPP, the PHCP, and the SP) are fitted to the point sets in Table 1.1 using the method of maximum pseudolikelihood, which is a common fitting method in stochastic geometry. The reason of using this method is that the definitions of the PHCP and the SP are based on their likelihood functions, thus maximizing the likelihood or pseudolikelihood is the most direct way for fitting. Since the likelihood function of the perturbed triangular lattice is generally unknown, it is not considered in this section. The fitting metric, which is used to compare the models, may be drawn from the classical statistics in stochastic geometry or some statistics relevant in wireless networks.

2.2.1 Fitting Method

For the PPP, the method of maximum pseudolikelihood coincides with maximum likelihood [22, 24]. The likelihood function for the PPP is $f(\varphi) = e^{-(\lambda-1)|W|}\lambda^{\varphi(W)}$, where λ is the intensity and W is the sampling region. The maximum likelihood estimate is $\hat{\lambda} = \varphi(W)/|W|$.

For the PHCP, R is decided by the method of maximum profile pseudolikelihood [22], which means for different values of R, we obtain their corresponding fitted PHCP models by the method of maximum pseudolikelihood and select the value of R whose fitted PHCP model has the largest maximum pseudolikelihood. The other parameters in (2.2) are obtained by fitting using the method of maximum pseudolikelihood given R.

For the SP, $\tilde{R}$ is selected from the range $[R, 4R]$ by the method of maximum profile pseudolikelihood. By fitting, a and b in the SP model (2.1) can then be obtained. We choose the lower bound to be R because the maximum pseudolikelihood of the SP model with $\tilde{R} < R$ would be smaller than that of the model with $\tilde{R} = R$, where R is the minimum distance between each two point of the point set. We choose the upper bound to be $4R$ because: 1) the base stations in the data sets we considered are located in a finite region

and the SP model with an $\tilde{R}$ that is too large is inaccurate to model the data; 2) $4R$ is a large enough upper bound, since, for the fitted SP model, the optimum value is always in the range $[R, 4R]$.

The reason why we use the method of maximum pseudolikelihood instead of maximum likelihood is that the likelihood is intractable for the PHCP and the SP, while, except for the computation of an integral over the sampling region, which can be approximated by a finite sum, the pseudolikelihood is known. As the conditional intensities take an exponential family form, the pseudolikelihood can then be maximized using standard statistical software for generalized linear or additive models. The simulations are all done with the software **R** [25].

We use the function *ppm* of the package "Spatstat" in **R** to perform the fitting, which contains the implementation of the method of maximum pseudolikelihood. It is closely related to the model fitting functions in **R** such as *lm* (for linear models) and *glm* (for generalized linear models). The method is computationally efficient. Details are provided in [22]. The computation times depend on the fitting model type and the number of points. The following are typical times for a standard computer (2.3 GHz processor, 4 GB memory). Consider the point set of the urban region. Fitting the PPP to the 64 points takes about 0.02 seconds; fitting the PHCP (with known R) takes about 0.06 seconds; fitting the SP (with known $\tilde{R}$) takes about 0.05 seconds. In the same region of the point set, fitting the PPP to 640 randomly generated points takes about 0.03 seconds; fitting the PPP to 6400 randomly generated points takes about 0.52 seconds. These numbers indicate that the complexity is $O(n^2)$, perhaps even $O(n \log n)$, as the number of points n grows.

We use the function *profilepl* of the package "Spatstat" in **R**, which uses the method of maximum profile pseudolikelihood, to find the optimal values of the interaction radius $\tilde{R}$ for the SP and the hard-core distance R for the PHCP that give the best fit. In the fitting, we search over a vector whose columns contain values of $\tilde{R}$ or R to find the optimum. Then with the optimal value of $\tilde{R}$ or R, we use the function *ppm* to get the values of other

parameters in the equations (1) or (2). The complexity of the fitting is in proportion to that of the function *ppm*.

2.2.2 Classical Statistics

Many statistics can be used to characterize the structure of a point process or a point set, such as the nearest-neighbor distance distribution function $G(r)$ and the empty space function $F(r)$. The J function, $J(r) = (1-G(r))/(1-F(r))$, measures how close a process is to a PPP. For the PPP, $J(r) \equiv 1$. $J(r) > 1$ at some r indicates the points are regular at these distances, while $J(r) < 1$ means the points are clustered. Hence, we can easily tell by visual inspection of $J(r)$ whether a point set or a point process is regular or clustered. But it is hard to get more information that can be used to discriminate different regular point processes.

Different from the J function that is related to the inter-point distance, Ripley's K function is related to point correlations. It is a second-order statistic and can be defined as $K(r) = \mathbb{E}[\Phi(b(x,r)) - 1 \mid x \in \Phi]/\lambda$, for $r \geq 0$, where λ is the intensity. $\lambda K(r)$ can be interpreted as the mean number of points $y \in \Phi$ that satisfy $0 < \|y-x\| \leq r$, given $x \in \Phi$. For the PPP, $K(r) = \pi r^2$.

The L function is defined as $L(r) = \sqrt{K(r)/\pi}$. $L(r) < r$ at some r indicates the points are regular at distance r, while $L(r) > r$ means the points are clustered.

Consider the point set of the urban region. The L function of the point set is plotted in Figs. 2.1-2.3 (black solid line). It is seen that the point set is regular for $r < 140$,[1] since $L(r) < r$ for $r < 140$. Clearly, $L(r) = 0$ for $r < 39$, which means no two points are closer than 39. Hence, the point set may be regarded as a realization of a hard-core process with hard-core distance $R = 39$. The grey regions in these figures are the pointwise maximum and minimum of 99 realizations of the fitted PPP, the fitted PHCP and the fitted SP, respectively. The values of the parameters obtained by fitting are $\hat{\lambda} = 4.06 \times 10^{-5}$ for the

[1]The unit of all distances in this chapter is meter.

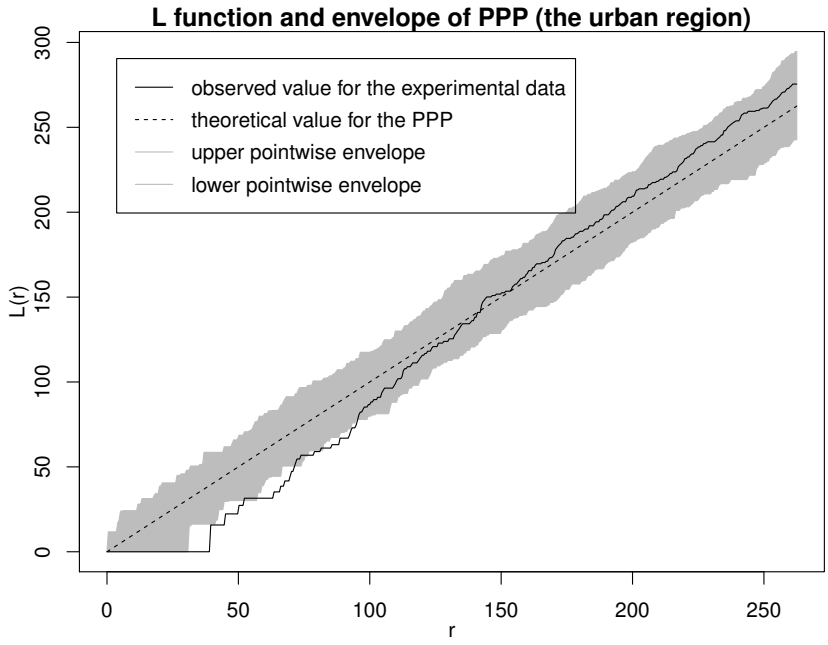

Figure 2.1. L function of BSs of the urban region (the solid line) and the envelope of 99 realizations of the fitted PPP model. The dashed line is the theoretical L function of the PPP.

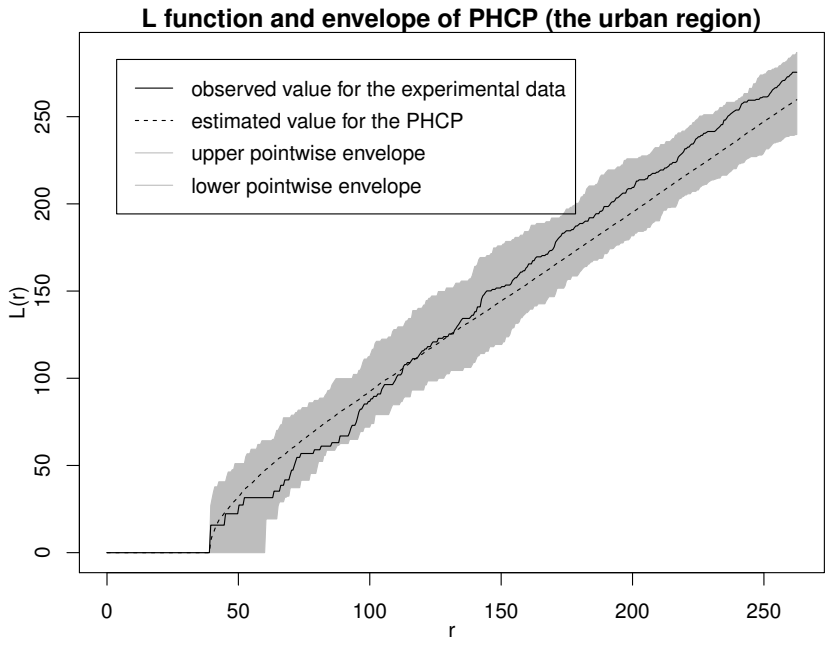

Figure 2.2. L function of BSs of the urban region (the solid line) and the envelope of 99 realizations of the fitted PHCP model. The dashed line is the average value of the L functions of 99 realizations of the fitted PHCP model.

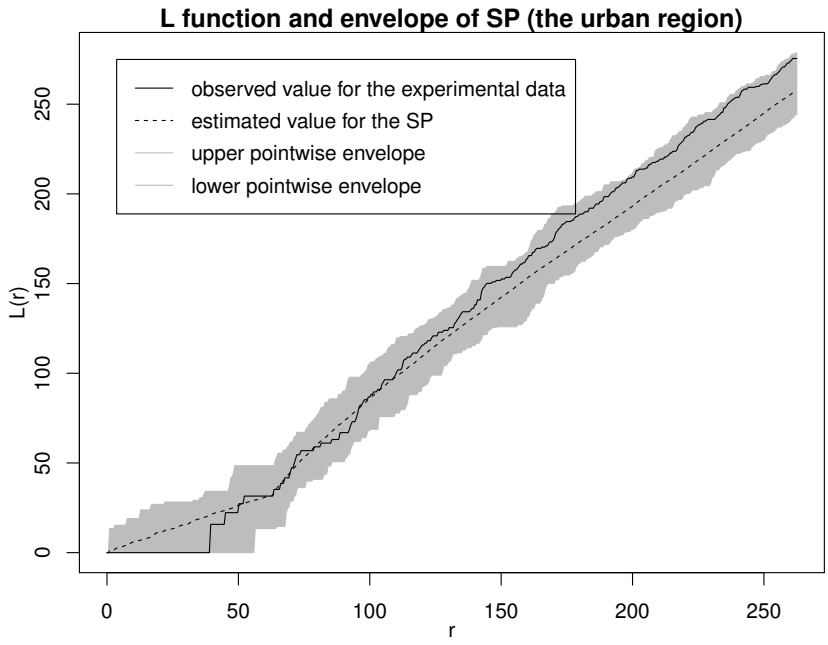

Figure 2.3. L function of BSs of the urban region (the solid line) and the envelope of 99 realizations of the fitted SP model. The dashed line is the average value of the L functions of 99 realizations of the fitted SP model.

PPP, $R = 39$ for the PHCP and $\tilde{R} = 63$ for the SP. Note that for the fitted PHCP, the R value coincides with that obtained by visual inspection.

According to the figures, the PPP is not an appropriate model, as the L function of the point set is not within the envelope of the PPP. But the PHCP and the SP fit well. Although the L function is more powerful than the J function when used to compare the three models, it cannot distinguish which of the PHCP and the SP is better. Other statistics are needed.

2.2.3 Definition of Coverage Probability

It is sensible to use a statistic that is related with a standard metric used in wireless networks to decide on the best model. For the three point sets, by evaluating the coverage probabilities of the point sets and fitted models through simulations, we find that the coverage probability is such a statistic that has two desirable properties: it has enough discriminative power to distinguish between different models, and it is relevant to cellular systems. Generally speaking, the coverage probability is the probability that a randomly located user achieves a given SINR threshold with respect to one of the BSs.

A mobile user is assumed to attempt to communicate with the nearest BS, while all other BSs act as interferers (the frequency reuse factor is 1). The received power, the interference, and, in turn, the coverage probability, depend on the transmit power of the BSs, the power loss during propagation, and the random channel effects. We make the following assumptions: (i) the transmit power of all BSs is constant 1; (ii) the path loss exponent $\alpha = 4$; (iii) all signals experience Rayleigh fading with mean 1; (iv) the shadowing effect is neglected; (v) the thermal noise W is ignored, i.e. SNR $= \infty$, and the SINR reduces to the SIR.

Under these assumptions, the SIR has the form

$$\mathrm{SIR}_z = \frac{h_0 \|x_0\|^{-\alpha}}{\sum_{i:x_i \in \Phi \setminus \{x_0\}} h_i \|x_i - z\|^{-\alpha}}, \tag{2.6}$$

where $\{h_0, h_1, ...\} \sim$ exponential(1) and independent, and $x_0 = \arg\min_{x\in\Phi} \|x - z\|$. We assume that the location z is in coverage if $\mathrm{SIR}_z > \theta$.

Definition 2.7 (Coverage probability)**.** *For a stationary process,* $\mathbb{P}(\mathrm{SIR}_z > \theta)$ *does not depend on* z*, and we call it the coverage probability:*

$$P_{\mathrm{c}}(\theta) = \mathbb{P}(\mathrm{SIR} > \theta). \tag{2.7}$$

It is the CCDF of the SIR and can also be interpreted as the covered area fraction for each realization of the BS point process.

The theoretical expression of $P_{\mathrm{c}}(\theta)$ for the PPP with intensity λ and $\alpha = 4$ has been derived in [8]:

$$P_{\mathrm{c}}(\theta) = \frac{1}{1 + \sqrt{\theta}\arctan(\sqrt{\theta})}. \tag{2.8}$$

Since the coverage probability of the PPP does not depend on the intensity, no fitting method based on adjusting the intensity is possible. On the other hand, the intensity is easily matched to the intensity of a given point set.

2.2.4 Results for Coverage Probability

The regions where the BSs reside are not infinite. Thus, for the fitted point process, which is stationary, we only consider a finite region that has the same area and shape as the point set under consideration.

In the finite region, $P_{\mathrm{c}}(\theta)$ can be estimated by determining the average fraction of the whole area where $\mathrm{SIR} > \theta$. In the following simulations, $P_{\mathrm{c}}(\theta)$ is obtained by evaluating 3,000,000 SIR values. In order to mitigate the boundary effect, we only use the central $[\frac{2}{3}\text{length} \times \frac{2}{3}\text{width}]$ area of the entire region to compute $P_{\mathrm{c}}(\theta)$. For the point sets, the SIRs of 3,000,000 randomly chosen locations (uniformly distributed) are computed. For point processes, 3,000 realizations are generated and for each realization, 1,000 randomly chosen locations are generated. The SIR is evaluated at all chosen locations.

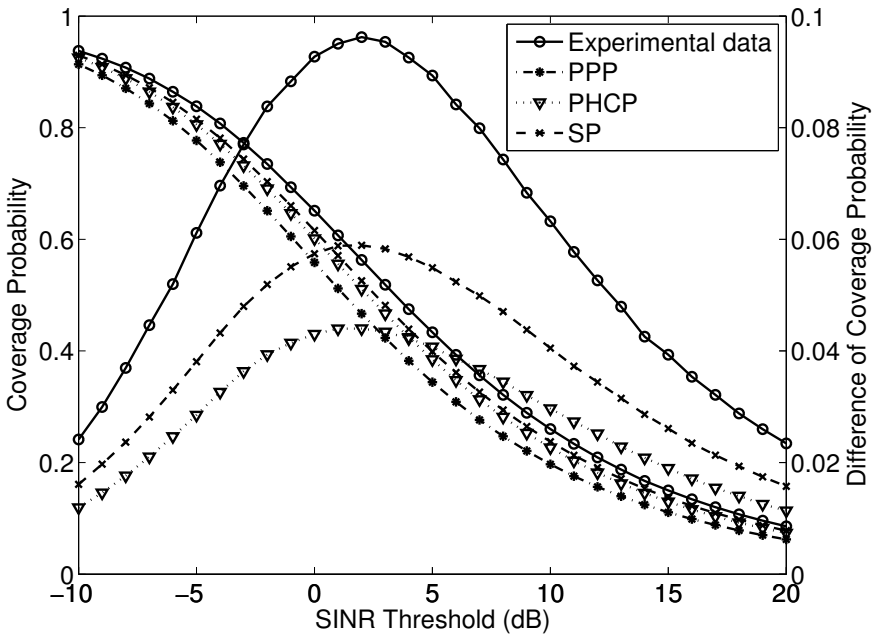

Figure 2.4. Left axis: the coverage curves of the experimental data of the urban region and different fitted point process models. Right axis: the difference between the coverage curve of the PPP and the other curves.

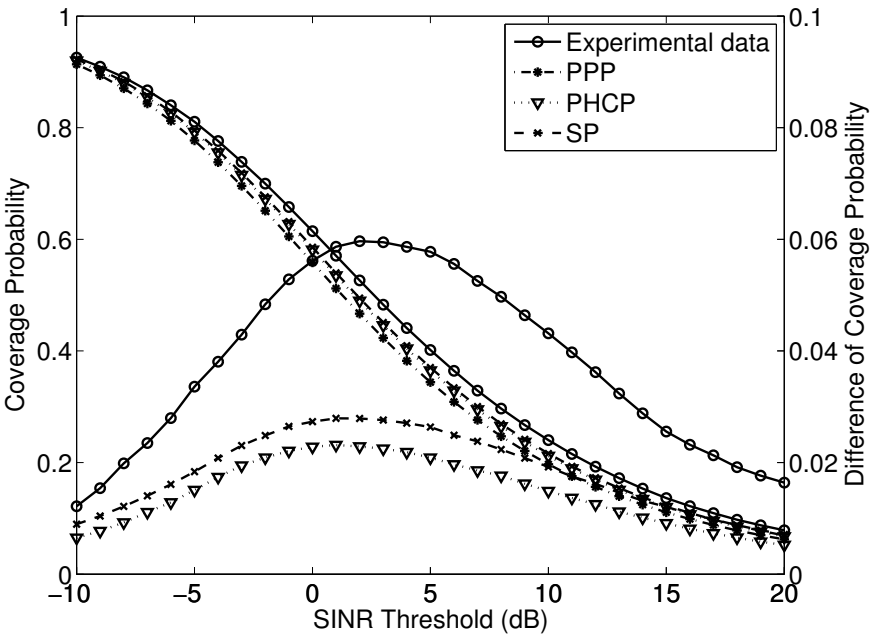

Figure 2.5. Left axis: the coverage curves of the experimental data of the rural region 1 and different fitted point process models. Right axis: the difference between the coverage curve of the PPP and the other curves.

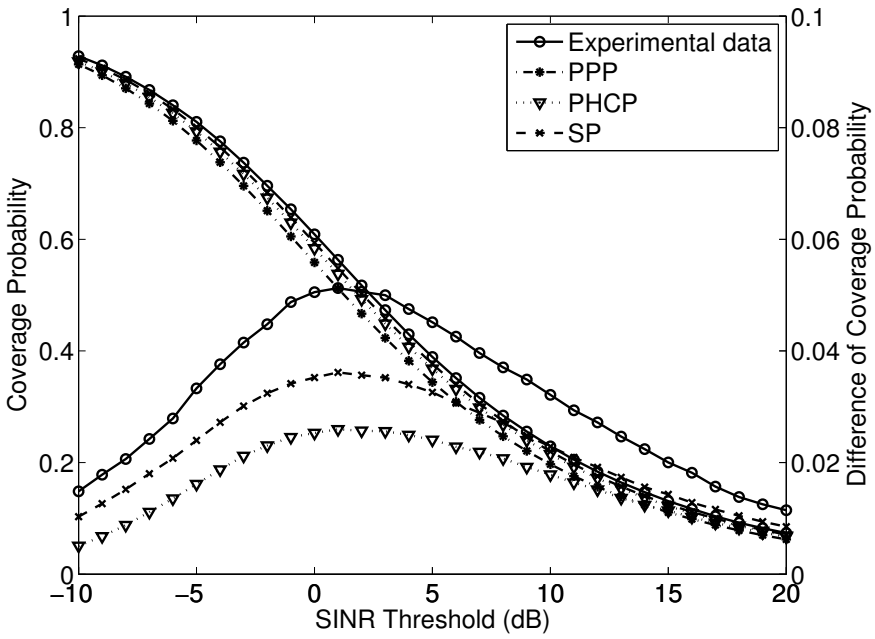

Figure 2.6. Left axis: the coverage curves of the experimental data of the rural region 2 and different fitted point process models. Right axis: the difference between the coverage curve of the PPP and the other curves.

Consider the point set of the urban region. The coverage curves of the experimental data and the fitted models of the PPP, the PHCP, and the SP are shown in Fig. 2.4. The left axis shows the coverage curves, while the right axis shows the difference between the coverage curve of the PPP and the other curves. Clearly, the curves of three models are all below the curve of the experimental data. Among the three point processes, the SP provides the best fit, followed by the PHCP and then the PPP.

We use the other two point sets in Table 1.1 to test the statistic. For the fitted models, the hard-core distances in the two rural regions are $R_1 = 1194$ and $R_2 = 1474$ and the interaction radii are $\tilde{R}_1 = 2120$ and $\tilde{R}_2 = 5490$. Figs. 2.5 and 2.6 show the coverage curves of the two point sets. The PPP still performs the worst. In Fig. 2.6, the SP is better than the PHCP, while in Fig. 2.5, the curves of the SP and the PHCP are quite close, thus, the two processes can be considered equivalent when fitted to that point set. Generally, it depends on the given point set. The SP is often better. Note that this is not because the PHCP is a special case of the SP. The method of maximum pseudolikelihood is used to do the fittings, but a larger pseudolikelihood does not imply a better matching coverage probability.

2.2.5 Average Rate

We can also distinguish the best fitted model in terms of the average ergodic rate. Similar results are obtained. The average ergodic rate (or Shannon throughput) is defined as $\bar{\gamma} = \mathbb{E}[\ln(1 + \mathrm{SIR})]$ and measured in nats/s/Hz. Denote $\bar{\gamma}_e$, $\bar{\gamma}_p$, $\bar{\gamma}_h$, $\bar{\gamma}_s$ as the average ergodic rates of the experimental data, the PPP, the PHCP, and the SP respectively. Let the simulation parameters remain the same. For the point set of the urban region, $\bar{\gamma}_e \approx 1.786$, $\bar{\gamma}_p \approx 1.513$, $\bar{\gamma}_h \approx 1.635$, $\bar{\gamma}_s \approx 1.682$. For the point set of the rural region 1, $\bar{\gamma}_e \approx 1.679$, $\bar{\gamma}_p \approx 1.506$, $\bar{\gamma}_h \approx 1.566$, $\bar{\gamma}_s \approx 1.572$. For the point set of the rural region 2, $\bar{\gamma}_e \approx 1.634$, $\bar{\gamma}_p \approx 1.515$, $\bar{\gamma}_h \approx 1.581$, $\bar{\gamma}_s \approx 1.605$. So we have $\bar{\gamma}_p < \bar{\gamma}_h < \bar{\gamma}_s < \bar{\gamma}_e$.

The theoretical average ergodic rate of the PPP is $\bar{\gamma}'_p \approx 1.49$, which is smaller than the

values of simulations of the PPP. The reason is that the theoretical average ergodic rate of the PPP considers all the points on the whole plane $\mathbb{R}^2$, while in the simulations, we only consider the points of the PPP in the same region of the given point set, which leads to the fact that the SIR value at any location is larger than the theoretical value at the same location and thus the theoretical average ergodic rate is smaller than the simulation values.

2.3 Fitting Using the Coverage Probability

We have fitted the PPP, the PHCP, and the SP to the given point sets by the method of maximum pseudolikelihood, but none of these models precisely describes the coverage probability of the data, and all their coverage curves are *below* the actual curve of the point set. If we want to find a point process that has a similar performance as the given point set, we cannot just use the three fitted models, because none of them is regular enough due to the limitation of the fitting methods. In this section, we adopt the method of minimum contrast as a fitting method and fit the SP, the PHCP, and the perturbed triangular lattice to the point sets in Table 1.1.

2.3.1 Fitting Method

In the method of minimum contrast, there is a suitable summary statistic S and a point process model with some adjustable parameters $\{\theta_i\}$. Ideally the chosen point process model has analytically tractable expressions for the summary statistic S as a function of $\{\theta_i\}$.

Here, the summary statistic is the coverage probability, and the chosen models are the SP, the PHCP and the perturbed triangular lattice. But there are no analytically tractable expressions for the coverage probability of the SP and the PHCP. For different values of the adjustable parameters, the coverage probabilities are estimated through simulations.

We assume the intensity of the fitted model is the same as the given point set. By this

method, the coverage curve of the fitted model should have the minimum difference from that of the given point set.

Definition 2.8 (Average squared error of the coverage probability)**.** *The average squared error of the coverage probability, denoted as E, measures the difference between two coverage curves. It is defined as:*

$$E(a,b) = \frac{1}{b-a}\int_a^b \Big(P_{c1}(t) - P_{c2}(t)\Big)^2 dt, \tag{2.9}$$

where $a, b \in \mathbb{R}$, t is the SIR threshold in dB, and $P_{c1}(t)$, $P_{c2}(t)$ denote two coverage curves.

The average squared error of the coverage probability is used as the contrast criterion of the method of minimum contrast. Under the condition of the fixed intensity, the relevant parameters in the model are adjusted to find the model that has the minimum average squared error between its coverage curve and the given point set's. Here, we set $a = -9.38$ dB and $b = 16.07$ dB (for the PPP, $P_{\mathrm{c}}(a) = 0.9$ and $P_{\mathrm{c}}(b) = 0.1$), because $[0.1, 0.9]$ is the coverage probability range where the curves differ the most and $[-10, 16]$ dB is a reasonable SIR interval for practical systems.

This fitting method is not restricted to the contrast criterion defined by the coverage probability. The criteria defined by other performance metrics in wireless networks and second-order statistics in stochastic geometry can also be used. Similarly, the method is not limited to Rayleigh fading either, when we simulate the network. Other fading types can also be applied depending on the propagation environment.

2.3.2 The SP and the PHCP

In the fitting method, the intensity of the fitted model is fixed. Thus, the PPP is not considered. As the accurate intensity values of the SP and the PHCP are unknown for given values of the parameters in (2.1) and (2.2), it is not quite suitable to use the method for the two processes. But there are some approximations of the intensity for the SP [26],

e.g.,

$$\lambda \approx W(a\Gamma)/\Gamma, \tag{2.10}$$

where $W(x)$ is the principle branch of the *Lambert W function* [27] and $\Gamma = \big(1 - \exp(-b)\big)\pi\tilde{R}^2$. This is the Poisson-saddlepoint approximation [26], which is more accurate than the mean field approximation.

If we use the approximated intensity (2.10) in the fitting method for the SP, we have to adjust the three parameters a, b, and $\tilde{R}$ in (2.1) to minimize the average squared error of the coverage probability. Note that, as b increases, the strength of the repulsion between the points in the SP increases, and as $\tilde{R}$ increases, the repulsion range increases. Both adjustments increase the regularity of the process. From (2.10), we have $a \approx \lambda \exp(\lambda\Gamma)$. a increases as b and $\tilde{R}$ increase with λ fixed. So in order to increase the regularity of the SP with fixed intensity, we can fix b, increase $\tilde{R}$ and a, or fix $\tilde{R}$, increase b and a according to (2.10). We can also first increase a, and then adjust b and $\tilde{R}$. But in this way, the regularity may not increase, or even decrease for some b and $\tilde{R}$. To get a more regular model, we can compare models with different settings of b and $\tilde{R}$ in simulations. The above three methods are used to obtain the fitting results of the SP in simulations.

TABLE 2.1

FITTING RESULTS OF THE STRAUSS PROCESS

Parameters	a	b	$\tilde{R}$	Actual intensity $\hat{\lambda}$	Desired intensity λ	$\hat{\lambda}/\lambda - 1$
Urban region	1×10^{-4}	3.745	85	3.737×10^{-5}	4.063×10^{-5}	-8.02%
Rural region 1	2.44×10^{-8}	1.892	3000	1.622×10^{-8}	1.645×10^{-8}	-1.40%
Rural region 2	5.00×10^{-8}	0.599	5490	2.086×10^{-8}	2.069×10^{-8}	0.82%

Given a point set, to obtain a fitted SP, we can first fit the SP to the point set using the method of the maximum pseudolikelihood, and then, based on the parameters we get, increase the regularity to minimize the average squared error of the coverage probability. Table 2.1 shows the fitting results of the SP for the three point sets in Table 1.1. As shown in Fig. 2.7, for each fitted model, the coverage curve matches the one of the corresponding point set very closely. Note that the simulation is not perfectly accurate, since the number of realizations of the point process used to calculate the coverage probability is limited to 3,000; also, when calculating the average squared error of the coverage probability, we only compute the average over a finite number of sample points on the coverage curve; and when we increase b and $\tilde{R}$, the step width is not infinitesimal. We say an SP model has the "minimum" average squared error of the coverage probability if $E < 10^{-5}$.

The fitted SP is not unique. For some different values of a, we can find different fitted models that satisfy $E < 10^{-5}$, by adjusting b and $\tilde{R}$. For instance, the SP with $a = 1.1 \times 10^{-4}$, $b = 2.547$, $\tilde{R} = 92$ is also a fitted model for the urban region, which is shown as the curve of another fitted SP model in Fig. 2.7.

Since the PHCP is a special case of the SP, its approximated intensity can be obtained by setting $b = \infty$ in (2.10), $\lambda \approx W(a\pi R^2)/(\pi R^2)$. To increase the regularity of the PHCP with fixed intensity, we can increase R. Table 2.2 shows the fitting results of the PHCP for the three point sets. The coverage curves of the fitted models and their corresponding point sets are visually indistinguishable, as shown in Fig. 2.8.

Although the models are fitted well to the point sets, there are two main shortcomings of the fitting for the SP and the PHCP. One is that the actual intensity is not the same as the density of the given point set as shown in Tables 2.1 and 2.2, and the difference can be as large as 10%. Note that each value of the actual intensity is obtained by averaging over 10,000 independent realizations of the model.

The other drawback is that we may not get a well fitted model for some point sets.

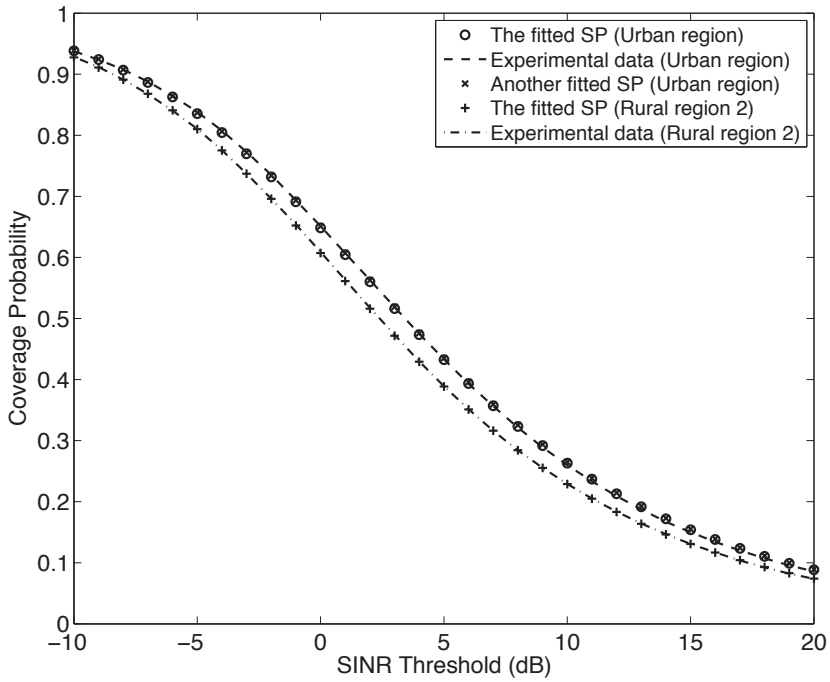

Figure 2.7. The coverage curves of the experimental data and the fitted SP models. The curves of the rural region 1, not shown in this figure, are very similar to those of the rural region 2.

TABLE 2.2

FITTING RESULTS OF THE POISSON HARD-CORE PROCESS

Parameters	a	R	Actual intensity $\hat{\lambda}$	Desired intensity λ	$\hat{\lambda}/\lambda - 1$
Urban region	9.38×10^{-5}	78	3.885×10^{-5}	4.063×10^{-5}	-4.38%
Rural region 1	2.28×10^{-8}	2500	1.626×10^{-8}	1.645×10^{-8}	-1.16%
Rural region 2	2.37×10^{-8}	2000	1.864×10^{-8}	2.069×10^{-8}	-9.91%

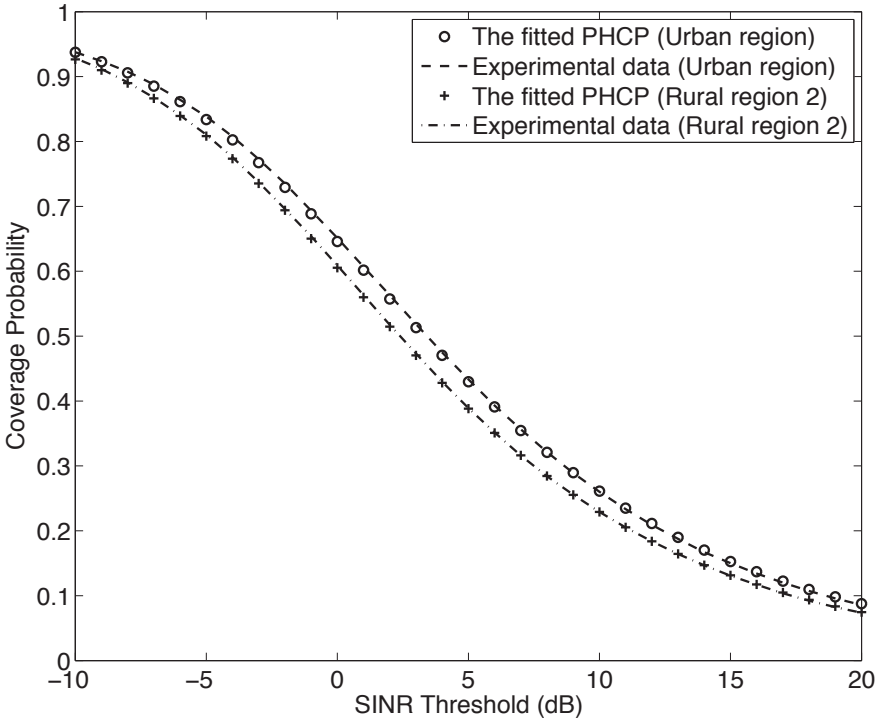

Figure 2.8. The coverage curves of the experimental data and the fitted PHCP models. The curves of the rural region 1, not shown in this figure, are very similar to those of the rural region 2.

In simulations, we use the function *rStrauss* in the **R** package "Spatstat" [28] to generate realizations for the SP and the function *rHardcore* for the PHCP. In *rStrauss* and *rHardcore*, the coupling-from-the-past (CFTP) algorithm [29] is used, but it is not practicable for all parameter values. Its computation time and storage increase rapidly with a, $\tilde{R}$ and R. For example, for a point set that has a coverage curve close to that of the triangular lattice, we cannot get the fitted SP or PHCP, due to the limited storage and time. It turns out, though, that the three point sets in Table 1.1 are not too regular to use *rStrauss* and *rHardcore*.

2.3.3 The Perturbed Triangular Lattice

There are no such shortcomings described in the previous subsection when the perturbed triangular lattice is fitted by the method of minimum contrast. The reasons are 1) the intensity is fixed once the lattice constant η is fixed; 2) as R increases from 0 to ∞, the coverage curve of the perturbed triangular lattice degrades from that of the triangular lattice to that of the PPP, and we can easily get the realizations of the perturbed triangular lattice for all values of η and R. To do the fitting, we first compute η and then increase R from 0 to find the fitted model.

Consider the point set of the urban region. The intensity of the point set is $\hat{\lambda} = 4.06 \times 10^{-5}$. Equating $\lambda_{tri} = \hat{\lambda}$, we get $\eta = 168.57$. Fig. 1.1 shows the locations of the BSs in the urban region. Figs. 2.9-2.11 give the realizations of the fitted PPP, the triangular lattice, and the triangular lattice with uniform perturbation on the disk $b(o, 0.52\eta)$, respectively. Note that the fitted PPP means that the intensity of the PPP is estimated by the method of maximum likelihood. To compute the coverage probability of the triangular lattice with $\eta = 168.57$, the lattice is generated on the same region as the point set. Under the same simulation conditions as those in Section 2.2, the coverage probability is obtained, which is shown in Fig. 2.12. As expected, the coverage probability of the lattice is larger than that of the given point set. The lattice provides an upper bound on the coverage probability.

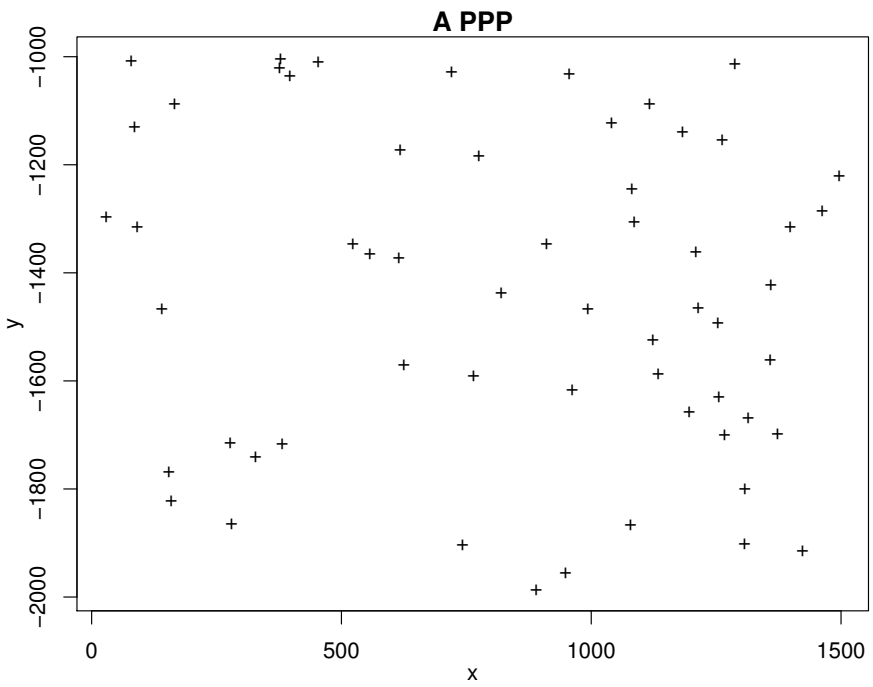

Figure 2.9. A realization of the PPP fitted to the urban data set.

To compare the coverage performances of the perturbed triangular lattices with the PPP and the triangular lattice, we simulate the cases with $R = 0.2\eta, 0.5\eta$ and 0.8η. Fig. 2.13 shows the coverage curves. As expected and observed in the figure, the coverage probability degrades as R increases. As $R \to \infty$, the perturbed triangular lattice approaches the PPP with intensity $\lambda = 4.06 \times 10^{-5}$. Therefore, the coverage curves of the perturbed triangular lattices with different R span the region between the PPP and the triangular lattice. It is thus guaranteed that we can obtain the desired perturbed triangular lattice that is fitted tightly to a point set.

For the point set of the urban region, the fitting value of R is $R = 0.52\eta$. Fig. 2.10 indicates that the disks centered at the triangular lattice points with radii 0.52η overlap slightly, as the distance between each two triangular lattice points is η. In Fig. 2.11, a realization of this perturbed triangular lattice is shown. The coverage curves of this perturbed triangular lattice and the point set closely overlap, as shown in Fig. 2.12. For

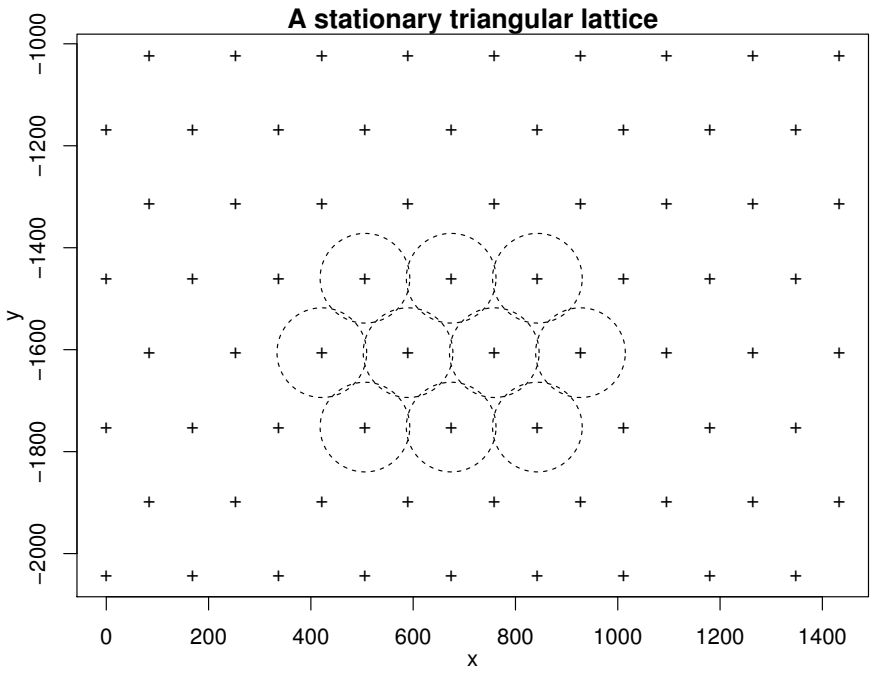

Figure 2.10. A realization of the triangular lattice on the urban region. The dashed disks have centers at the lattice points and their radii are 0.52η.

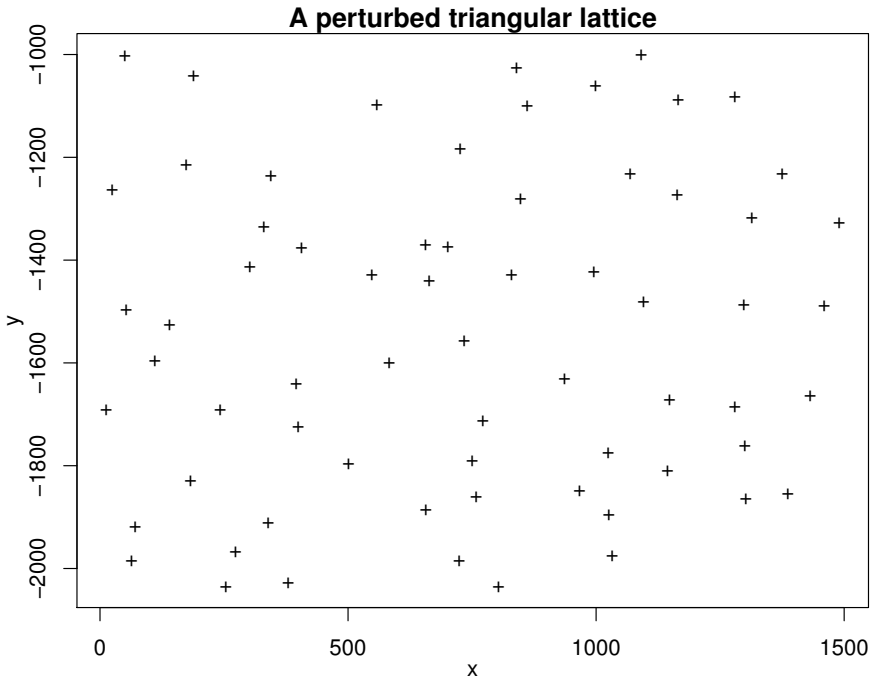

Figure 2.11. A realization of the triangular lattice with uniform perturbation on the disk $b(o, 0.52\eta)$ fitted to the urban data set.

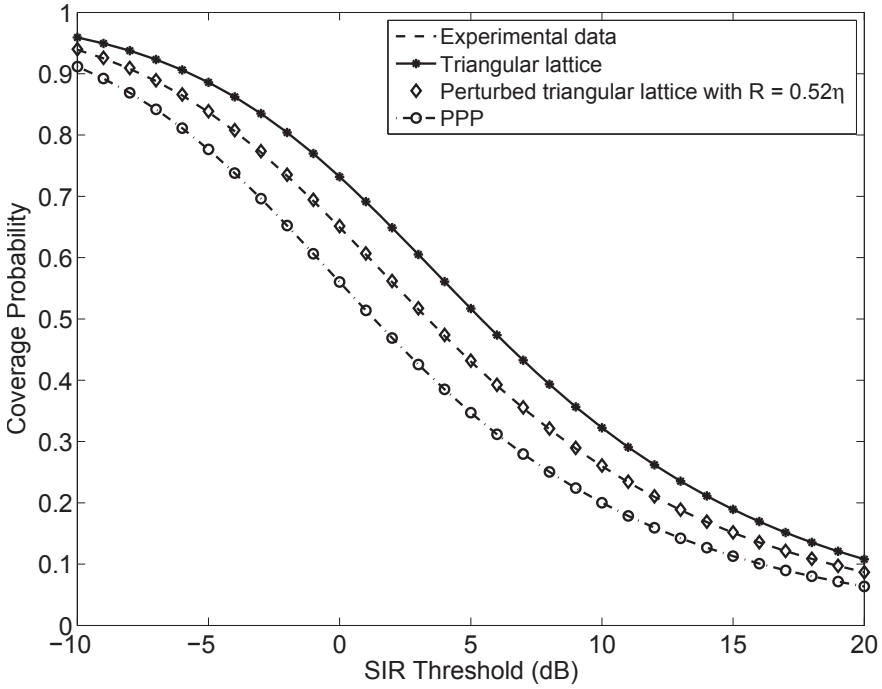

Figure 2.12. The coverage curves of the experimental data (the urban region), the triangular lattice, the triangular lattice with uniform perturbation on the disk $b(o, 0.52\eta)$ and the PPP.

the point sets of the rural region 1 and the rural region 2, the fitting values are $R_1 = 0.70\eta$ and $R_2 = 0.74\eta$, respectively. So the point set of the urban region is the most regular of the three, followed by the point set of the rural region 1 and then the point set of the rural region 2.

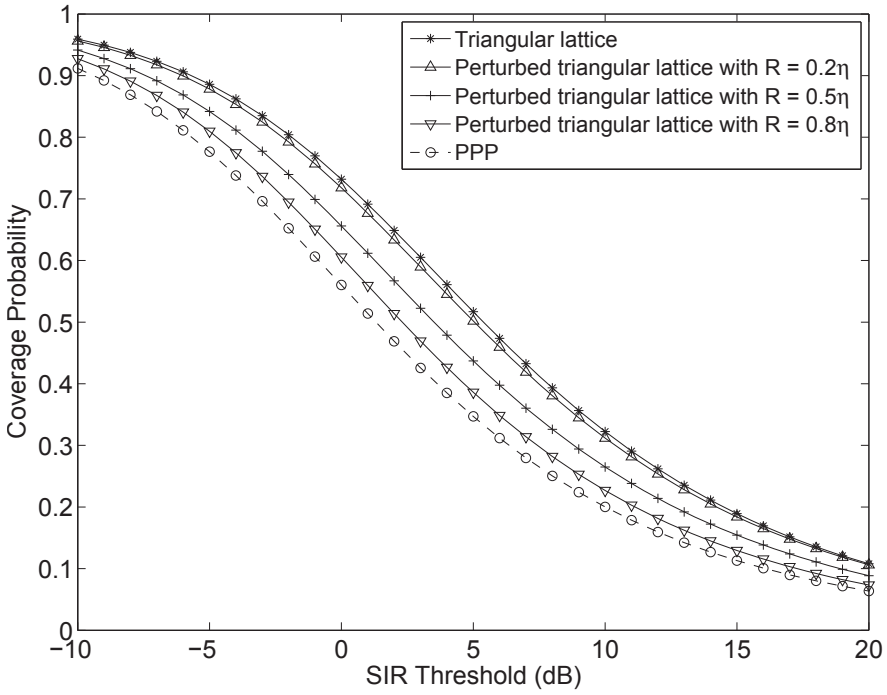

Figure 2.13. The coverage curves of the triangular lattice, the perturbed triangular lattices and the PPP.

To obtain a point set from the model that has approximately the same performance of the coverage probability as the given point set, we can generate a realization of the triangular lattice with uniform perturbation on the disk $b(o, R)$. Although the coverage curve of the realization may have some deviations, its average, the coverage probability, is quite exactly that of the point set.

Thus, we can model the given point set as a realization of the triangular lattice with uniform perturbation on the disk $b(o, R)$, where R can be determined by minimizing the average squared error of the coverage probability, which is of great significance in practice. When analyzing performance metrics that are related with the distribution of the BSs in real cellular networks, we can use the perturbed triangular lattice instead of the lattice or the PPP to model the BSs. Although the perturbed triangular lattice is not as tractable as the PPP, it still has some desirable properties. For the PPP, the distribution of the area of the Voronoi cell is usually approximated by a generalized gamma function [11, 30, 31]. Its typical support is unbounded for the PPP, while for the perturbed triangular lattice, the area is bounded and depends on R.

2.4 Deployment Gain

Here we define a metric that measures how close the point set is to the PPP. This metric can be considered as a "distance" between the point set and the PPP whose coverage curve only depends on the SIR threshold θ. We call this metric the *deployment gain*. It is a function of the coverage probability and is a gain in the SIR, relative to the PPP, provided by the deployment.

Definition 2.9 (Deployment gain)**.** *The deployment gain, denoted by $G(p_t)$, is the SIR difference between the coverage curves of the given point set and the PPP at a given target coverage probability p_t.*

As such, it mimics the notion of the coding gain[2] commonly used in coding theory. We can evaluate different deployment gains at different p_t, for different considerations. In the rest of the chapter, we choose $p_t = 0.5$. At this target probability, the coverage curves are steep, and the gap between curves is easy to observe. More importantly, $G(0.5)$ gives

[2]Coding gain [32, Ch. 1], always a function of the target bit-error-rate (BER), is a measure to quantify the performance of a given code, and is defined by the difference in minimum signal-to-noise-ratio (SNR) required to achieve the same BER with and without the code.

a good approximation of the *average deployment gain*, which is the value by which the coverage curve of the PPP is right shifted such that the difference between the new curve and the curve of the point set is minimized.

Definition 2.10 (Average deployment gain)**.** *Let the difference between two curves be the average squared error defined in (2.9). The average deployment gain, denoted by $\hat{S}_g$, is then defined as:*

$$\hat{S}_g = \arg\min_x \int_a^b \left(P_{\mathrm{c}}^{\mathrm{th}}(t-x) - P_{\mathrm{c}}^{\mathrm{ed}}(t) \right)^2 dt, \tag{2.11}$$

where $a = -9.38$ dB and $b = 16.07$ dB, $P_{\mathrm{c}}^{\mathrm{th}}(t)$ is the theoretical value of the coverage probability for the PPP, and $P_{\mathrm{c}}^{\mathrm{ed}}(t)$ is the experimental value of the coverage probability for the data.

For fixed α, the theoretical expression of the coverage probability of the PPP [8] is

$$P_{\mathrm{c}}^{\mathrm{th}}(\theta) = \frac{1}{1+\rho(\theta,\alpha)}, \tag{2.12}$$

where $\rho(\theta,\alpha) = \theta^{2/\alpha} \int_{\theta^{-2/\alpha}}^{\infty} 1/(1+u^{\alpha/2}) du$. For $\alpha = 4$, $P_{\mathrm{c}}^{\mathrm{th}}(\theta)$ is equal to $P_{\mathrm{c}}(\theta)$ in (2.8).

The average deployment gain $\hat{S}_g$ is a measure of regularity. The point set with a larger average deployment gain has a better performance than the one with a smaller value. For the triangular lattice, when $\alpha = 4$, $\hat{S}_g^l = 4.38$ dB, which is the maximal value of the average deployment gain. Similar to $\hat{S}_g$, $G(0.5)$ is also a measure of regularity and satisfies that $|G(0.5) - \hat{S}_g|/\hat{S}_g < 5\%$, which is verified in simulations. Hence, we can evaluate $G(0.5)$ instead of $\hat{S}_g$ in practice, since $G(0.5)$ is much easier to obtain.

Fig. 2.14 shows the coverage curves of the experimental data and the PPP and the right shifted curves of the PPP by the average deployment gains, when $\alpha = 4$. As the figure shows, the right shifted curve of the PPP and the curve of the point set are well matched. For the point sets of the urban region, the rural region 1 and the rural region 2, the average deployment gains are, respectively, $\hat{S}_{g0} = 2.09$ dB, $\hat{S}_{g1} = 1.28$ dB and $\hat{S}_{g2} = 1.10$ dB. While, the deployment gains at $p_t = 0.5$ are, respectively, $G_0(0.5) = 2.07$ dB, $G_1(0.5) = 1.26$ dB

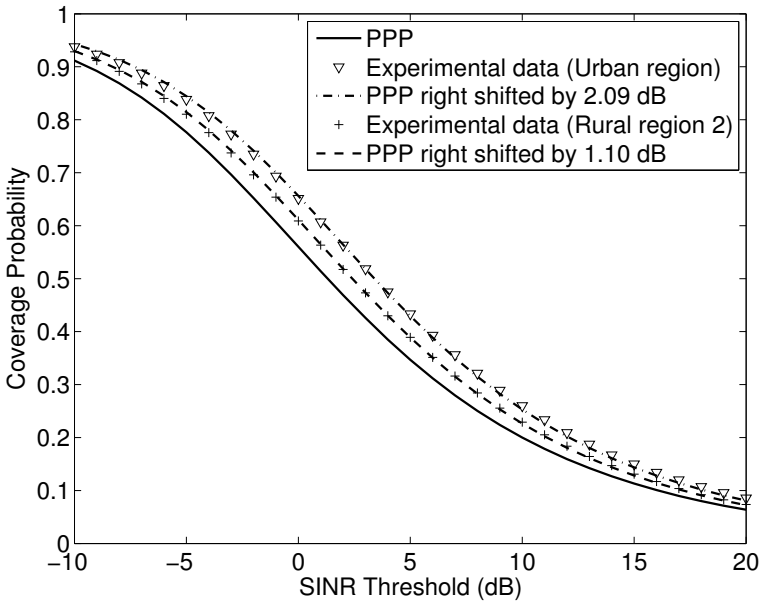

Figure 2.14. The coverage curves of the experimental data and the PPP and the curves of the PPP right shifted by 2.09 dB and 1.10 dB, which are the average deployment gains ($\alpha = 4$). The coverage curve of the experimental data (Rural region 1) and the curve of the PPP right shifted by 1.28 dB are not shown in this figure, but they are well matched, similar to the cases of the other two regions.

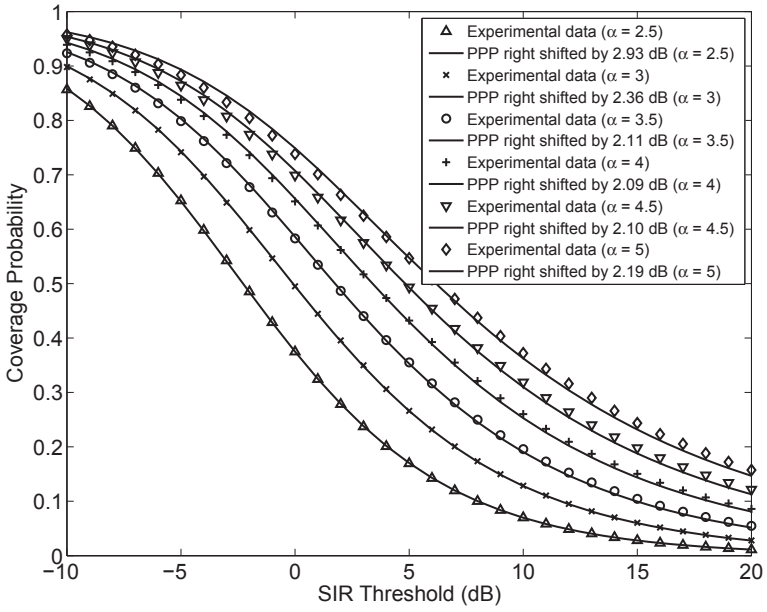

Figure 2.15. The coverage curves of the experimental data (the urban region) and the curves of the PPP right shifted by the corresponding average deployment gains $\hat{S}_g = 2.93, 2.36, 2.11, 2.09, 2.10, 2.19$ (dB) under different values of $\alpha = 2.5, 3, 3.5, 4, 4.5, 5$.

and $G_2(0.5) = 1.08$ dB, which are very close to the average deployment gains. Because $G_0(0.5) > G_1(0.5) > G_2(0.5)$, in terms of the deployment gain, the deployment of the point set of the urban region is the best, followed by the point set of the rural region 1 and then the point set of the rural region 2.

In the above case, the path loss exponent $\alpha = 4$ is fixed. If the value of α varies, $G(0.5)$ and $\hat{S}_g$ will also change. Fig. 2.15 shows the coverage curves of the experimental data (the urban region) and the curves of the PPP right shifted by the corresponding $\hat{S}_g$ under different values of α. For the triangular lattice, as the parameter η of the triangular lattice in the SIR can be eliminated, the coverage probability and the average deployment gain do not depend on η. Fig. 2.16 shows the deployment gains $G(0.5)$ and the average deployment gains $\hat{S}_g$ of all point sets and the triangular lattice when α takes different values, which indicates that $\hat{S}_g$ and $G(0.5)$ are not monotonic as a function of α, but first decrease and then increase as α increases from 2.5 to 5. In this figure, the lines or dashed lines indicate the average deployment gains, and the marks indicate the deployment gains. The inequality $|G(0.5) - \hat{S}_g|/\hat{S}_g < 5\%$ is also satisfied here. The figure also reveals that $G_0(0.5) > G_1(0.5) > G_2(0.5)$ for all $\alpha \in \{2.5, 3, 3.5, 4, 4.5, 5\}$, and the deployment gain of the triangular lattice gives an upper bound.

We have demonstrated that in all cases considered, the coverage probability is very closely approximated by the coverage curve of the PPP, right shifted along the SIR axis by the deployment gain. This general behavior has important implications for the analysis of point process models that are more accurate than the PPP. For the coverage performance evaluation of an arbitrary cellular model, we may take the value analytically obtained for the PPP, and adjust the SIR threshold θ by the deployment gain. Since the coverage probability (or the SIR distribution) affects most first-order metrics, the deployment gain can be used to estimate other metrics (e.g. the average ergodic rate), according to their definitions. Of course, the deployment gain of a model or point set first needs to be established.

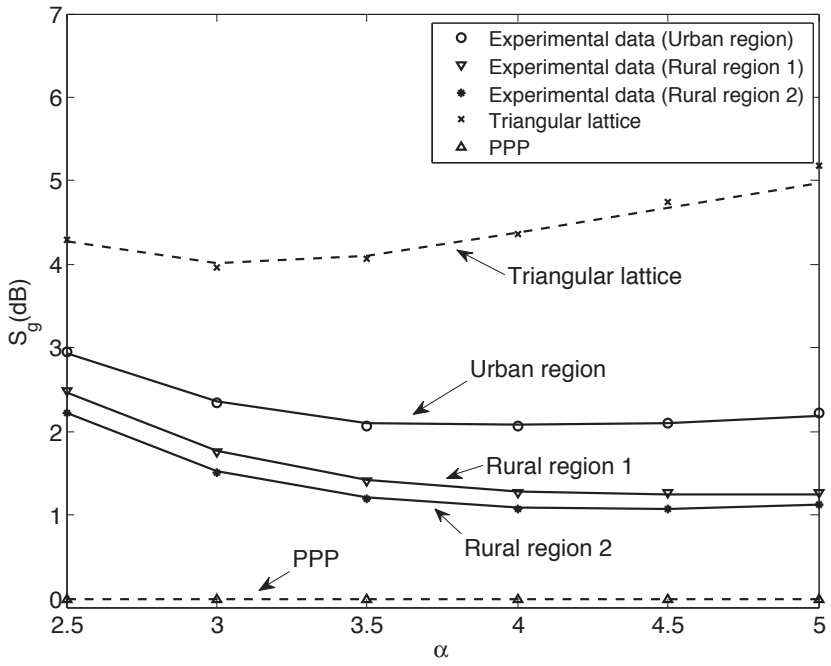

Figure 2.16. The deployment gains $G(0.5)$ and the average deployment gains $\hat{S}_g$ of the experimental data and the triangular lattice when α takes different values. ($G(0.5)$: the marks, $\hat{S}_g$: the lines or dashed lines.)

One important implication is the estimation of the average ergodic rate of the network using the deployment gain. Since the coverage probability is the CCDF of the SIR and the average ergodic rate only depends on the PDF of the SIR, we can first obtain the approximated CDF of the SIR by the deployment gain, and then compute the average ergodic rate. Using the definition of the average ergodic rate $\bar{\gamma}$ and the theoretical expression of $P_{\mathrm{c}}(\theta)$ for the PPP in (2.8), $\bar{\gamma}$ can be expressed as

$$\begin{aligned}\bar{\gamma} &= \mathbb{E}[\ln(1+\mathrm{SIR})] \\ &= -\int_0^{\infty} \ln(1+Gx) dP_{\mathrm{c}}(x) \\ &\overset{(a)}{=} \int_0^{\infty} P_{\mathrm{c}}\left(\frac{e^x-1}{G}\right) dx, \end{aligned} \tag{2.13}$$

where the unit of G is 1, not dB. (a) follows since the CCDF of the random variable $X = \ln(1+G\cdot\mathrm{SIR})$ is $\mathbb{P}(X>x) = \mathbb{P}\big(\mathrm{SIR} > (\exp(x)-1)/G\big) = P_{\mathrm{c}}\big((\exp(x)-1)/G\big)$ and the expectation of a positive random variable can be expressed as the integral over the CCDF. Numerically evaluating the above integral, we can obtain the approximated average ergodic rate of the three point sets. For the point set of the urban region, $\bar{\gamma} \approx 1.770$. For the point set of the rural region 1, $\bar{\gamma} \approx 1.660$. For the point set of the rural region 2, $\bar{\gamma} \approx 1.6311$. Compared with the values obtained in Section 2.2.5, the difference is smaller than 2%.

2.5 Summary

We proposed a general procedure for point process fitting and applied it to publicly available base station data. To the best of our knowledge, this is the first time public data was used for model fitting in cellular systems. We also introduced the deployment gain, which is a metric on the regularity of a point set or a point process and greatly simplifies the analysis of general point process models.

Two methods are used to fit different point processes to real deployments of BSs in

wireless networks in the UK. One is the method of maximum pseudolikelihood, the other is the method of minimum contrast, which minimizes the average squared error of the coverage probability between the point process model and the point set. Using the former method for fitting, we can decide which model fits best in terms of the coverage probability. But the fitted model cannot perfectly fit the coverage probability—there is still a significant gap between the fit and the data. Conversely, using the latter method, the fitted model fits the data perfectly with respect to the metric.

The deployment gain can be used to evaluate the coverage probability and compare the coverage performances of different point sets analytically. It has considerable practical significance in system design. For example, it can help guide the placement of additional BSs and judge the goodness of a concrete deployment of BSs, which includes recognizing how much better the deployment is than the PPP and how much the deployment could be improved theoretically.

Our work sheds light on real BSs modeling in cellular networks in terms of coverage. For a specified BS data set, we can use the methodology in this chapter to model it. The SP, the PHCP and the perturbed triangular lattice are shown to be accurate models. However, for detailed theoretical analyses, these models may not be suitable. They do not have the tractability of the PPP, since their probability generating functionals are unknown. We can carry out the analysis for the PPP instead and then add the deployment gain to the coverage curve to evaluate the performance of the real deployments.

CHAPTER 3

ASYMPTOTIC DEPLOYMENT GAIN

In this chapter, we propose a novel approach to evaluate the coverage probability of cellular networks, where BSs follow a general class of point processes, using the asymptotic deployment gain (ADG).

3.1 System Model and Asymptotic Deployment Gain

3.1.1 System Model

We consider a cellular network that consists of BSs and mobile users. The BSs are modeled as a general m.i. point process Φ of intensity λ on the plane. We assume that Φ is mixing[1] [5, Def. 2.31], which implies that the second moment density $\rho^{(2)}(x_1, x_2) \to \lambda^2$ as $\|x_1 - x_2\| \to \infty$. Intuitively, $\rho^{(2)}(x_1, x_2)$ is the probability that there are two points of Φ at x_1 and x_2 in the infinitesimal volumes dx_1 and dx_2. Rigorously, it is the density pertaining to the second factorial moment measure [5, Def. 6.4], which is given by

$$\alpha^{(2)}(A \times B) = \mathbb{E}\Big(\sum_{x,y \in \Phi}^{\neq} \mathbf{1}_A(x)\mathbf{1}_B(y) \Big) = \int_{A \times B} \rho^{(2)}(y - x)dxdy,$$

[1]The distribution of Φ, denoted by P, is the probability measure pertaining to the outcome measure space $(\mathcal{N}, \mathfrak{N})$, where $\mathcal{N}$ is the set of all counting measures and $\mathfrak{N}$ is the σ-algebra of counting measures. For an event Y, the translated event Y_x is defined as $Y_x \triangleq \{\varphi \in \mathcal{N} : \varphi_{-x} = \{x_1 - x, x_2 - x, \dots\} \in Y\}$, $Y \in \mathfrak{N}$. A stationary point process is mixing if $P(E \bigcap Y_x) \to P(E)P(Y)$, as $\|x\| \to \infty$, $\forall E, Y \in \mathfrak{N}$. Mixing implies that if two events are defined on disjoint finite regions of the plane, the two events become independent as the distance between the regions grows. Moreover, mixing implies ergodicity, which means that it is sufficient to analyze one realization of the point process on a window large enough to obtain statistically meaningful results.

where A, B are two compact subsets of $\mathbb{R}^2$, and the $\neq$ symbol indicates that the sum is taken only over distinct point pairs. Since the point processes considered are m.i., $\rho^{(2)}(x_1, x_2)$ only depends on $\|x_1 - x_2\|$. Without ambiguity, we let $\rho^{(2)}(x_2 - x_1) \triangleq \rho^{(2)}(x_1, x_2)$. Similarly, the nth moment density $\rho^{(n)}(x_1, x_2, \ldots, x_n)$ is the density (with respect to the Lebesgue measure) pertaining to the nth-order factorial moment measure $\alpha^{(n)}$, and we let $\rho^{(n)}(x_2 - x_1, \ldots, x_n - x_1) \triangleq \rho^{(n)}(x_1, \ldots, x_n)$.

We assume all BSs are always transmitting and the transmit power is fixed to 1. Each mobile user receives signals from its nearest BS, and all other BSs act as interferers (the frequency reuse factor is 1). Every signal is assumed to experience path loss and fading. We consider both non-singular and singular path loss models, which are, respectively, $\ell(x) = (1 + \|x\|^\alpha)^{-1}$ and $\ell(x) = \|x\|^{-\alpha}$, where $\alpha > 2$. (Since $\ell(x)$ only depends on $\|x\|$, in this chapter, $\ell(x)$ and $\ell(\|x\|)$ are equivalent.) We assume that the fading is independent and identically distributed (i.i.d.) for signals from all BSs. The fading can be small-scale fading, shadowing or a combination of the two. We mainly focus on Nakagami-m fading, which includes Rayleigh fading as a special case, and the combination of Nakagami-m fading and log-normal shadowing. The thermal noise is assumed to be additive and constant with power W. We define the mean SNR as the received SNR at a distance of $r = 1$, where its value is $1/(2W)$ for the non-singular path loss model and $1/W$ for the singular path loss model.

To formulate the SINR and the coverage probability, we first define the nearest-point operator NP_φ for a point pattern $\varphi \subset \mathbb{R}^2$ as

$$\mathrm{NP}_\varphi(x) \triangleq \arg\min_{y \in \varphi} \{\|y - x\|\}, \quad x \in \mathbb{R}^2. \tag{3.1}$$

If the nearest point is not unique, the operator picks one of the nearest points uniformly

at random. The SINR at location $z \in \mathbb{R}^2$ has the form

$$\mathrm{SINR}_z = \frac{h_u \ell(u-z)}{W + \sum_{x \in \Phi \setminus \{u\}} h_x \ell(x-z)}, \tag{3.2}$$

where $u = \mathrm{NP}_\Phi(z)$ and h_x denotes the i.i.d. fading variable for $x \in \Phi$ with the cumulative distribution function (CDF) F_h and the probability density function (PDF) f_h. For a m.i. point process, the coverage probability $\mathbb{P}(\mathrm{SINR}_z > \theta)$ does not depend on z, and we define

$$P_\mathrm{c}(\theta) = \mathbb{P}(\mathrm{SINR} > \theta). \tag{3.3}$$

Hence, without loss of generality, we focus on the coverage probability at the origin o. Since each user communicates with its nearest BS, the interference at o only comes from the BSs outside the open disk $b(o,r) \triangleq \{x \in \mathbb{R}^2 : \|x\| < r\}$, where $r = \|\mathrm{NP}_\Phi(o)\|$. The total interference, denoted by $I(\Phi)$, is

$$I(\Phi) = \sum_{x \in \Phi \setminus \mathrm{NP}_\Phi(o)} h_x \ell(x). \tag{3.4}$$

3.1.2 Asymptotic Deployment Gain

In Section 2.4, we introduced the deployment gain (DG) for interference-limited networks. Here we redefine the DG, to include the thermal noise.

Definition 3.1 (Deployment gain)**.** *The deployment gain, denoted by $G(p_\mathrm{t})$, is the ratio of the θ values between the coverage probability curves of the given point process (or point set) and the PPP at a given target coverage probability p_t, i.e.,*

$$G(p_\mathrm{t}) = \frac{P_\mathrm{c}^{-1}(p_\mathrm{t})}{(P_\mathrm{c}^{\mathrm{PPP}})^{-1}(p_\mathrm{t})}, \tag{3.5}$$

where $P_\mathrm{c}^{\mathrm{PPP}}(\theta)$ and $P_\mathrm{c}(\theta)$ are, respectively, the coverage probabilities of the PPP and the given point process Φ.

This definition is analogous to the notion of the coding gain commonly used in coding theory [32, Ch. 1].

Fig. 3.1 shows the coverage probability of the PPP, the Matérn cluster process (MCP) [5, Ch. 3], [40], and the randomly translated triangular lattice. The intensities of all the three point processes are the same. We observe that for $p_{\mathrm{t}} > 0.3$, the DG is approximately constant, e.g. the DG of the MCP is about -3 dB. In Fig. 3.1, the coverage probability curves of the PPP that are shifted by $G(0.6)$ (in dB) of the MCP and the triangular lattice are also drawn. We see that the shifted curves overlap quite exactly with the curves of the MCP and the triangular lattice, respectively, for all $p_{\mathrm{t}} > 0.3$. It is thus sensible to study the DG as $p_{\mathrm{t}} \to 1$ and find out whether the DG approaches a constant. To do so, analogous to the notion of the asymptotic coding gain, we define the asymptotic deployment gain (ADG).

Definition 3.2 (Asymptotic deployment gain)**.** *The ADG, denoted by $\hat{G}$, is the deployment gain $G(p_{\mathrm{t}})$ when $\theta \to 0$, or, equivalently, when $p_{\mathrm{t}} \to 1$:*

$$\hat{G} = \lim_{p_{\mathrm{t}} \to 1} G(p_{\mathrm{t}}). \tag{3.6}$$

Note that, the ADG may not exist for some point processes and fading types. In the following section, we will provide some sufficient conditions for the existence of the ADG. For Rayleigh fading, the ADG of the MCP exists.

Similar to the DG, the ADG measures the coverage probability but characterizes the difference between the coverage probability of the PPP and a given point process as the coverage probability approaches 1 instead of for a target coverage probability, and by observation from Fig. 3.1, the ADG closely approximates the DG for all practical values of the coverage probability. Hence, given the ADG of a point process, we can evaluate its coverage probability by shifting (in dB) the corresponding PPP results, that is to say, $P_{\mathrm{c}}(\theta) \approx P_{\mathrm{c}}^{\mathrm{PPP}}(\theta/\hat{G})$ and $P_{\mathrm{c}}(\theta) \sim P_{\mathrm{c}}^{\mathrm{PPP}}(\theta/\hat{G})$, $\theta \to 0$. In Fig. 3.1, we observe that

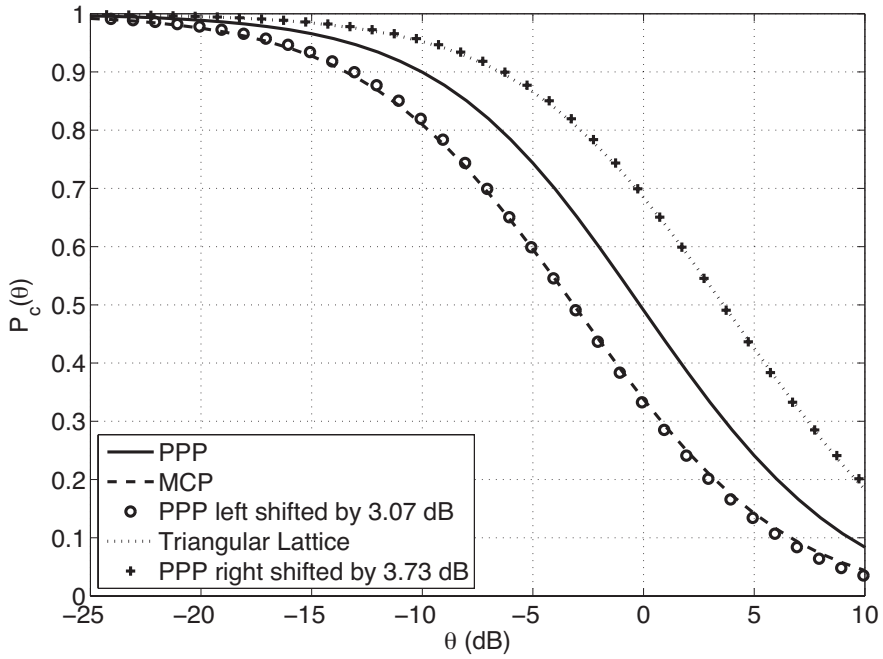

Figure 3.1. The coverage probability of the PPP with intensity $\lambda = 0.1$, the MCP with $\lambda_{\mathrm{p}} = 0.01$, $\bar{c} = 10$ and $r_{\mathrm{c}} = 5$ (see Section 3.2.4 for an explanation of these parameters), and the triangular lattice with density $\lambda = 0.1$ for Rayleigh fading, path loss model $\ell(x) = (1 + \|x\|^4)^{-1}$ and no noise, which are simulated on a 100×100 square. The lines are the coverage probability curves of the three point processes, while the markers indicate the coverage probability curves of the PPP shifted by the DGs of the MCP and the triangular lattice at $p_{\mathrm{t}} = 0.6$.

$\hat{G} \approx 3.73$ dB ≈ 2.4 for the triangular lattice and $\hat{G} \approx -3.07$ dB ≈ 0.5 for the MCP. Note that the ADG relative to the PPP permits an immediate calculation of the ADG between two arbitrary point processes.

3.2 Existence of the Asymptotic Deployment Gain

In this section, we derive several important asymptotic properties of the SINR distribution, given some general assumptions about the point process and the CDF of the fading variables. These asymptotic properties, in turn, prove the existence of the ADG.

Some important and recurrent notations used in this section are summarized in Table 3.1.

TABLE 3.1

SOME IMPORTANT AND RECURRENT NOTATIONS IN SECTION 3.2.

Notation	Description
$\mathrm{NP}_{\varphi}(x)$	$\arg\min_{y\in\varphi}\{\|y-x\|\}, \quad x\in\mathbb{R}^2$
ξ	$\|\mathrm{NP}_{\Phi}(o)\|$
$\xi_{\max}$	$\sup_{x\in\mathbb{R}^2}\min_{y\in\Phi}\{\|x-y\|\}$
Φ_o^{ζ}	$(\Phi \mid \mathrm{NP}_{\Phi}(o)=\zeta)$, where $\zeta\in\mathbb{R}^2\setminus\{o\}$
$I(\Phi_o^{\zeta})$	$\sum_{x\in\Phi_o^{\zeta}\setminus\{\zeta\}} h_x\ell(x)$
Φ^{ζ}	$(\Phi \mid \zeta\in\Phi)$
$\hat{I}(\Phi^{\zeta})$	$\sum_{x\in\Phi^{\zeta}\bigcap B_{\zeta/2}\setminus\{\zeta\}} h_x\ell(x)$

3.2.1 Definition of a General Class of Base Station Models

First we give several notations, based on which we introduce the precise class of point processes we focus on. We define the contact distance $\xi \triangleq \|\mathrm{NP}_\Phi(o)\|$, and define the supremum of ξ as $\xi_{\max} \triangleq \sup_{x\in\mathbb{R}^2} \min_{y\in\Phi}\{\|x-y\|\}$. Due to the ergodicity of the point process (which follows from the mixing property) [5, Ch. 2], $\xi_{\max}$ does not depend on the realization of Φ. $\xi_{\max} = \infty$ in many mixing point processes.

We define $\Phi_o^\zeta \triangleq (\Phi \mid \mathrm{NP}_\Phi(o) = \zeta)$, where $\zeta \in \mathbb{R}^2 \setminus \{o\}$, as the conditional point process that satisfies $\mathrm{NP}_\Phi(o) = \zeta$, which implies $\zeta \in \Phi_o^\zeta$ and $\Phi_o^\zeta(b(o, \|\zeta\|)) = 0$.[2] So given that ζ is the closest point of Φ to o, the total interference is $I(\Phi_o^\zeta)$. However, it is tricky to directly handle the conditional point process conditioned on that there is an empty disk, if the point process is not the PPP. Thus, we compare the interference in Φ_o^ζ with the interference from a point process where the desired BS ζ is not necessarily the closest one. To this end, we define $\Phi^\zeta \triangleq (\Phi \mid \zeta \in \Phi)$ and consider its interference outside a disk of radius $\|\zeta\|/2$ around the origin:

$$\hat{I}(\Phi^\zeta) = \sum_{x\in\Phi^\zeta \bigcap B_{\zeta/2}\setminus\{\zeta\}} h_x \ell(x), \tag{3.7}$$

where $B_{\zeta/2} \triangleq \mathbb{R}^2 \setminus b(o, \|\zeta\|/2)$. Note that it is not necessary to set the radius of the disk to $\|\zeta\|/2$; in fact, the radius could be any quantity that is smaller than $\|\zeta\|$. Since we can use standard Palm theory [5] for Φ^ζ, it is easier to deal with Φ^ζ than Φ_o^ζ.

To motivate the above notations, we give an illustration of them in Fig. 3.2. Both Φ_o^ζ and Φ^ζ have a point at ζ, and we let $\|\zeta\| = y$. All points of Φ_o^ζ are located in the striped region (outside $b(o, y)$), and $I(\Phi_o^\zeta)$ is the interference from all these points except ζ. In contrast, Φ^ζ may have points throughout the whole plane, but $\hat{I}(\Phi^\zeta)$ is the interference only from the points of Φ^ζ in the shaded region (outside $b(o, y/2)$) except ζ.

[2] For a point process Φ, $\Phi(B)$ is a random variable that denotes the number of points in set $B \subset \mathbb{R}^2$.

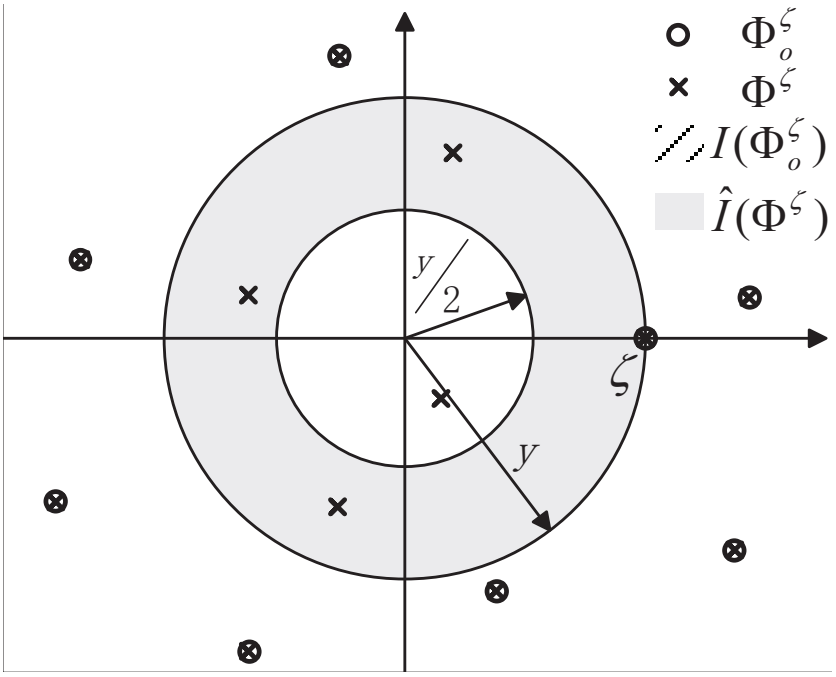

Figure 3.2. An illustration of Φ_o^ζ, Φ^ζ, $I(\Phi_o^\zeta)$ and $\hat{I}(\Phi^\zeta)$, where $\|\zeta\| = y$.

Using the above notations, we define a general class of point process distributions that we use to rigorously state our main result on the SINR distribution.

Definition 3.3 (Set $\mathcal{A}$)**.** *The set $\mathcal{A} = \{P_\Phi\}$ is the set of all m.i. point process distributions P_Φ that are mixing and that satisfy the following four conditions. If a point process Φ is distributed as $P_\Phi \in \mathcal{A}$,*

1. *for all $n \geq 2$, the nth moment density of Φ is bounded, i.e., $\exists q_n < \infty$, such that $\rho^{(n)}(x_1, \ldots, x_n) < q_n$, for $x_1, \ldots, x_n \in \mathbb{R}^2$;*
2. *for all $y > 0$, $\exists \zeta \in \mathbb{R}^2$ with $\|\zeta\| = y$, such that $\mathbb{P}(\Phi^\zeta(b(o, y)) = 0) \neq 0$;*
3. *$\exists y_0 > 0$, such that for all $y > y_0$ and $\zeta \in \mathbb{R}^2$ with $\|\zeta\| = y$, $\hat{I}(\Phi^\zeta)$ stochastically dominates $I(\Phi_o^\zeta)$, i.e., $\mathbb{P}(I(\Phi_o^\zeta) > z) \leq \mathbb{P}(\hat{I}(\Phi^\zeta) > z)$, for all $z \geq 0$;*
4. *$\forall n \in \mathbb{N}$, the n-th moment of the contact distance ξ is bounded, i.e., $\exists b_n < \infty$, s.t. $\mathbb{E}(\xi^n) < b_n$.*

To clarify the need for these conditions, we offer the following remarks:

1. By the mixing property, we have that $\rho^{(2)}(x_1, x_2) \to \lambda^2$, as $\|x_1 - x_2\| \to \infty$, which indicates that when $\|x_1 - x_2\|$ is large enough, $\rho^{(2)}(x_1, x_2)$ is bounded. The first condition is stronger than that. It guarantees that the nth moment measure of Φ is absolutely continuous with respect to the Lebesgue measure, which, in turn, implies that Φ is *locally finite* [5, Ch. 2.2]. A point process is locally finite if and only if $\Phi(B) < \infty$ a.s., for any $B \subset \mathbb{R}^2$ with $\nu(B) < \infty$, where $\nu(\cdot)$ is the Lebesgue measure. Local finiteness is a standard assumption in point process theory, but it is too weak for our purposes. For example, Condition 1 excludes some extreme[3] cases, such as the Gauss-Poisson point process as described in [5, Sec. 3.4], which is locally finite.

2. Since Φ is a m.i. point process, the second condition is equivalent to requiring that for all $y > 0$, $\forall \zeta \in \mathbb{R}^2$ with $\|\zeta\| = y$, such that $\mathbb{P}(\Phi^{\zeta}(b(o, y)) = 0) \neq 0$. That is to say, if $\zeta \in \Phi$, the probability of no points of Φ being located in $b(o, \|\zeta\|)$ is positive. The condition also implies that $\xi_{\max} = \infty$. Because if $\xi_{\max} < \infty$, for all $y > \xi_{\max}$, there surely is at least one point of Φ in $b(o, y)$, which leads to a contradiction since it would imply that $\mathbb{P}(\Phi^{\zeta}(b(o, y)) > 0) = 1$. So, the condition excludes the m.i. and mixing point processes where there exists $r_0 > 0$, such that for all $x \in \mathbb{R}^2$, there is at least one point in the region $b(x, r_0)$. Those point processes may be constructed, but are rarely considered in the context of wireless networks.

3. The third condition is based on the two random variables $I(\Phi_o^{\zeta})$ and $\hat{I}(\Phi^{\zeta})$, whose expressions contain the fading variables. But, in fact, the condition is independent of the fading type, since the fading variables are i.i.d. and their expectation is bounded. The condition means that there exists $y_0 > 0$, such that for all $y > y_0$ and $\zeta \in \mathbb{R}^2$ with $\|\zeta\| = y$, the CCDF of the interference from $\Phi^{\zeta} \bigcap B_{\zeta/2} \setminus \{\zeta\}$ is always no smaller than the CCDF of the interference from $\Phi_o^{\zeta} \setminus \{\zeta\}$. Most point processes meet the condition, since an extra region $b(o, y) \setminus b(o, y/2)$ is included in $\hat{I}(\Phi^{\zeta})$, but not in $I(\Phi_o^{\zeta})$. Some point processes that are seldom considered may violate the condition. For example, albeit somewhat artificial, for small $\epsilon > 0$, the expectation of $\Phi_o^{\zeta}(b(o, \|\zeta\| + \epsilon))$ is much greater than that of $\Phi^{\zeta}(b(o, \|\zeta\| + \epsilon))$, which, at last, leads to the violence of the third condition. Such kind of point processes are beyond our consideration.

4. The fourth condition is satisfied by most point processes that are considered. A sufficient condition of the fourth condition is that $F_{\xi}^{\mathrm{c}}(x) < \exp(-c_0 x)$, as $x \to \infty$, where F_{ξ}^{c} is the CCDF of ξ and $c_0 \in \mathbb{R}^+$. One simple example is the PPP with intensity λ, whose CCDF of ξ is $F_{\xi}^{\mathrm{c}}(x) = \exp(-\lambda \pi x^2)$.

In summary, the four conditions in Def. 3.3 are quite mild; they are satisfied by most point processes that are usually considered in wireless networks and in stochastic geometry, such as the PPP, the MCP, the Thomas cluster process [5, Ch. 3], the Matérn hard-core

[3]We call this point process extreme since, conditioned on a point at o, there is a positive probability of having another point on a subset of Lebesgue measure zero.

process (MHP) [5, Ch. 3] and the Ginibre process [48]. The triangular lattice is not included, since it is not mixing and $\xi_{\max} < \infty$. We will prove that the laws of the PPP, the MCP and the MHP belong to $\mathcal{A}$ in Section 3.2.4.

3.2.2 Main Results

Before presenting the main theorem, we state a property of the distribution of $I(\Phi_o^\zeta)$.

Lemma 3.4. *Assume the fading variable h satisfies that $\forall n \in \mathbb{N}$, $\mathbb{E}(h^n) < +\infty$. For a point process Φ with $P_\Phi \in \mathcal{A}$, the following statements hold:*

1. *for $\ell(x) = (1+\|x\|^\alpha)^{-1}$, all moments of the interference $I(\Phi_o^\zeta)$ are bounded, i.e., $\forall n \in \mathbb{N}$, $\exists c_n \in \mathbb{R}^+$, such that $\mathbb{E}(I(\Phi_o^\zeta)^n) < c_n$, where c_n does not depend on ζ;*
2. *for $\ell(x) = \|x\|^{-\alpha}$, all moments of the interference $I(\Phi_o^\zeta)$ are bounded, and $\forall n \in \mathbb{N}$, $\exists c_n \in \mathbb{R}^+$, such that $\mathbb{E}(I(\Phi_o^\zeta)^n) < c_n \max\{1, \|\zeta\|^{2-\alpha n}\}$.*

Proof. See Appendix A.1. □

Since $I(\Phi_o^\zeta)$ can be interpreted as the total interference at o if the nearest base station to o is at ζ, Lemma 3.4 shows that all moments of the total interference are bounded. If the path loss model is non-singular, the bound can be chosen to be independent of $\|\zeta\|$. However, if the path loss model is singular, the bound depends on $\|\zeta\|$, and if $\|\zeta\|$ goes to 0, it can be proved that $\mathbb{E}(I(\Phi_o^\zeta))$ becomes arbitrarily large for some BS processes, e.g., the PPP.[4]

Now we are equipped to state our main result: if the CDF of the fading variable h decays polynomially around 0 and all moments of h are bounded, then as a result of the boundedness of the moments of the interference, the outage probability $1 - P_{\mathrm{c}}(\theta)$ expressed in dB, as a function of the SINR threshold θ, also in dB, has the same slope as $\theta \to 0$, for all Φ with $P_\Phi \in \mathcal{A}$.

[4]Note that for the PPP with intensity λ, if we de-conditioned on $\|\zeta\|$, by Campbell's theorem, the mean interference $\mathbb{E}(I(\Phi)) = \sum_{x \in \Phi \setminus \mathrm{NP}_\Phi(o)} h_x \|x\|^{-\alpha} = \mathbb{E}(h) \int_0^\infty \frac{(2\pi\lambda)^2}{\alpha-2} x^{3-\alpha} e^{-\lambda\pi x^2} dx$. So, $\mathbb{E}(I(\Phi))$ is finite for $2 < \alpha < 4$, and infinite for $\alpha \geq 4$.

Theorem 3.5. *For a point process Φ with $P_\Phi \in \mathcal{A}$, if the fading variable satisfies*

1. $\exists m \in (0, +\infty)$, *s.t.* $F_h(t) \sim at^m$, *as* $t \to 0$, *where* $a > 0$ *is constant,*

2. $\forall n \in \mathbb{N}$, $\mathbb{E}(h^n) < +\infty$,

then we have

$$\frac{1 - P_{\mathrm{c}}(\theta)}{\theta^m} \to \kappa, \qquad \text{as } \theta \to 0, \tag{3.8}$$

where $0 < \kappa < \infty$ *does not depend on* θ *and is given by*

$$\kappa = \int_0^\infty \mathbb{E}_{I(\Phi_o^\zeta)}\Big[a\ell(y)^{-m}\big(I(\Phi_o^\zeta) + W\big)^m\Big] f_\xi(y)dy \tag{3.9}$$

$(\|\zeta\| = y)$ *and* f_ξ *is the PDF of* ξ.

Proof. See Appendix A.2. □

Theorem 1 shows that the ADG exists and how it depends on the other network parameters. The following theorem quantifies the ADG.

Corollary 3.6. *Under the same condition as in Theorem 3.5, the ADG of* Φ *exists and is given by*

$$\hat{G} = \Big(\frac{\kappa^{\mathrm{PPP}}}{\kappa}\Big)^{\frac{1}{m}}, \tag{3.10}$$

where κ^{PPP} *is the value for the PPP and* κ *is the value for* Φ. *For the PPP with intensity* λ,

$$\kappa^{\mathrm{PPP}} = 2\lambda\pi \int_0^\infty \mathbb{E}_{I_r}\Big[\frac{m^{m-1}}{\Gamma(m)}\ell(r)^{-m}\big(I_r + W\big)^m\Big] r\exp(-\lambda\pi r^2)dr, \tag{3.11}$$

where $I_r = \sum_{x\in\Phi\bigcap b(o,r)^{\mathrm{c}}} h_x\ell(x)$.

Proof. Given a target coverage probability p_{t}, define $\theta_1 \triangleq P_{\mathrm{c}}^{-1}(p_{\mathrm{t}})$ and $\theta_2 \triangleq (P_{\mathrm{c}}^{\mathrm{PPP}})^{-1}(p_{\mathrm{t}})$. As $p_{\mathrm{t}} \to 1$, we have $\theta_1 \to 0$ and $\theta_2 \to 0$. By Theorem 3.5, $1 - P_{\mathrm{c}}(\theta_1) \sim \kappa\theta_1^m$ and $1 - P_{\mathrm{c}}^{\mathrm{PPP}}(\theta_2) \sim \kappa^{\mathrm{PPP}}\theta_2^m$. Since $p_{\mathrm{t}} = P_{\mathrm{c}}(\theta_1) = P_{\mathrm{c}}^{\mathrm{PPP}}(\theta_2)$, as $p_{\mathrm{t}} \to 1$, $\kappa\theta_1^m = \kappa^{\mathrm{PPP}}\theta_2^m$. Thus, $\hat{G} = \lim_{p_{\mathrm{t}}\to 1}\theta_1/\theta_2 = (\kappa^{\mathrm{PPP}}/\kappa)^{1/m}$. □

Note that Rayleigh fading meets the requirements in Theorem 3.5 with $m = 1$. For the special case of the PPP with intensity λ, no noise and Rayleigh fading, the coverage probability can be expressed as (2.12). It follows that $\kappa^{\mathrm{PPP}} = \lim_{\theta\to 0} \frac{1-P_{\mathrm{c}}(\theta)}{\theta} = \frac{2}{\alpha-2}$. For $\alpha = 4$, $P_{\mathrm{c}}(\theta) = 1/(1 + \sqrt{\theta}\arctan\sqrt{\theta})$, and $\kappa^{\mathrm{PPP}} = 1$.

κ plays a key role in evaluating the ADG. For a non-Poisson point process, κ can be obtained by simulations; it does not seem possible to derive an exact analytical expression. The main difficulties for getting the analytical expression are: first, the contact distance distributions for many non-Poisson point processes are not available; second, the nth moment densities ($n \geq 2$) for most non-Poisson point processes are generally unknown, even for $n = 2$; and lastly but most importantly, the knowledge on the non-Poisson point processes conditioned on that there is an empty ball around the origin is required but currently unavailable, e.g. the conditional intensities, the conditioned second moment densities, etc. While Palm theory provides techniques for point processes conditioned on one fixed point (atom), it is not directly applicable to our situation, which requires conditioning on events in a region.

A point process has different ADGs depending on the value of m and other network parameters. So it is sensible to compare the ADGs of different point process models only under the same network parameters.

We have proved that the ADG exists with certain constrains on the fading and point processes. In the rest of this section, we consider some special cases.

3.2.3 Special Cases - Fading Types

Regarding the fading, we mainly consider Nakagami-m fading and *composite fading*, which is a combination of Nakagami-m fading and log-normal shadowing.

3.2.3.1 Nakagami-m Fading

The fading variable $h \sim \text{gamma}(m, \frac{1}{m})$. On the one hand, we have

$$\lim_{t\to 0} \frac{F_h(t)}{t^m} = \lim_{t\to 0} \frac{(mt)^{m-1}\exp(-mt)}{\Gamma(m)t^{m-1}} = \frac{m^{m-1}}{\Gamma(m)} < +\infty. \tag{3.12}$$

On the other hand, since $F_h^{\text{c}}(x)$ has an exponential tail, all moments of h are finite. Thus, Nakagami-m fading meets the requirements in Theorem 3.5.

In addition, we find an interesting phenomenon that for a point process Φ with $P_\Phi \in \mathcal{A}$, the behavior of the CCDF of the fading at the tail determines the tail behavior of the CCDF of the interference $I(\Phi_o^\zeta)$. The following corollary formalizes this property. As usual, $f(x) = \Omega(g(x))$ as $x \to \infty$ means $\limsup_{x\to\infty} \left|\frac{f(x)}{g(x)}\right| > 0$.

Corollary 3.7. *For a point process Φ with $P_\Phi \in \mathcal{A}$, if the fading has at most an exponential tail, i.e., $-\log F_h^{\text{c}}(x) = \Omega(x)$, $x \to \infty$, where $F_h^{\text{c}}(x)$ is the CCDF of the fading variable h, then the interference tail is bounded by an exponential, i.e., $-\log F^{\text{c}}_{I(\Phi_o^\zeta)}(x) = \Omega(x)$, $x \to \infty$, where $F^{\text{c}}_{I(\Phi_o^\zeta)}(x)$ is the CCDF of $I(\Phi_o^\zeta)$.*

Proof. See Appendix A.3. □

A similar property has been derived in [45], namely, that in ad hoc networks modeled by m.i. point processes, an exponential tail in the fading distribution implies an exponential tail in the interference distribution. The result in [45] cannot be directly applied to cellular networks, because in the cellular network that we consider, each user communicates with its nearest BS u and thus no interferers can be closer than u, while the authors in [45] assume the receiver communicates with a transmitter at a fixed location and there can be some interferers closer to the receiver than the transmitter.

3.2.3.2 Composite Fading

The signals from all BSs experience both Nakagami-m fading and log-normal shadowing. The same kind of fading[5] has been investigated in [50], and its special case, which was composed of Rayleigh fading and log-normal shadowing, was studied in [51, 52]. Denoting the fading variable with respect to Nakagami-m fading by $\tilde{h}$ and the fading variable with respect to log-normal shadowing by $\hat{h}$, the composite fading variable can be represented as $h = \tilde{h}\hat{h}$, where $\tilde{h}$ and $\hat{h}$ are independent.

For log-normal shadowing, we use the definition from [57]. Without loss of generality, we assume $\hat{h} = 10^{X/10}$, where $X \sim \mathcal{N}(0, \sigma^2)$. The CDF of $\hat{h}$, denoted by $F_{\hat{h}}(t)$, is

$$F_{\hat{h}}(t) = \frac{1}{2}\mathrm{erfc}\bigg(- \frac{10\log t}{\sigma\sqrt{2}\log 10}\bigg) = \frac{1}{\sqrt{\pi}}\int_{-\frac{10\log t}{\sigma\sqrt{2}\log 10}}^{\infty} \exp(-v^2)dv, \tag{3.13}$$

where erfc is the complementary error function. It is straightforward to obtain that[6] $\mathbb{E}[\hat{h}] = \exp((\frac{\log 10}{10})^2\frac{\sigma^2}{2})$ and $\mathbb{E}[\hat{h}^2] = \exp((\frac{\log 10}{10})^2 2\sigma^2)$, and to show that as $t \to \infty$, $F^{\mathrm{c}}_{\hat{h}}(t)$ decays faster than t^{-n} for any $n \in \mathbb{N}$, but slower than $\exp(-at)$ for any $a > 0$.

For composite fading, we have the following lemma about the distribution of h.

Lemma 3.8. *If $\tilde{h} \sim$ gamma$(m, \frac{1}{m})$, $10\log\hat{h}/\log 10 \sim \mathcal{N}(0, \sigma^2)$, and $\tilde{h}$ is independent of $\hat{h}$, the distribution of $h = \tilde{h}\hat{h}$ has the following properties:*

1. *F_h decays polynomially around 0 and*

$$\lim_{t\to 0}\frac{F_h(t)}{t^m} = \frac{m^{m-1}}{\Gamma(m)}\exp\left(\Big(\frac{m\log 10}{10\sqrt{2}}\Big)^2\sigma^2\right) < \infty;$$

2. *$F^{\mathrm{c}}_h(t) = o(t^{-n})$, as $t \to \infty$, for any $n \in \mathbb{N}$, and $-\log F^{\mathrm{c}}_h(t) = o(t)$, $t \to \infty$.*

---

[5]Note that in the presence of shadowing, it may be more appropriate to assume that each mobile user is associated with the BS that offers the highest received power. Here, we assume that each user is connected to the BS that offers the highest average received power, or equivalently, which is the closest to the user.

[6]Note that the mean of $\hat{h}$ is not 1. Actually, we could normalize it to 1 and replace it with the normalized variable in our results, but since it does not affect our results, for convenience, we just leave it as it is.

Proof. See Appendix A.4. □

The two properties in Lemma 3.8 indicate that the composite fading retains the asymptotic property of Nakagami-m fading for $t \to 0$ and that of log-normal shadowing for $t \to \infty$, respectively. They also imply that the composite fading meets the requirements in Theorem 3.5.[7]

Regarding the distribution of the interference at the tail, we have the following corollary.

Corollary 3.9. *For a point process Φ with $P_\Phi \in \mathcal{A}$ and composite fading, the interference tail is upper bounded by a power law with arbitrary parameter β, i.e., $F^{\mathrm{c}}_{I(\Phi_o^\zeta)}(y) = o(y^{-\beta})$, $\forall \beta \in \mathbb{N}$, as $y \to +\infty$.*

Proof. We can simply apply the Markov inequality and have that $\forall \beta \in \mathbb{N}$,

$$\mathbb{P}(I(\Phi_o^\zeta) > y) \leq \frac{\mathbb{E}(I(\Phi_o^\zeta)^\beta)}{y^\beta}. \tag{3.14}$$

Hence, using Lemma 3.4, we have $F^{\mathrm{c}}_{I(\Phi_o^\zeta)}(y) = o(y^{-\beta})$, $\forall \beta \in \mathbb{N}$, as $y \to +\infty$. □

3.2.4 Special Cases - Point Processes

As for the point processes, we specifically concentrate on the PPP, the MCP and the MHP. We first briefly describe the MCP and the MHP.

Matérn Cluster Process: As a class of clustered point processes on the plane built on a PPP, the MCPs are doubly Poisson cluster processes, where the parent points form a uniform PPP Φ_{p} of intensity λ_{p} and the daughter points are uniformly scattered on the

[7]It is worth noting that in [53], it is proved that with increasing shadowing variance, the received powers at the origin for all m.i. point processes converge weakly to those of a PPP. This implies that if shadowing is considered in the BS association, the Poisson result applies in the limit $\sigma^2 \to \infty$. However, it does not mean that the ADG $\hat{G} \to 1$, as $\sigma^2 \to \infty$ in our scenario with compound fading. We assume BS association is based on distance, and shadowing is affecting the coverage probability rather than being included in the decision on which BS is the serving one. In fact, as $\sigma^2 \to \infty$, it can be shown using (3.9), (3.10), the multinomial theorem and the Dominated Convergence Theorem that $\hat{G}$ approaches a constant different from 1.

ball of radius $r_{\rm c}$ centered at each parent point $x_{\rm p}$ with intensity $\lambda_0(x) = \frac{\bar{c}}{\pi r_{\rm c}^2}\mathbf{1}_{B(x_{\rm p},r_{\rm c})}(x)$, where $B(x_{\rm p}, r_{\rm c}) \triangleq \{x \in \mathbb{R}^2 : \|x - x_{\rm p}\| \leq r_{\rm c}\}$ is the closed disk of radius $r_{\rm c}$ centered at $x_{\rm p}$. The mean number of daughter points in one cluster is $\bar{c}$. So the intensity of the process is $\lambda = \lambda_{\rm p}\bar{c}$.

Matérn Hard-core Process: The MHPs are a class of repulsive point processes, where points are forbidden to be closer than a certain minimum distance. There are several types of MHPs. Here we only consider the MHP of type II [5, Ch. 3], which is generated by starting with a basic uniform PPP $\Phi_{\rm b}$ of intensity $\lambda_{\rm b}$, adding to each point x an independent random variable $m(x)$, called a mark, uniformly distributed on $[0, 1]$, then flagging for removal all points that have a neighbor within distance $r_{\rm h}$ that has a smaller mark and finally removing all flagged points. The intensity of the MHP is $\lambda = \frac{1-\exp(-\lambda_{\rm b}\pi r_{\rm h}^2)}{\pi r_{\rm h}^2}$. The highest density $\lambda_{\max} = 1/(\pi r_{\rm h}^2)$ is achieved as $\lambda_{\rm b} \to \infty$.

Lemma 3.10. *The distributions of the PPP, the MCP and the MHP belong to the set $\mathcal{A}$.*

Proof. See Appendix A.5. □

By Lemma 3.10, regarding Nakagami-m fading and composite fading, we have the following corollary directly from Theorem 3.5.

Corollary 3.11. *If the fading is Nakagami-m or the composite fading, then for the PPP, the MCP and the MHP,*

$$\frac{1 - P_{\rm c}(\theta)}{\theta^m} \to \kappa, \qquad \text{as } \theta \to 0, \tag{3.15}$$

where κ is given by (3.9)*. In* (3.9)*, for Nakagami-m fading, $a = \frac{m^{m-1}}{\Gamma(m)}$; for the composite fading, $a = \frac{m^{m-1}}{\Gamma(m)} \exp\left(\left(\frac{m \log 10}{10\sqrt{2}}\right)^2 \sigma^2\right)$.*

It is worth noting that the Thomas cluster process (TCP) is an important concrete Neyman-Scott process [5, Ch. 3], along with the MCP. Similar to the MCP, the TCP has also been studied in wireless networks (e.g., [40]). The difference between the two point

processes is that for the TCP, the daughter points are normally scattered with variance σ_t^2 around each parent point x_p with intensity $\lambda_0(x) = \frac{\bar{c}}{2\pi\sigma_t^2} \exp\Big(- \frac{\|x-x_\mathrm{p}\|^2}{2\sigma_t^2} \Big)$. It can be shown that the distribution of the TCP also belongs to the set $\mathcal{A}$. The proof is similar to the proof for the MCP.

The applicability of the ADG framework is not restricted to the case of full frequency reuse. For example, to analyze the benefits of partial frequency reuse, an independent thinning of the base station point process could be considered, as in [8]. Similar to the proof of Lemma 3.10, we can prove that after an independent thinning of the PPP, the MHP and the MCP, the distributions of the new point processes Φ' belong to $\mathcal{A}$. That said, it is unclear whether for *all* point processes in $\mathcal{A}$, their independently thinned version still belongs to $\mathcal{A}$. This is an interesting open problem that we will consider it in our future work.

3.3 Applications of the Asymptotic Deployment Gain

Since the ADG characterizes the gap of the coverage probability between a point process and the PPP, any statistic that depends on the distribution of the SINR (e.g., the average ergodic rate and the mean SINR) can be approximated using the ADG. In this section, we focus on the average ergodic rate and the mean SINR.

3.3.1 Average Ergodic Rate

We assume that the base station adopts adaptive modulation/coding to achieve the Shannon bound of the rate for the instantaneous SINR. That is to say, each BS adjusts its rate of transmission to $\gamma = \ln(1 + \mathrm{SINR})$. The average ergodic rate (expressed in nats) is $\bar{\gamma} \triangleq \mathbb{E}[\ln(1 + \mathrm{SINR})]$.

Denoting the ADG of Φ as $\hat{G}$ and the coverage probability of the corresponding PPP as $P_\mathrm{c}^\mathrm{PPP}(\theta)$, the coverage probability for Φ is approximated as $P_\mathrm{c}^\mathrm{PPP}(\theta/\hat{G})$. The average

ergodic rate can be expressed as

$$\bar{\gamma} \approx -\int_0^\infty \ln(1+\theta) dP_{\rm c}^{\rm PPP}\left(\frac{\theta}{\hat{G}}\right) = -\int_0^\infty \ln(1+\hat{G}\theta) dP_{\rm c}^{\rm PPP}(\theta) \overset{(a)}{=} \int_0^\infty P_{\rm c}^{\rm PPP}\left(\frac{e^x-1}{\hat{G}}\right) dx,$$

where (a) follows since the CCDF of the random variable $X = \ln(1+\hat{G}\cdot \mathrm{SINR})$ is $\mathbb{P}(X > x) = \mathbb{P}\big(\mathrm{SINR} > (e^x-1)/\hat{G}\big) = P_{\rm c}^{\rm PPP}\big((e^x-1)/\hat{G}\big)$ and the expectation of a positive random variable can be expressed as the integral over the CCDF.

3.3.2 Mean SINR

Just as the coverage probability and the average ergodic rate, the mean SINR is also an important criterion that has been discussed in wireless networks, e.g. in [54]. Denote M_Φ as the mean SINR for Φ, and $M_{\rm PPP}$ the mean SINR for the PPP with the same intensity as that of Φ. It can be proved that the mean SINR for the PPP is infinite if the path loss model is singular. Briefly, for $\zeta = \mathrm{NP}_\Phi(o)$, letting $y = \|\zeta\|$, we have

$$\begin{aligned}
\mathbb{E}(\mathrm{SINR}) &= \mathbb{E}\left(\frac{h_\zeta \ell(\zeta)}{W + I(\Phi_o^\zeta)}\right) \overset{(a)}{\geq} \mathbb{E}(h)\mathbb{E}_y\left(\frac{\ell(\zeta)}{W + \mathbb{E}[I(\Phi_o^\zeta)]}\right) \overset{(b)}{\geq} \mathbb{E}(h)\mathbb{E}_y\left(\frac{y^{-\alpha}}{W + c_1 \max\{1, y^{2-\alpha}\}}\right) \\
&= \mathbb{E}(h)\left(\int_0^1 \frac{x^{-\alpha}}{W + c_1 x^{2-\alpha}} f_{\|\zeta\|}(x)dx + \int_1^\infty \frac{x^{-\alpha}}{W + c_1} f_{\|\zeta\|}(x)dx\right) \\
&\geq \mathbb{E}(h)\left(\int_0^1 \frac{x^{-1}}{W + c_1} 2\pi\lambda e^{-\lambda\pi x^2} dx + \int_1^\infty \frac{x^{-\alpha}}{W + c_1} f_{\|\zeta\|}(x)dx\right) = \infty,
\end{aligned}$$

where $f_{\|\zeta\|}(x) = 2\pi\lambda x e^{-\lambda\pi x^2}$ is the contact distance distribution for the PPP, (a) follows from Jensen's inequality, and (b) follows from Lemma 3.4.

So, we only consider the non-singular path loss model. We have $\mathbb{E}(\mathrm{SINR}) = \mathbb{E}(h)\mathbb{E}\big(\frac{\ell(\zeta)}{W+I(\Phi_o^\zeta)}\big) \leq \frac{\mathbb{E}(h)}{W}\mathbb{E}(\ell(\zeta)) < \infty$. Given the ADG $\hat{G}$ of Φ, we have a simple approximation for M_Φ:

$$M_\Phi \approx \hat{G} M_{\rm PPP}, \tag{3.16}$$

where $M_{\rm PPP}$ can be expressed as $M_{\rm PPP} = \int_0^\infty P_{\rm c}^{\rm PPP}(\theta)d\theta$. Therefore, the ADG can also be

interpreted as the approximate gain in the mean SINR.

3.4 Simulations

In this section, we present simulation results on a 100×100 square, where we consider the non-singular path loss model and fix the path loss exponent to $\alpha = 4$ and the intensity of the point processes to $\lambda = 0.1$. For the MCP, we let $\lambda_{\mathrm{p}} = 0.01$, $\bar{c} = 10$ and $r_{\mathrm{c}} = 5$; for the MHP, we let $\lambda_{\mathrm{b}} = 0.263$ and $r_{\mathrm{h}} = 1.7$. We present our results in two subsections corresponding to the SINR distribution and the applications of the ADG.

3.4.1 SINR Distribution

3.4.1.1 Nakagami-m Fading

In this part, we present simulation results of the outage probability for the PPP, the MCP, and the MHP under Nakagami-m fading.

Fig. 5.1 shows the outage curves $1 - P_{\mathrm{c}}(\theta)$ of the PPP for $m \in \{0.5, 1, 2\}$ and different mean SNR values. Note that the SNR value here is $1/(2W)$. As θ approaches 0, the slopes of the curves for $m = 0.5$ are all 5 dB/decade, the slopes for $m = 1$ are all 10 dB/decade, and the slopes for $m = 2$ are all 20 dB/decade, in agreement with Corollary 3.11. We also observe that there is only a rather small gap between the cases of SNR = 20 dB and SNR $= \infty$, thus the thermal noise does not significantly affect the asymptotic performance of the coverage probability. We will neglect noise in the rest of this section.

In Fig. 5.2, we find that for the same point process, a different m implies a different asymptotic slope. In fact, the slope is $10m$ dB/decade, just as Corollary 3.11 indicates. For the same m, different point processes have the same asymptotic slope, thus in the high-reliability regime, the coverage probability of a non-Poisson process can be obtained accurately simply by shifting the coverage probability curve of the PPP with the same intensity by the ADG. Besides, we observe that for any m, the coverage probability of

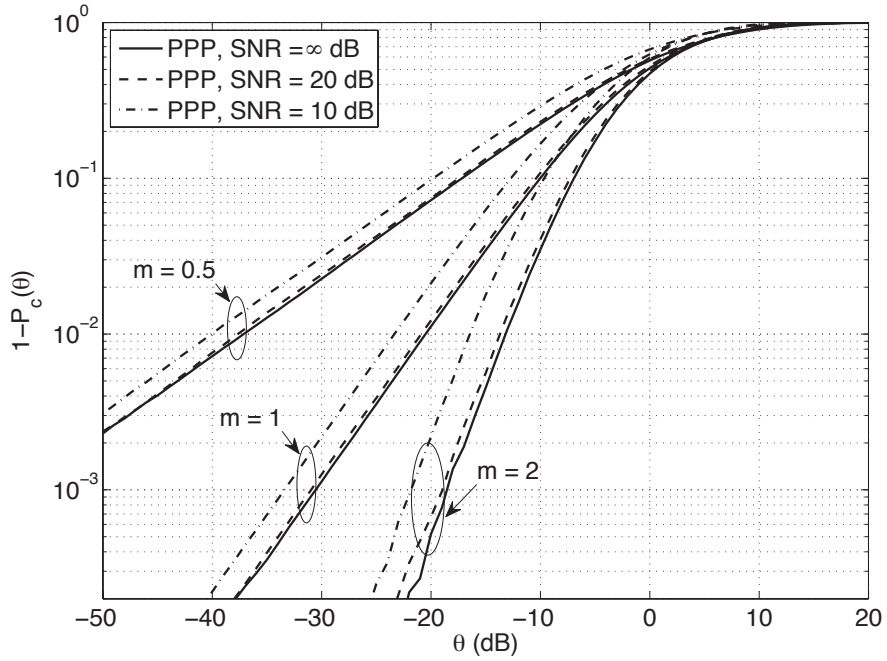

Figure 3.3. Nakagami-m fading: the outage probability $1 - P_{\rm c}(\theta)$ vs. θ for the PPP when $m \in \{0.5, 1, 2\}$ under different SNR settings.

the MHP is the largest of the three processes, followed by the PPP and then the MCP. Intuitively, it is because the MHP is more regular than the PPP and the MCP is more clustered than the PPP. In addition, since the value of κ for the MCP and the MHP can be approximated through the simulation, by Corollary 3.6, we can approximate their ADGs. Denote by $\hat{G}_m^{\rm MCP}$ the ADG for the MCP with respect to m, and by $\hat{G}_m^{\rm MHP}$ that of the MHP. We obtain that for the MCP, $\hat{G}_{0.5}^{\rm MCP} \approx 0.47$, $\hat{G}_1^{\rm MCP} \approx 0.49$, $\hat{G}_2^{\rm MCP} \approx 0.37$ and $\hat{G}_4^{\rm MCP} \approx 0.29$; for the MHP, $\hat{G}_{0.5}^{\rm MHP} \approx 1.38$, $\hat{G}_1^{\rm MHP} \approx 1.58$, $\hat{G}_2^{\rm MHP} \approx 1.48$ and $\hat{G}_4^{\rm MHP} \approx 1.45$. Note that $\hat{G}_1^{\rm MCP}$ is consistent with the approximated value 0.49 obtained from Fig. 3.1.

3.4.1.2 Composite Fading

We consider the combination of Nakagami-m fading and log-normal shadowing in this part. In Fig. 3.5, the outage probabilities for the PPP, the MCP and the MHP are exhibited. The MHP still has the best outage probability, followed by the PPP and the

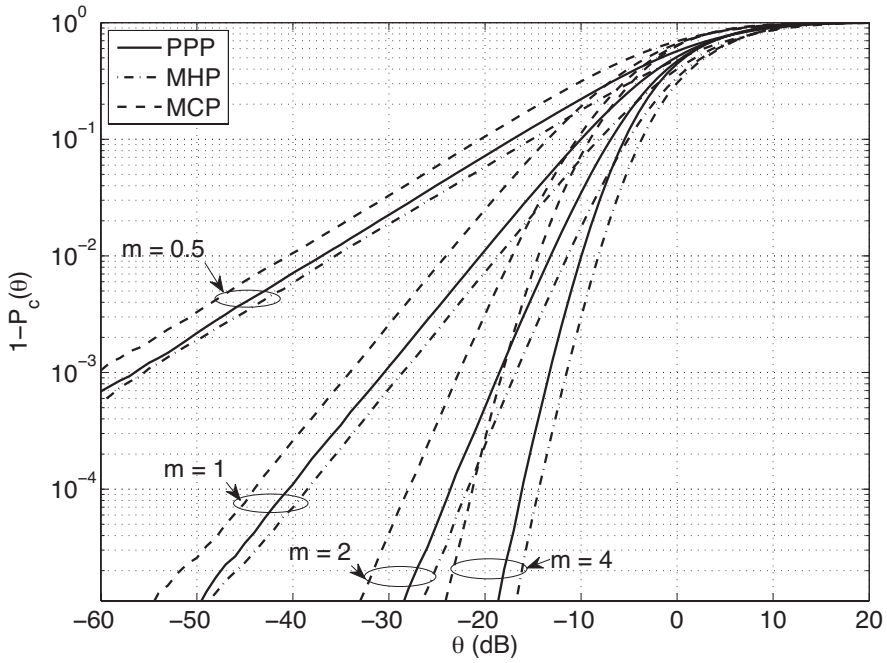

Figure 3.4. Nakagami-m fading: the outage probability $1 - P_{\rm c}(\theta)$ vs. θ for the PPP, the MCP and the MHP when $m \in \{0.5, 1, 2, 4\}$ (no noise).

MCP. We also observe that the value of σ does not affect the slope of the outage curve as $\theta \to 0$, which is $10m$ dB/decade. The ADGs of the MCP and MHP can also be estimated: for $m = 1$ and $\sigma = 2$, $\hat{G}_1^{\rm MCP} \approx 0.51$ and $\hat{G}_1^{\rm MHP} \approx 1.55$; for $m = 2$ and $\sigma = 4$, $\hat{G}_2^{\rm MCP} \approx 0.40$ and $\hat{G}_2^{\rm MHP} \approx 1.37$.

3.4.2 Applications of the ADG

In this subsection, we evaluate the average ergodic rate and the mean SINR for the PPP, the MCP and the MHP through simulations, and also estimate them using the ADGs. The ADG values are approximated by the DG values at $p_{\rm t} = 1 - 10^{-4}$ for the three point processes, which are presented in Table 3.2.

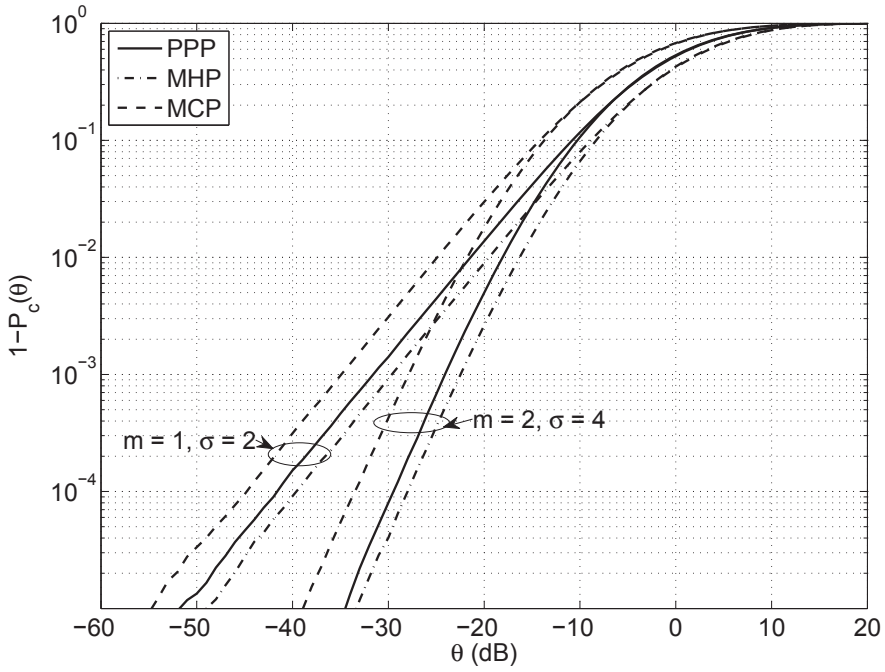

Figure 3.5. Compound fading: the outage probability $1 - P_{\rm c}(\theta)$ vs. θ for the PPP, the MCP and the MHP when $m = 1, \sigma = 2$ and $m = 2, \sigma = 4$ (no noise, $\alpha = 4$).

TABLE 3.2

THE ADGS FOR DIFFERENT α (RAYLEIGH FADING, NO NOISE).

ADG	$\alpha = 2.5$	$\alpha = 3.0$	$\alpha = 3.5$	$\alpha = 4$	$\alpha = 4.5$
MCP	0.46	0.40	0.41	0.49	0.42
MHP	1.27	1.37	1.37	1.58	1.40

3.4.2.1 Average Ergodic Rate

In Fig. 3.6, the average ergodic rates $\bar{\gamma}$ for the three point processes as a function of α are shown as the lines. We also use the simulation results of the PPP and the ADGs in Table 3.2 to estimate the average ergodic rates for the MCP and the MHP. The estimated values are shown as the markers in Fig. 3.6. From the figure, we observe that the average ergodic rates estimated using the ADGs provide fairly good approximations to the empirical values. We also observe that $\bar{\gamma}$ increases as α grows, which is obvious since the interference decays much faster than the desired signal power.

3.4.2.2 Mean SINR

In Fig. 3.7, the lines are the mean SINRs for the three point processes as a function of α. The markers indicate the mean SINRs for the MCP and the MHP estimated using the simulation results of the PPP and the ADGs. The approximations using the ADGs are acceptable, although not perfect. The gaps between the values estimated using the ADG and the empirical value are mainly due to the fact that the mean is heavily affected by the tail of the CCDF of the SINR, while the ADG approximation is accurate for small and moderate values of θ.

3.5 Summary

In this chapter, we examined the asymptotic properties of the SINR distribution for a variety of motion-invariant point processes, given some general assumptions on the point process and general fading assumptions. The assumptions on the point process are satisfied by many commonly used point processes, e.g. the PPP, the MHP, the MCP and the TCP. Similarly, the fading assumptions are satisfied by Nakagami-m fading and composite fading. We proved that $1 - P_{\mathrm{c}}(\theta) \sim \kappa\theta^m$, as $\theta \to 0$, which shows that the ADG exists.

Under the same system configurations on the fading and path loss, different point

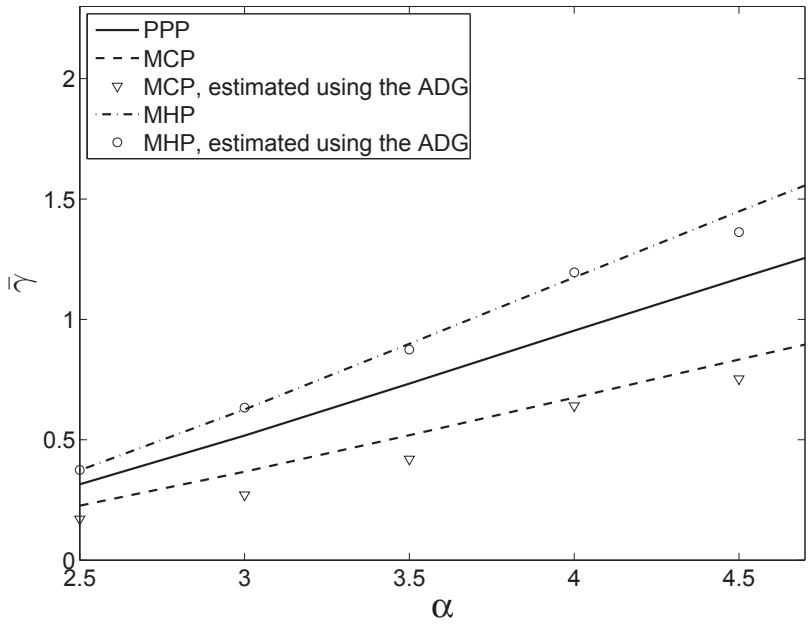

Figure 3.6. The average ergodic rate $\bar{\gamma}$ vs. α for the PPP, the MCP and the MHP. The lines are the average ergodic rates obtained directly from simulations, while the markers are the average ergodic rates estimated using the ADGs.

processes with the same intensity have different ADGs. Thus, the ADG can be used as a simple metric to characterize the coverage probability. Given the ADG of a point process, we can obtain the precise CCDF of the SINR near 1 by shifting the coverage probability curve of the PPP with the same intensity by the ADG (in dB), and numerical studies show that the shifted coverage probability curve is highly accurate for all practical coverage probabilities.

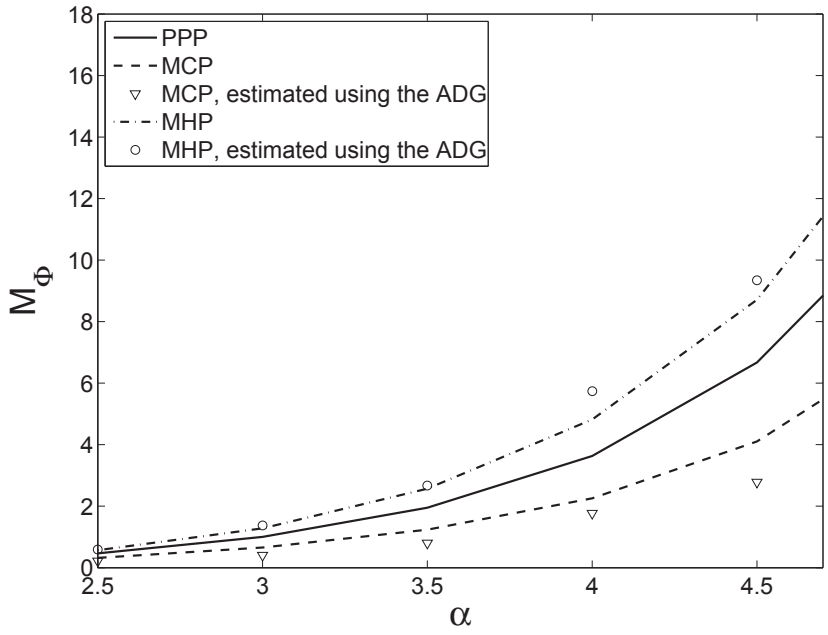

Figure 3.7. The mean SINR M_Φ vs. α for the PPP, the MCP and the MHP. The lines are the mean SINRs obtained directly from simulations, while the markers are the mean SINRs estimated using the ADGs (i.e., by (3.16)).

CHAPTER 4

SIR ASYMPTOTICS IN GENERAL NETWORK MODELS

In this chapter, we extend our asymptotic results in Chapter 3 to more scenarios. We show our results as the leaves of the tree in Fig. 4.1. Visually, the tree provides the structure of the main part of this chapter. We discuss the asymptotic results for all combinations of the assumptions.

Besides, we study the impact of the nearest interferer on the asymptotic properties of the SIR distribution, to see whether the nearest interferer plays a dominant role in determining the asymptotics.

The rest of this chapter is organized as follows. In Section 4.1, we introduce the system model. We analyze the asymptotic properties of the lower and upper tails of the SIR distribution in Sections 4.2 and 4.3, respectively. In Section 4.4, the impact of the nearest interferer on the asymptotic is investigated. A summary is given in Section 4.5.

4.1 System Models

We consider general network models, including ad hoc networks and cellular networks, where the transmitters/BSs are assumed to follow a stationary point process Φ. Without loss of generality, we focus on the SIR distribution at the typical receiver at the origin o. We assume that the desired transmitter/base station is x_0 and all transmitters/BSs transmit at the same unit power level. Note that in ad hoc networks, x_0 does not belong to Φ, but in cellular networks, x_0 is a point of Φ. Also, in ad hoc networks, if Φ is not simple, we assume there is an interferer at the same location as x_0. Let Φ^* be the collection of all interferers in both ad hoc networks and cellular networks. All signals experience i.i.d.

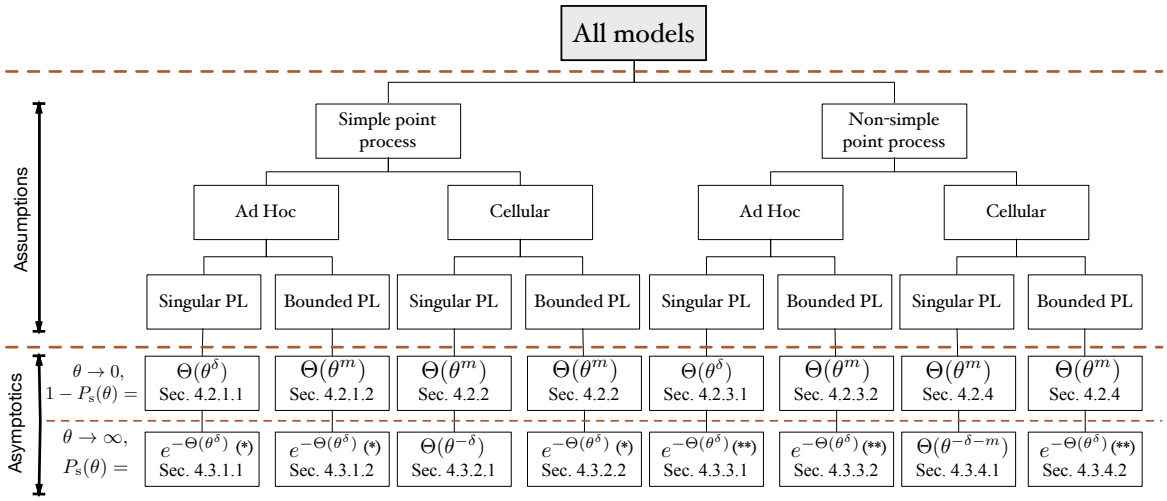

Figure 4.1. The organization of the chapter sorted by the assumptions and the asymptotic results.

fading with unit mean and the cumulative distribution function (CDF) of the fading is denoted by F_h. The SIR is given by

$$\mathrm{SIR} \triangleq \frac{S}{I} = \frac{h_{x_0}\ell(x_0)}{\int_{\mathbb{R}^2} h_x \ell(x)\Phi^*(\mathrm{d}x)}, \tag{4.1}$$

where (h_x) are the fading random variables and $\ell(\cdot)$ is the path loss law. We use the integral form of the interference instead of the usual sum over all interferers, since Φ^* is not necessarily simple. Note that for simple point processes, S and I are independent in ad hoc networks but correlated in cellular networks; for non-simple point processes, S and I are always correlated, since there is always one interferer at the same location as the desired transmitter/BS.

Using the notation of the interference-to-(average)-signal ratio (ISR) defined in [61], in

general, the success probability can be expressed as

$$P_{\mathrm{s}}(\theta) = \mathbb{E}\bar{F}_h\left(\theta \cdot \frac{I}{\mathbb{E}_h\left(S\right)}\right)$$
$$= \mathbb{E}\bar{F}_h(\theta \cdot \bar{\mathrm{ISR}}), \tag{4.2}$$

where $\mathbb{E}_h\left(S\right) = \mathbb{E}\left(S \mid \Phi\right) = \ell(x_0)$ is the mean received signal power averaged only over the fading and $\bar{F}_h$ is the CCDF of the fading random variables.

In the following two sections, we will first discuss the asymptotic properties of the lower tail of the SIR distribution (near 0) and then the upper tail of the SIR distribution (near ∞). Note that in the rest of this chapter, by "tail" we mean the "upper tail", whereas "lower tail" refers to the asymptotics near 0.

4.2 Lower Tail of the SIR Distribution

4.2.1 Simple Ad Hoc Models

4.2.1.1 Singular Path Loss Model

Consider the wireless network where all transmitters follow a simple stationary point processes Φ of intensity λ and the distance between the transmitter and the corresponding receiver is a constant $b > 0$. We add an additional transmitter-receiver pair with the the receiver at the origin o and its desired transmitter at $x_0 = (b, 0) \notin \Phi$ and analyze the SIR distribution at o. We assume all transmitters are always transmitting[1] at unit power and in the same frequency band. Every signal is assumed to experience i.i.d. fading with mean 1. The path loss model is $\ell(x) = \|x\|^{-\alpha}$, where $\alpha > 2$. The lower tail of the CDF of the SIR has the following property:

Theorem 4.1. *Let Φ be a simple stationary point processes with intensity λ, and let the*

[1]This is not a restriction due to the generality of the point process model (most MAC schemes preserve the stationarity of the transmitters).

desired received signal strength be given by $S = hb^{-\alpha}$ *and the interference be given by* $I = \sum_{x\in\Phi} h_x \|x\|^{-\alpha}$. *If the fading random variable* h *satisfies* $\mathbb{E}[h^{-\delta}] < \infty$, *we have*

$$1 - P_{\mathrm{s}}(\theta) \sim \theta^{\delta}\pi\lambda b^2 \mathbb{E}[h^{\delta}]\mathbb{E}[h^{-\delta}], \quad \theta \to 0. \tag{4.3}$$

In particular, if $h \sim \exp(1)$, $1 - P_{\mathrm{s}}(\theta) \sim \theta^{\delta}\pi\lambda b^2 \Gamma(1+\delta)\Gamma(1-\delta)$, *as* $\theta \to 0$.

Proof. Using the same method as in the proof of Theorem 5.6 in [42], we can show that

$$\mathbb{P}(I \geq y) \sim \pi\lambda \mathbb{E}[h^{\delta}] y^{-\delta}, \quad y \to \infty. \tag{4.4}$$

Note that in the proof of Theorem 5.6 in [42], the reduced Palm measure is used. In our case, we use the standard probability measure, since in our model, the transmitter and receiver do not belong to Φ, while in Theorem 5.6 in [42], the result is conditioned on that there is a transmitter at the origin belonging to Φ. The success probability can be rewritten as

$$\begin{aligned} P_{\mathrm{s}}(\theta) &= 1 - \mathbb{P}\left(I > h_{x_0} b^{-\alpha}\theta^{-1}\right) \\ &= 1 - \mathbb{E}_h\left[\mathbb{P}\left(I > hb^{-\alpha}\theta^{-1} \mid h\right)\right]. \end{aligned} \tag{4.5}$$

Thus,

$$\begin{aligned} \lim_{\theta\to 0} \frac{1 - P_{\mathrm{s}}(\theta)}{\theta^{\delta}} &= \lim_{\theta\to 0} \frac{\mathbb{E}_h\left[\mathbb{P}\left(I > hb^{-\alpha}\theta^{-1} \mid h\right)\right]}{\theta^{\delta}} \\ &\overset{(a)}{=} \mathbb{E}_h\left[\lim_{\theta\to 0} \frac{\mathbb{P}\left(I > hb^{-\alpha}\theta^{-1} \mid h\right)}{\theta^{\delta}}\right] \\ &\overset{(b)}{=} \pi\lambda b^2 \mathbb{E}[h^{\delta}]\mathbb{E}[h^{-\delta}], \end{aligned} \tag{4.6}$$

where (a) follows from the dominated convergence theorem and (b) follows from (4.4). □

Note that Nakagami-m fading, Rician fading and lognormal fading satisfy the conditions

in Theorem 4.1.

In this model, the distance between the nearest interferer and the origin could be arbitrarily small irrespective of the type of the point process and thus the ratio of the average desired signal strength and the nearest interferer's signal strength averaged over the fading could be arbitrarily small due to the singular path loss. In the rest of this subsection, we study whether the nearest interferer determines the asymptotic property of $P_{\mathrm{s}}(\theta)$, as $\theta \to 0$. The following proposition [61, Lemma 7] gives the property about the upper tail of the CCDF of the nearest interferer's signal strength.

Proposition 4.2. *For all stationary point processes, the tail of the CCDF of the nearest interferer's signal strength I_0 at the receiver o is*

$$\mathbb{P}(I_0 > y) \sim \lambda\pi\mathbb{E}\left[h^{\delta}\right] y^{-\delta}, \quad y \to \infty. \tag{4.7}$$

Proposition 4.2 implies that the CDF of the ratio of the desired signal strength and the nearest interferer's signal strength, denoted by $\frac{S}{I_0}$, satisfies

$$\begin{aligned}
\mathbb{P}\left(\frac{S}{I_0} < \theta\right) &= P(I_0 > hb^{-\alpha}\theta^{-1}) \\
&\sim \lambda\pi E(h^{\delta})\mathbb{E}_h\left[\left(hb^{-\alpha}\theta^{-1}\right)^{-\delta}\right] \\
&= \lambda\pi b^2 E[h^{\delta}]\mathbb{E}[h^{-\delta}]\theta^{\delta}, \quad \theta \to 0.
\end{aligned} \tag{4.8}$$

So, $\mathbb{P}\left(\mathrm{SIR} < \theta\right) > \mathbb{P}\left(\frac{S}{I_0} < \theta\right) \sim \lambda\pi b^2\mathbb{E}\left[h^{\delta}\right]\mathbb{E}\left[h^{-\delta}\right]\theta^{\delta}$, as $\theta \to 0$.

By Theorem 4.1, we find that $\mathbb{P}\left(\mathrm{SIR} < \theta\right) \sim \mathbb{P}\left(\frac{S}{I_0} < \theta\right)$, as $\theta \to 0$. So the nearest interferer alone determines the asymptotic behavior of $P_{\mathrm{s}}(\theta)$ (not just the pre-constant), as $\theta \to 0$. For Nakagami-m fading, $\mathbb{E}[h^{\delta}]\mathbb{E}[h^{-\delta}] = \frac{\Gamma(m)^2}{\Gamma(m+\delta)\Gamma(m-\delta)}$. So, both m and δ affect the pre-constant, but only δ determines the decay order.

4.2.1.2 Bounded Path Loss Model

We assume that the path loss model is $\ell(x) = (\epsilon + \|x\|^\alpha)^{-1}$, where $\alpha > 2$ and $\epsilon > 0$, and that signals experience Nakagami-m fading with mean 1, i.e., the fading variables are distributed as $h \sim \text{gamma}(m, \frac{1}{m})$. We have

$$\lim_{t\to 0} \frac{F_h(t)}{t^m} = \lim_{t\to 0} \frac{(mt)^{m-1}\exp(-mt)}{\Gamma(m)t^{m-1}} = \frac{m^{m-1}}{\Gamma(m)}. \tag{4.9}$$

So as $\theta \to 0$,

$$\begin{aligned} 1 - P_{\text{s}}(\theta) &= \mathbb{P}\left(\frac{h_0(\epsilon + b^\alpha)^{-1}}{I} < \theta\right) \\ &= \mathbb{E}\left[F_h\left(\theta(\epsilon + b^\alpha)I\right)\right] \\ &\overset{(a)}{\sim} \theta^m \frac{m^{m-1}}{\Gamma(m)}(\epsilon + b^\alpha)^m \mathbb{E}[I^m], \quad \epsilon > 0, \end{aligned} \tag{4.10}$$

where $I = \sum_{x\in\Phi} h(\epsilon + \|x\|^\alpha)^{-1}$ and (a) follows by the dominated convergence theorem (similar to the proof of Theorem 3.5 in Section 3.2.2). By Lemma 3.4 in Section 3.2.2, we have $\mathbb{E}[I^m] < \infty$, for $\epsilon > 0$.

4.2.2 Simple Cellular Models

For both singular and bounded path loss models with Nakagami-m fading, the results in Table 1.2 have been proved in Chapter 3.

4.2.3 Non-simple Ad Hoc Models

4.2.3.1 Singular Path Loss Model

We assume that in the wireless network, all transmitters follow a duplicated-2-point stationary point processes Φ of intensity λ, where every point has a partner point colocated. We add an additional transmitter-receiver pair with the receiver at the origin o and its desired transmitter at $x_0 = (b, 0) \notin \Phi$ and an additional transmitter $x_1 = (b, 0) \notin \Phi$ as

an interferer. We analyze the SIR distribution at o. As in Section 4.2.1.1, we assume all transmitters are always transmitting at unit power and in the same frequency band; the path loss model is $\ell(x) = \|x\|^{-\alpha}$, where $\alpha > 2$; every signal is assumed to experience i.i.d. fading with mean 1 and PDF f_h.

Φ can no longer be represented as a random set, since a set can only contain one instance of each element. Let Φ_{s} be the simple point process version of Φ, which means that at every point location of Φ, there is only one point of Φ_{s}. So Φ_{s} is a random set. Viewing Φ and Φ_{s} as random counting measures, we have $\Phi = 2\Phi_{\mathrm{s}}$. The intensity of Φ_{s} is $\lambda_{\mathrm{s}} = \lambda/2$. Let $\tilde{I} \triangleq \sum_{x\in\Phi_{\mathrm{s}}} (h_{x,1} + h_{x,2})\, \ell(x)$, where $h_{x,1}$ and $h_{x,2}$ are the two fading variables of the transmitters at the location of x. The total interference, including the one from the partner node of the desired transmitter, is then given by $I = h_1 b^{-\alpha} + \tilde{I}$. The SIR at the receiver at o can be expressed as

$$\mathrm{SIR} = \frac{h_0 b^{-\alpha}}{h_1 b^{-\alpha} + \tilde{I}}, \tag{4.11}$$

where $\{h_0, h_1\}$ are fading variables.

The following theorem characterizes the lower tail of the SIR distribution.

Theorem 4.3. *Let Φ be a stationary processes with intensity λ, where every transmitter is colocated with another one. We focus on a receiver at the origin o, with the desired received signal strength $S = h_0 b^{-\alpha}$ and the interference $I = \sum_{x\in\Phi_{\mathrm{s}}} (h_{x,1} + h_{x,2}) \|x\|^{-\alpha} + h_1 b^{-\alpha}$. If the fading random variables h_a, h_b satisfy $\mathbb{E}[h_a^{\delta}] < \infty$, $\mathbb{E}[h_a^{-\delta}] < \infty$ and $\mathbb{P}(h_a < \theta h_b) = \Theta(\theta^K)$ as $\theta \to 0$[2], where $K > 1$, then we have*

$$1 - P_{\mathrm{s}}(\theta) \sim \theta^{\delta} \frac{\pi\lambda b^2}{2} \mathbb{E}[(h_a + h_b)^{\delta}] \mathbb{E}[h^{-\delta}], \quad \theta \to 0, \tag{4.12}$$

[2]Note that there exist distributions that violate the fading constraints in Theorem 4.3. For example, if h follows an inverse Gamma distribution with its PDF $f_h(x) = \frac{\beta^a}{\Gamma(a)} x^{-a-1} \exp(-\beta/x)$, where $a, \beta > 0$, we have $\mathbb{E}[h^{\delta}] = \infty$ for $a < \delta$.

where h, h_a, h_b are iid fading random variables. Specifically, Nakagami-m fading meets the fading constraints wherein $K = m$.

Proof. See Appendix A.6. □

Comparing (4.12) with (4.3), we observe that by duplication of the transmitters, only the pre-constant changes, since for the interference, the duplication can be interpreted as the duplication of the fading variable and the decay order is determined only by δ.

4.2.3.2 Bounded Path Loss Model

The system model is the same as that in Section 4.2.3.1, except that $\ell(x) = (\epsilon + \|x\|^\alpha)^{-1}$, where $\alpha > 2$ and $\epsilon > 0$, and that signals experience Nakagami-m fading with mean 1.

As $\theta \to 0$, we have

$$\begin{aligned} 1 - P_{\mathrm{s}}(\theta) &= \mathbb{P}\left(\frac{h_0(\epsilon + b^\alpha)^{-1}}{h_1(\epsilon + b^\alpha)^{-1} + \tilde{I}} < \theta \right) \\ &= \mathbb{E}\left[F_h\left(\theta(\epsilon + b^\alpha)\left(h_1(\epsilon + b^\alpha)^{-1} + \tilde{I} \right) \right) \right] \\ &\overset{(a)}{\sim} \theta^m \frac{m^{m-1}}{\Gamma(m)} (\epsilon + b^\alpha)^m \mathbb{E}\left[\left(h_1(\epsilon + b^\alpha)^{-1} + \tilde{I} \right)^m \right], \end{aligned} \tag{4.13}$$

where (a) follows by the dominated convergence theorem (similar to the proof of Theorem 3.5 in Section 3.2.2). By Lemma 3.4 in Section 3.2.2, we have $\mathbb{E}[\tilde{I}^n] < \infty$ for any $n \in \mathbb{N}$, and thus $\mathbb{E}\left[\left(h_1(\epsilon + b^\alpha)^{-1} + \tilde{I} \right)^m \right] < \infty$ follows using binomial expansion.

For example, the non-simple ad hoc models can be applied to the scenario where there is a jamming transmitter located at the desired transmitter's position. Our results show that adding jamming transmitters does not change the asymptotic order as $\theta \to 0$ and only the pre-constant changes. Besides, by analyzing the non-simple ad hoc models, we know how the limiting case when an interferer gets really close to the receiver behaves and we can contrast the ad hoc models with the cellular models under the same duplication in the next subsection.

4.2.4 Non-simple Cellular Models

Consider a downlink cellular network model. The base station (BS) locations are modeled as a stationary point process $\Phi \in \mathbb{R}^2$ with intensity λ, where every point has a partner point colocated. Hence Φ is no longer a simple point process. Without loss of generality, we assume that the typical user is located at the origin o and is served by one of the two nearest BSs. All transmitters are assumed to be always transmitting signals using unit power and in the same frequency band. Every signal is assumed to experience i.i.d. Nakagami-m fading with mean 1 and PDF f_h and there is no noise and shadowing.

For both the singular path loss model $\ell(x) = \|x\|^{-\alpha}$ and the bounded path loss model $\ell(x) = (\epsilon + \|x\|^{\alpha})^{-1}$, where $\alpha > 2$, we can simply modify the proof of Theorem 3.5 in Chapter 3 and prove that $1 - P_{\mathrm{s}}(\theta) \sim \theta^m$, as $\theta \to 0$.

This model can be applied to the analysis of edge users of two adjacent cells in cellular networks, since each edge user has an interferer that has the same distance to the user as the serving BS. The application's model is a bit different from our model, since the interferers, excluding the nearest one, do not have partner points colocated. But in our model, the duplication of the interferers in the SIR expression can be interpreted as the sum of two i.i.d. the fading variables. Therefore, the only difference between the results of the application and our model is the pre-constant, and the asymptotic order remains the same.

4.2.5 Discussion

In Table 1.2, for those entries where the lower or upper tail of the SIR distribution decays by the power law, the results are true for essentially all motion-invariant (m.i.) point processes. So if it turns out that the distribution of $\|x_0\|$ or the distributions of the distances from interferers to the origin determine the decay order, the decay order is a function of δ.

For $\theta \to 0$, to study the asymptotic properties of $\mathbb{P}\left(\frac{S}{I} < \theta\right)$, at least one of the two

conditions, $S \to 0$ or $I \to \infty$, has to be met, otherwise, $\mathbb{P}\left(\frac{S}{I} < \theta\right) = 0$ for some θ.

In ad hoc models, for both the singular and bounded path loss models, $S \to 0$ is only determined by the lower tail of the fading distribution and $I \to \infty$ is determined by both the tail of the fading distribution and the distributions of all interferers. It is proved that for ad hoc models with bounded path loss, $1 - P_{\mathrm{s}}(\theta)$ decays polynomially, and the decay order is only determined by the fading parameter m. For ad hoc models with singular path loss, it is proved that the lower tail of the distributions of the interferer distances, other than the fading distirbution, dominates the decay order and thus the decay order is only determined by δ.

4.3 Tail of the SIR Distribution

4.3.1 Simple Ad Hoc Models

4.3.1.1 Singular Path Loss Model

We first consider the PPP with Rayleigh fading and then discuss the case of the PPP with Nakagami-m fading.

The success probability $P_{s,\mathrm{PPP}}(\theta)$ for the PPP is [5, Ch. 5.2]

$$P_{s,\mathrm{PPP}}(\theta) = \exp\left(-\pi\lambda\theta^{\delta}b^2\Gamma(1+\delta)\Gamma(1-\delta)\right). \tag{4.14}$$

Hence, $P_{s,\mathrm{PPP}}(\theta) = e^{-\Theta(\theta^{\delta})}$, as $\theta \to \infty$.

Note in (4.14), $P_{s,\mathrm{PPP}}(\theta)$ is in the form of the void probability of a ball. As $\theta \to \infty$, $P_{s,\mathrm{PPP}}(\theta)$ is equal to void probability of a ball with radius $d_0 = \theta^{\delta/2}b(\Gamma(1+\delta)\Gamma(1-\delta))^{1/2}$, i.e., the probability that there is no interferer with distance less than d_0 to o.

For $h \sim \exp(1)$, we have $\mathbb{P}(h > \beta) = \exp(-\beta)$. From the above result, we observe that $P_{s,\mathrm{PPP}}(\theta) = \mathbb{P}\left(h > \theta b^{\alpha} I\right)$ does not have an exponential tail $e^{-\Theta(\theta)}$ simply as the fading random variable does. It is the interference term in the denominator that determines the power of θ.

For the simple PPP case with Nakagami-m fading, we have the following proposition.

Proposition 4.4. *For the PPP Φ with intensity λ, the desired received signal strength at the origin is given by $S = hb^{-\alpha}$ and the interference is expressed as $I = \sum_{x\in\Phi} h_x \|x\|^{-\alpha}$, where (h_x) are i.i.d. Nakagami-m fading variables, then we have*

$$P_{s,\mathrm{PPP}}(\theta) = e^{-\Theta(\theta^\delta)}, \quad \theta \to \infty. \tag{4.15}$$

Proof. By (4.14), it has been showed that (4.15) holds for $m = 1$. First, we consider the case with $m = 2$. The Laplace transform of the interference I for the PPP has been derived in [5, Ch. 5.2], which is $\mathcal{L}_I(s) = \mathbb{E}[e^{-sI}] = \exp\left(-\pi\lambda\mathbb{E}(h^\delta)\Gamma(1-\delta)s^\delta\right)$. By taking the derivative of $\mathcal{L}_I(s)$, we have

$$\mathbb{E}[Ie^{-sI}] = \pi\lambda\mathbb{E}(h^\delta)\Gamma(1-\delta)\delta s^{\delta-1}\exp\left(-\pi\lambda\mathbb{E}(h^\delta)\Gamma(1-\delta)s^\delta\right). \tag{4.16}$$

Thus, the success probability is expressed as

$$\begin{aligned}
P_{s,\mathrm{PPP}}(\theta) &= \mathbb{P}\left(h > \theta b^\alpha I\right) \\
&= \mathbb{E}_I\left[\int_{\theta b^\alpha I}^{\infty} 4xe^{-2x}\mathrm{d}x\right] \\
&\overset{(a)}{=} \mathbb{E}_I\left[2\theta b^\alpha I e^{-2\theta b^\alpha I} + \int_{2\theta b^\alpha I}^{\infty} e^{-x}\mathrm{d}x\right] \\
&= 2\theta b^\alpha \mathbb{E}_I\left[Ie^{-2\theta b^\alpha I}\right] + \mathbb{E}_I\left[e^{-2\theta b^\alpha I}\right] \\
&= \left(\pi\lambda\mathbb{E}(h^\delta)\Gamma(1-\delta)\delta 2^\delta b^2\theta^\delta + 1\right)\exp\left(-\pi\lambda\mathbb{E}(h^\delta)\Gamma(1-\delta)2^\delta b^2\theta^\delta\right),
\end{aligned} \tag{4.17}$$

where (a) follows using the integration by parts. Therefore, as $\theta \to \infty$, $-\log\left(P_{s,\mathrm{PPP}}(\theta)\right) = \Theta(\theta^\delta)$.

For $m \geq 3$, we can obtain the same result by the same reasoning as the case with $m = 2$, i.e., applying the $(m-1)$-th derivative of $\mathcal{L}_I(s)$ and integration by parts. □

4.3.1.2 Bounded Path Loss Model

We consider the PPP case with Nakagami-m fading and assume that the path loss model is $\ell(x) = (\epsilon + \|x\|^{\alpha})^{-1}$, where $\alpha > 2$ and $\epsilon > 0$.

For $m = 1$, the success probability $P_{s,\mathrm{PPP}}(\theta)$ can be expressed as

$$P_{s,\mathrm{PPP}}(\theta) = \mathbb{E}\left[\exp\left(-\left(\epsilon + b^{\alpha}\right)\theta I\right)\right], \tag{4.18}$$

which is in the form of the Laplace transform of the interference I. We have

$$\begin{aligned}
\mathcal{L}_I(s) &\triangleq \mathbb{E}\left[\exp\left(-sI\right)\right] \\
&= \exp\left(-\lambda \int_{\mathbb{R}^2} \left(1 - \mathbb{E}_h\left[\exp\left(-sh\left(\epsilon + \|x\|^{\alpha}\right)^{-1}\right)\right]\right) \mathrm{d}x\right) \\
&= \exp\left(-2\pi\lambda \int_0^{\infty} \left(1 - \frac{1}{1 + s\left(\epsilon + r^{\alpha}\right)^{-1}}\right) r \mathrm{d}r\right) \\
&\overset{(a)}{=} \exp\left(-2\pi\lambda s (s+\epsilon)^{\delta - 1} \int_0^{\infty} \frac{r}{1 + r^{\alpha}} \mathrm{d}r\right) \\
&= \exp\left(-\frac{\pi\lambda}{\operatorname{sinc}\delta} s (s+\epsilon)^{\delta - 1}\right),
\end{aligned} \tag{4.19}$$

where (a) follows by using the substitution $r(s+\epsilon)^{-\delta/2} \to r$.

Thus, $P_{s,\mathrm{PPP}}(\theta) = \exp\left(-\frac{\pi\lambda}{\operatorname{sinc}\delta}\left(\epsilon + b^{\alpha}\right)\theta\left(\left(\epsilon + b^{\alpha}\right)\theta + \epsilon\right)^{\delta - 1}\right)$. We have

$$\log\left(P_{s,\mathrm{PPP}}(\theta)\right) \sim -A\theta^{\delta}, \quad \theta \to \infty, \tag{4.20}$$

where $A = \frac{\pi\lambda}{\operatorname{sinc}\delta}\left(\epsilon + b^{\alpha}\right)^{\delta}$.

For $m \in \mathbb{N}^{+}$, we have the following proposition.

Proposition 4.5. *For the PPP Φ with intensity λ, the desired received signal strength at the origin is given by $S = h(\epsilon + b^{\alpha})^{-1}$ and the interference is expressed as $I = \sum_{x \in \Phi} h_x(\epsilon +$*

$\|x\|^{\alpha})^{-1}$, *where* $\{h_x\}$ *are i.i.d. Nakagami-m fading variables, then we have*

$$P_{s,\mathrm{PPP}}(\theta) = e^{-\Theta(\theta^{\delta})}, \quad \theta \to \infty. \tag{4.21}$$

Proof. The proof is similar to that of Proposition 4.4. □

4.3.2 Simple Cellular Models

4.3.2.1 Singular Path Loss Model

For general fading models, the SIR asymptotics have been derived in [61].

4.3.2.2 Bounded Path Loss Model

By the same reasoning as in the proof of Theorem 4 in [61], we have

$$P_s(\theta) \sim \lambda\theta^{-\delta} \int_{\mathbb{R}^2} \mathbb{E}_o^! \left[\bar{F}_h \left(\left(\theta\epsilon + \|x\|^{\alpha}\right) I_{\infty}\right)\right] \mathrm{d}x, \quad \theta \to \infty, \tag{4.22}$$

where $I_{\infty} = \sum_{x\in\Phi} h_x \ell(x)$.

We consider the PPP case with Nakagami-m fading. For $m = 1$, as $\theta \to \infty$,

$$\begin{aligned} P_{s,\mathrm{PPP}}(\theta) &\sim \lambda\theta^{-\delta} \int_{\mathbb{R}^2} \mathbb{E}_o^! \left[\exp\left(-\left(\theta\epsilon + \|x\|^{\alpha}\right) I_{\infty}\right)\right] \mathrm{d}x \\ &\overset{(a)}{=} \lambda\theta^{-\delta} \int_{\mathbb{R}^2} \exp\left(-2\pi\lambda \left(\theta\epsilon + \|x\|^{\alpha}\right) \left(\theta\epsilon + \|x\|^{\alpha} + 1\right)^{\delta-1} \int_0^{\infty} \frac{r}{1+r^{\alpha}} \mathrm{d}r\right) \mathrm{d}x \\ &= \lambda\theta^{-\delta} \exp\left(-\frac{\pi\lambda}{\operatorname{sinc}\delta}\theta^{\delta}\epsilon^{\delta}\right) \int_{\mathbb{R}^2} \exp\left(-\frac{\pi\lambda}{\operatorname{sinc}\delta} \left(\left(\theta\epsilon + \|x\|^{\alpha}\right) \left(\theta\epsilon + \|x\|^{\alpha} + 1\right)^{\delta-1} - \theta^{\delta}\epsilon^{\delta}\right)\right) \mathrm{d}x, \end{aligned} \tag{4.23}$$

where (a) follows by using the result in (4.19).

Since $\log\left(\int_{\mathbb{R}^2} \exp\left(-\frac{\pi\lambda}{\operatorname{sinc}\delta}\left(\left(\theta\epsilon + \|x\|^{\alpha}\right)\left(\theta\epsilon + \|x\|^{\alpha} + 1\right)^{\delta-1} - \theta^{\delta}\epsilon^{\delta}\right)\right) \mathrm{d}x\right) = o(\theta^{\delta})$, as $\theta \to \infty$, we have $P_{\mathrm{s}}(\theta) = e^{-\Theta(\theta^{\delta})}$, as $\theta \to \infty$.

4.3.3 Non-simple Ad Hoc Models

4.3.3.1 Singular Path Loss Model

The system model is the same as that in Section 4.2.3.1, except that Φ_{s} is assumed to be a uniform (and thus simple) PPP with intensity $\lambda/2$ and the fading is Rayleigh.

The success probability $P_{s,\mathrm{PPP}}(\theta)$ is

$$\begin{aligned} P_{s,\mathrm{PPP}}(\theta) &= \mathbb{P}\left(\frac{h_0 b^{-\alpha}}{h_1 b^{-\alpha} + \tilde{I}} > \theta\right) \\ &= \mathbb{E}\left[e^{-h_1\theta}\right]\mathbb{E}\left[e^{-\theta b^{\alpha}\tilde{I}}\right] \\ &= \frac{1}{1+\theta}\exp\left(-\frac{\pi\lambda}{2}\theta^{\delta}b^{2}\mathbb{E}\left[\left(h_a + h_b\right)^{\delta}\right]\Gamma(1-\delta)\right), \end{aligned} \tag{4.24}$$

where h_0, h_1, h_a, h_b are fading variables. Takeing the logarithm on both sides, we have $-\log(P_{s,\mathrm{PPP}}(\theta)) - \log(1+\theta) \sim \Theta(\theta^{\delta})$, as $\theta \to \infty$. Thus, $P_{\mathrm{s}}(\theta) = e^{-\Theta(\theta^{\delta})}$, as $\theta \to \infty$.

Note that if we had k colocated interferers, the prefactor at the right-hand side of (4.24) would be $(1+\theta)^{-k}$. When $k = 2$, the prefactor is the same as in the result for cellular worst-case users in [65, Eq. (19)].

4.3.3.2 Bounded Path Loss Model

The system model is the same as that in Section 4.2.3.2, except that Φ_{s} is assumed to be a uniform PPP with intensity $\lambda/2$ and the fading is Rayleigh.

The success probability $P_{s,\mathrm{PPP}}(\theta)$ is

$$\begin{aligned}
P_{s,\mathrm{PPP}}(\theta) &= \mathbb{P}\left(\frac{h_0\left(\epsilon+b^\alpha\right)^{-1}}{h_1\left(\epsilon+b^\alpha\right)^{-1}+\tilde{I}} > \theta\right) \\
&= \mathbb{E}\left[e^{-h_1\theta}\right]\mathbb{E}\left[e^{-\theta(\epsilon+b^\alpha)\tilde{I}}\right] \\
&= \frac{1}{1+\theta}\exp\left(-\pi\lambda\int_0^\infty\left(1-\mathbb{E}\left[e^{-g_2 s_1(\epsilon+r^\alpha)^{-1}}\right]\right)r\mathrm{d}r\right) \\
&= \frac{1}{1+\theta}\exp\left(-\pi\lambda\int_0^\infty\left(1-\frac{1}{\left(1+s_1\left(\epsilon+r^\alpha\right)^{-1}\right)^2}\right)r\mathrm{d}r\right) \\
&\overset{(a)}{=} \frac{1}{1+\theta}\exp\left(-2\pi\lambda s_1(s_1+\epsilon)^{\delta-1}\int_0^\infty\frac{r^\alpha+\frac{s_1+2\epsilon}{2(s_1+\epsilon)}}{\left(r^\alpha+1\right)^2}r\mathrm{d}r\right) \\
&\overset{(b)}{\sim} \frac{1}{1+\theta}\exp\left(-2\pi\lambda s_1(s_1+\epsilon)^{\delta-1}\int_0^\infty\frac{r^\alpha+\frac{1}{2}}{\left(r^\alpha+1\right)^2}r\mathrm{d}r\right), \quad \theta\to\infty \\
&\sim \frac{1}{1+\theta}\exp\left(-\frac{\pi\lambda(\delta+1)}{2\,\mathrm{sinc}\,\delta}s_1(s_1+\epsilon)^{\delta-1}\right), \quad \theta\to\infty,
\end{aligned} \tag{4.25}$$

where h_0, h_1, h_a, h_b are fading variables, $s_1 \triangleq \theta\left(\epsilon+b^\alpha\right)$, $g_2 \triangleq h_a + h_2 \sim \mathrm{Gamma}(2,1)$, (a) follows by using the substitution $r(s_1+\epsilon)^{-\delta/2} \to r$, and (b) follows by the dominated convergence theorem. Thus, $P_{\mathrm{s}}(\theta) = e^{-\Theta(\theta^\delta)}$, as $\theta\to\infty$.

4.3.4 Non-simple Cellular Models

4.3.4.1 Singular Path Loss Model

The system model is the same as that in Section 4.2.4, except that $\ell(x) = \|x\|^{-\alpha}$, where $\alpha > 2$.

Let x_0 denote the serving BS of the typical user, and let $x_1 = x_0$ denote the BS colocated with x_0. Define $R \triangleq \|x_0\|$. The downlink SIR of the typical user can be expressed as

$$\mathrm{SIR} = \frac{h_0 R^{-\alpha}}{h_1 R^{-\alpha} + \sum_{x\in\Phi_{\mathrm{s}}\setminus\{x_0\}}\left(h_{x,1}+h_{x,2}\right)\ell(x)}, \tag{4.26}$$

where $h_0, h_1, \{h_{x,1}\}, \{h_{x,2}\} \sim \mathrm{gamma}(m, \frac{1}{m})$ are independent fading variables and Φ_{s} is the

simple point process version of Φ. Let $\tilde{I} \triangleq \sum_{x\in\Phi_{\mathrm{s}}\setminus\{x_0\}} (h_{x,1}+h_{x,2})\,\ell(x)$. $\tilde{I}$ can be rewritten as

$$\tilde{I} = \sum_{x\in\Phi_{\mathrm{s}}} \sum_{y\in\Phi_{\mathrm{s}}\setminus\{x\}} \left((h_{y,1}+h_{y,2})\,\|y\|^{-\alpha}\right) \mathbf{1}(\Phi(b(o,\|x\|)=0)), \tag{4.27}$$

where $b(o,r)$ denotes the open disk of radius r at o.

For the tail property of the SIR, we have the following theorem.

Theorem 4.6. *For all stationary BS point processes, where every BS is colocated with another one and the typical user is served by one nearest BS, if the fading is Nakagami-m, then*

$$P_{\mathrm{s}}(\theta) \sim \theta^{-(m+\delta)} \frac{\lambda\pi m^{-\delta}}{2(m+\delta)\left(\Gamma(m)\right)^2} \mathbb{E}_o^!(I_\infty^{-\delta}) \left(\sum_{i=0}^{m} \binom{m}{i} \Gamma(m+i)\bar{\Gamma}(m-i)\right), \quad \theta\to\infty, \tag{4.28}$$

where $\delta \triangleq 2/\alpha$, $I_\infty \triangleq \sum_{y\in\Phi_{\mathrm{s}}} (h_{y,1}+h_{y,2})\,\|y\|^{-\alpha}$, *and*

$$\bar{\Gamma}(m-i) = \begin{cases} \delta\Gamma(m-i+\delta), & i<m \\ \Gamma(1+\delta), & i=m. \end{cases} \tag{4.29}$$

Proof. See Appendix A.7. □

By Theorem 4.6, we know that in the log-log plot of $P_{\mathrm{s}}(\theta)$ v.s. θ, the slope of $P_{\mathrm{s}}(\theta)$ is $-10(m+\delta)$ dB/decade, as $\theta\to\infty$. The slope only depends on the fading type and the path loss exponent.

4.3.4.2 Bounded Path Loss Model

The system model is the same as that in Section 4.3.4.1, except that Φ_{s} is assumed to be a uniform PPP with intensity $\lambda/2$, the fading is Rayleigh and $\ell(x) = (\epsilon+\|x\|^{\alpha})^{-1}$,

where $\alpha > 2$ and $\epsilon > 0$. We have

$$\begin{aligned} P_{s,\mathrm{PPP}}(\theta) &= \mathbb{P}\left(\frac{h_0 \ell(R)}{h_1 \ell(R) + \tilde{I}} > \theta\right) \\ &= \mathbb{E}\left[e^{-h_1 \theta}\right] \mathbb{E}\left[e^{-\theta(\epsilon + R^\alpha)\tilde{I}}\right] \\ &= \frac{1}{1+\theta} \mathbb{E}\left[e^{-\theta(\epsilon + R^\alpha)\tilde{I}}\right]. \end{aligned} \tag{4.30}$$

Using the same method as in Section 4.3.2.2, we obtain that as $\theta \to \infty$,

$$\begin{aligned} P_{s,\mathrm{PPP}}(\theta) &\sim \frac{1}{1+\theta} \frac{\lambda \theta^{-\delta}}{2} \int_{\mathbb{R}^2} \exp\left(-2\pi\lambda \left(\theta\epsilon + \|x\|^\alpha\right) \left(\left(\theta\epsilon + \|x\|^\alpha\right) + \epsilon\right)^{\delta - 1} \int_0^\infty \frac{r^\alpha + \frac{1}{2}}{\left(r^\alpha + 1\right)^2} r \mathrm{d}r\right) \mathrm{d}x \\ &\sim \frac{1}{1+\theta} \frac{\lambda \theta^{-\delta}}{2} \exp\left(-2\pi\lambda\theta^\delta\epsilon^\delta \int_0^\infty \frac{r^\alpha + \frac{1}{2}}{\left(r^\alpha + 1\right)^2} r \mathrm{d}r\right) \\ &\quad \cdot \int_{\mathbb{R}^2} \exp\left(-2\pi\lambda \left(\left(\theta\epsilon + \|x\|^\alpha\right) \left(\left(\theta\epsilon + \|x\|^\alpha\right) + \epsilon\right)^{\delta - 1} - \theta^\delta\epsilon^\delta\right) \int_0^\infty \frac{r^\alpha + \frac{1}{2}}{\left(r^\alpha + 1\right)^2} r \mathrm{d}r\right) \mathrm{d}x. \end{aligned} \tag{4.31}$$

Thus, $\log(P_{\mathrm{s}}(\theta)) = \Theta(\theta^\delta)$, as $\theta \to \infty$.

4.3.5 Discussion

For $\theta \to \infty$, to study the asymptotic properties of $\mathbb{P}\left(\frac{S}{I} > \theta\right)$, we need either $S \to \infty$ or $I \to 0$, or both.

In simple ad hoc models, for both the singular and bounded path loss models, the tail of the distribution of S is determined only by the tail of the fading distribution and the lower tail of the distribution of I is determined by the lower tail of the fading distribution and the tail of the nearest-interferer distance distribution. For Nakagami-m fading, the distribution of the fading variable has an exponential tail and its lower tail follows a power law. If we fix the locations of all the interferers (i.e., conditioned on Φ), the lower tail of the distribution of I decays faster than any power law, since I is a sum of an infinite number of weighted fading variables. If we fix all fading variables, the lower tail of the

distribution of I depends on the tail of the distribution of the nearest-interferer distance. Note that, we have not yet proved our results for all m.i. point processes. For the PPP, the tail of the distribution of the nearest-interferer distance decays exponentially and thus the lower tail of the distribution of I is bounded by an exponential decay. So, $P_{\mathrm{s}}(\theta)$ decays faster than any power law and it is proved to decay exponentially.

In non-simple ad hoc models, one interferer's location is fixed. Thus, a necessary condition for $I \to 0$ is that the fading variable goes to 0. Similar to the simple ad hoc models, $P_{\mathrm{s}}(\theta)$ decays faster than any power law and it is proved to decay exponentially.

In simple cellular models with singular path loss, $S \to \infty$ is determined by the tail of the fading distribution and the lower tail of the distribution of $\|x_0\|$, and the lower tail of the distribution of I decays faster than any power law. It is proved that $P_{\mathrm{s}}(\theta)$ decays by the power law and the lower tail of the distribution of $\|x_0\|$ (and not the fading distribution) dominates the decay order, so the decay order is a function of δ. In non-simple cellular models with singular path loss, there is an interferer at the desired transmitter's location. It is proved that $P_{\mathrm{s}}(\theta)$ decays by the power law, and both the lower tail of the distribution of $\|x_0\|$ and the ratio of two i.i.d fading variables determine the decay order, so the decay order is a function of δ and the fading parameter. For both simple and non-simple cellular models with bounded path loss, $S \to \infty$ is determined only by the tail of the fading distribution, and the lower tail of the distribution of I decays faster than any power law. It is proved that $P_{\mathrm{s}}(\theta)$ decays exponentially.

4.4 Impact of the Interferer on the Aymptotics

In this section, we study how the nearest interferer affects the aymptotics. In other words, we analyze the SIR asymptotics if we only consider the interference from the nearest interferer I_0. In ad hoc networks, we assume the distance from the nearest interferer to the receiver at the origin is R with PDF f_R and $\mathbb{E}[R^t] < \infty$, for all $t > 0$. In cellular networks, we assume the distance from the nearest BS to the receiver at the origin is R_0

with PDF f_{R_0}, the distance from the nearest interferer to the receiver at the origin is R with conditional PDF $f_{R|R_0}$ and $\mathbb{E}[R_0^t] < \infty$ and $\mathbb{E}[R^t \mid R_0] < \infty$, for all $t > 0$. We define $\mathrm{SIR}_0 \triangleq \frac{S}{I_0}$ and $P_0(\theta) \triangleq \mathbb{P}(\mathrm{SIR}_0 > \theta)$.

Table 4.1 summarizes the asymptotic properties of $P_0(\theta)$. Note that the shading indicate that the results are the same as those in Table 1.2. Those entries indicate that the nearest interferer alone determines the decay order, and other interferers may only affect the pre-constant.

TABLE 4.1

ASYMPTOTIC PROPERTIES OF $P_0(\theta)$ ("SIMPLE": SIMPLE POINT PROCESSES; "DUPLICATED": DUPLICATED-2-POINT POINT PROCESSES)

Models	$\theta \to 0$	$\theta \to \infty$
Simple & Ad Hoc & Singular path loss	$1 - P_0(\theta) = \Theta(\theta^{\delta})$	$P_0(\theta) = \Theta(\theta^{-m})$
Simple & Ad Hoc & Bounded path loss	$1 - P_0(\theta) = \Theta(\theta^{m})$	$P_0(\theta) = \Theta(\theta^{-m})$
Simple & Cellular & Singular path loss	$1 - P_0(\theta) = \Theta(\theta^{m})$	$P_0(\theta) = \Theta(\theta^{-\delta})$
Simple & Cellular & Bounded path loss	$1 - P_0(\theta) = \Theta(\theta^{m})$	$P_0(\theta) = \Theta(\theta^{-m})$
Duplicated & Ad Hoc & Singular path loss	$1 - P_0(\theta) = \Theta(\theta^{m})$	$P_0(\theta) = \Theta(\theta^{-m})$
Duplicated & Ad Hoc & Bounded path loss	$1 - P_0(\theta) = \Theta(\theta^{m})$	$P_0(\theta) = \Theta(\theta^{-m})$
Duplicated & Cellular & Singular path loss	$1 - P_0(\theta) = \Theta(\theta^{m})$	$P_0(\theta) = \Theta(\theta^{-m})$
Duplicated & Cellular & Bounded path loss	$1 - P_0(\theta) = \Theta(\theta^{m})$	$P_0(\theta) = \Theta(\theta^{-m})$

4.4.1 Lower Tail of the SIR Distribution

4.4.1.1 Simple Ad Hoc Models

For the singular path loss model, the result has been proved in Proposition 4.2. For the bounded path loss model, we have

$$\begin{aligned} 1 - P_0(\theta) &= \mathbb{P}\left(\frac{h_0\ell(b)}{h\ell(R)} < \theta\right) \\ &= \mathbb{E}_R\mathbb{P}\left(h_0 < \theta h\ell(b)^{-1}\ell(R) \mid R\right) \\ &= \mathbb{E}_R\mathbb{P}\left(h_0 < \theta h\ell(b)^{-1}(\epsilon + R^\alpha)^{-1} \mid R\right). \end{aligned} \tag{4.32}$$

As was stated after Theorem 4.3, for Nakagami-m fading, we have $\mathbb{P}\left(h_0 < \theta h\right) = \Theta(\theta^m)$ as $\theta \to 0$. Using the dominated convergence theorem and L'Hospital's rule, we can prove that as $\theta \to 0$,

$$1 - P_0(\theta) = \Theta(\theta^m). \tag{4.33}$$

4.4.1.2 Simple Cellular Models

We can simply modify the proof of Theorem 3.5 in Section 3.2.2 and prove that $1 - P_0(\theta) = \Theta(\theta^m)$, as $\theta \to 0$.

4.4.1.3 Non-simple Ad Hoc Models

For the singular path loss model, we have

$$\begin{aligned} 1 - P_0(\theta) &= \mathbb{P}\left(\frac{h_0\ell(b)}{h\ell(\min\{R, b\})} < \theta\right) \\ &= \mathbb{P}(R < b)\mathbb{E}_R[\mathbb{P}\left(h_0 < \theta h\ell(b)^{-1}\ell(R) \mid R\right) \mid R < b] + \mathbb{P}(R \geq b)\mathbb{E}_R[\mathbb{P}\left(h_0 < \theta h\right) \mid R \geq b] \\ &= \mathbb{P}(R < b)\mathbb{E}_R[\mathbb{P}\left(h_0 < \theta h\ell(b)^{-1}\ell(R) \mid R\right) \mid R < b] + \mathbb{P}(R \geq b)\mathbb{P}\left(h_0 < \theta h\right). \end{aligned} \tag{4.34}$$

From Section 4.4.1.1, we know that the first term in (4.34) is $\Theta(\theta^{\delta})$ and the second term is $\Theta(\theta^{m})$. So, $1 - P_0(\theta) = \Theta(\theta^{m})$, as $\theta \to 0$.

For the bounded path loss model, we can apply the same methods as in the corresponding cases in Section 4.4.1.1 and obtain the results in Table 4.1.

4.4.1.4 Non-simple Cellular Models

We have $R = R_0$. Thus, $\mathrm{SIR}_0 = h_0/h_1$. We can easily obtain the results in Table 4.1.

4.4.2 Tail of the SIR Distribution

4.4.2.1 Simple Ad Hoc Models

For both singular and bounded path loss models, we have

$$\begin{aligned} P_0(\theta) &= \mathbb{P}\left(\frac{h_0 \ell(b)}{h \ell(R)} > \theta\right) \\ &= \mathbb{E}_R \mathbb{P}\left(h < \theta^{-1} h_0 \ell(b) \ell(R)^{-1} \mid R\right). \end{aligned} \tag{4.35}$$

Since $\mathbb{E}[R^t] < \infty$, for all $t > 0$, using the dominated convergence theorem and L'Hospital's rule, we obtain that $P_0(\theta) = \Theta(\theta^{-m})$, as $\theta \to \infty$.

4.4.2.2 Simple Cellular Models

For the singular path loss model, we define $\bar{R}_2$ as the distance from the origin to its nearest point of $\Phi_o^!$ and assume $\mathbb{E}(\bar{R}_2^2) < \infty$. We have

$$\begin{aligned}
P_0(\theta) &= \mathbb{P}\left(\frac{h_0\ell(R_0)}{h\ell(R)} > \theta\right) \\
&= \mathbb{E}\sum_{x\in\Phi} \bar{F}_{h_0}\left(\theta\|x\|^\alpha h\|\bar{x}_2\|^{-\alpha}\right)\mathbf{1}\left(\Phi(b(o,\|x\|))=0\right)\mathbf{1}\left(\Phi(b(o,\|\bar{x}_2\|))=1\right) \\
&= \lambda\int_{\mathbb{R}^2} \mathbb{E}_o^! \bar{F}_{h_0}\left(\theta\|x\|^\alpha h\|\bar{x}_2\|^{-\alpha}\right)\mathbf{1}\left(b(o,\|x\|)\text{empty}\right)\mathbf{1}\left(\Phi_x(b(o,\|\bar{x}_2\|))\setminus\{x\}=0\right)\mathrm{d}x \\
&\overset{(a)}{=} \lambda\theta^{-\delta}\int_{\mathbb{R}^2} \mathbb{E}_o^! \bar{F}_{h_0}\left(\|x\|^\alpha h\|\bar{x}_2\|^{-\alpha}\right)\mathbf{1}\left(b(o,\|x\|\theta^{-\delta/2})\text{ empty}\right) \\
&\quad\cdot\mathbf{1}\left(\Phi_{x\theta^{-\delta/2}}(b(o,\|\bar{x}_2\|))\setminus\{x\theta^{-\delta/2}\}=0\right)\mathrm{d}x \\
&\overset{(b)}{\sim} \lambda\theta^{-\delta}\int_{\mathbb{R}^2} \mathbb{E}\bar{F}_{h_0}\left(\|x\|^\alpha h\|\bar{x}_2\|^{-\alpha}\right)\mathbf{1}\left(\Phi_o^!(b(o,\|\bar{x}_2\|))=0\right)\mathrm{d}x, \quad \theta\to\infty \\
&\overset{(c)}{=} \lambda\theta^{-\delta}\mathbb{E}\left[\left(h\bar{R}_2^{-\alpha}\right)^{-\delta}\right]\int_{\mathbb{R}^2}\bar{F}_{h_0}\left(\|x\|^\alpha\right)\mathrm{d}x, \quad \theta\to\infty \\
&= \lambda\theta^{-\delta}\mathbb{E}\left[h^{-\delta}\right]\mathbb{E}\left[\bar{R}_2^2\right]\pi\mathbb{E}(h^\delta), \quad \theta\to\infty,
\end{aligned} \tag{4.36}$$

where $\Phi_x = \{y\in\Phi : y+x\}$ is a translated version of Φ, (a) follows by using the substitution $x\theta^{\delta/2}\to x$, (b) follows since $\mathbf{1}\left(b(o,\|x\|\theta^{-\delta/2})\text{ empty}\right)\to 1$, and (c) follows by using the substitution $x(h\|\bar{x}_2\|^{-\alpha})^{\delta/2}\to x$. Thus, $P_0(\theta)=\Theta(\theta^{-\delta})$, as $\theta\to\infty$.

For the bounded path loss model, we have

$$\begin{aligned}
P_0(\theta) &= \mathbb{P}\left(\frac{h_0\ell(R_0)}{h\ell(R)} > \theta\right) \\
&= \mathbb{E}_{R_0}\mathbb{E}_{R|R_0}\mathbb{P}\left(h < \theta^{-1}h_0\ell(R_0)\ell(R)^{-1} \mid R, R_0\right).
\end{aligned} \tag{4.37}$$

Since $\mathbb{E}[R_0^t]<\infty$ and $\mathbb{E}[R^t \mid R_0]<\infty$, for all $t>0$, using the dominated convergence theorem and L'Hospital's rule, we obtain that $P_0(\theta)=\Theta(\theta^{-m})$, as $\theta\to\infty$.

4.4.2.3 Non-simple Ad Hoc Models

For both singular and bounded path loss models, we can apply the same methods as in the corresponding cases in Section 4.4.1.1 and obtain the results in Table 4.1.

4.4.2.4 Non-simple Cellular Models

We have $R = R_0$. Thus, $\mathrm{SIR}_0 = h_0/h_1$. We can easily obtain the results in Table 4.1.

4.4.3 Discussion

Intuitively, since $I \geq I_0$ and $\frac{S}{I_0} \geq \frac{S}{I}$, we have $1 - P_0(\theta) \leq 1 - P_{\mathrm{s}}(\theta)$ and thus, as $\theta \to 0$, $1 - P_0(\theta)$ decays faster than or in the same order as $1 - P_{\mathrm{s}}(\theta)$; also, since $P_0(\theta) \geq P_{\mathrm{s}}(\theta)$, as $\theta \to \infty$, $P_0(\theta)$ decays slower than or in the same order as $P_{\mathrm{s}}(\theta)$. This is consistent with the results in Tables 1.2 and 4.1.

4.4.3.1 $\theta \to 0$

For $\theta \to 0$, to study the asymptotic properties of $\mathbb{P}\left(\frac{S}{I_0} < \theta\right)$, at least one of the two conditions, $S \to 0$ or $I_0 \to \infty$, has to be met, otherwise, $\mathbb{P}\left(\frac{S}{I_0} < \theta\right) = 0$ for some θ.

In ad hoc models, for both the singular and bounded path loss models, $S \to 0$ is only determined by the distribution of the fading variable near 0; for the singular path loss model, $I_0 \to \infty$ is determined by both the tail of the fading distribution and the lower tail of the nearest-interferer distance distribution, while for the bounded path loss model, $I_0 \to \infty$ is determined only by the tail of the fading distribution. Thus, for ad hoc models with bounded path loss, the decay order is only determined by the fading parameter m. For simple ad hoc models with singular path loss, it is proved that the lower tail of the nearest-interferer distance distribution, other than the fading distribution, dominates the decay order and thus the decay order is only determined by δ. For non-simple ad hoc models with singular path loss, since $R \leq b$, $\mathbb{P}(R = b) > 0$ and $\Theta(\theta^m)$ decays faster than

$\Theta(\theta^{\delta})$, the decay order is the same as that of simple ad hoc models with bounded path loss.

In cellular models, R_0 can be arbitrarily small and it always holds that $R \geq R_0$. For simple point processes, it is proved that it is the fading variable, not the path loss exponent (or δ), that determines the decay order. For non-simple point processes, since $R = R_0$, the fading variable alone determines the decay order.

4.4.3.2 $\theta \to \infty$

For $\theta \to \infty$, to study the asymptotic properties of $\mathbb{P}\left(\frac{S}{I_0} > \theta\right)$, at least one of the two conditions, $S \to \infty$ or $I_0 \to 0$, has to be met.

In simple ad hoc models, for both the singular and bounded path loss models, $S \to \infty$ is determined only by the tail of the fading distribution and $I_0 \to 0$ is determined by both the lower tail of the fading distribution and the tail of the nearest-interferer distance distribution. It is proved that the fading distribution, other than the nearest-interferer distance distribution, dominates the decay order.

The non-simple ad hoc models have the same results as the simple case, since only the nearest-interferer distance near ∞ may affect the asymptotic property and in the non-simple case, the nearest-interferer distance cannot be larger than b.

In simple cellular models, for the singular path loss model, $S \to \infty$ is determined by the tail of the fading distribution and the lower tail of the distribution of R_0; $I_0 \to 0$ is determined by both the lower tail of the fading distribution and the tail of the distribution of R. It is proved that the lower tail of the distribution of R_0/R (especially, that of R_0), other than the fading distribution, dominates the decay order, so the decay order is a function of δ. For the bounded path loss model, $S \to \infty$ is determined only by the tail of the fading distribution; $I_0 \to 0$ is determined by both the lower tail of the fading distribution and the tail of the distribution of R. It is proved that the fading distribution, other than the distribution of R, dominates the decay order.

In non-simple cellular models, since $R = R_0$, the fading distribution alone determines the decay order.

4.5 Summary

We considered a variety of wireless networks including ad hoc networks and cellular networks, where transmitters/BSs follow general point processes, and analyzed the asymptotic properties of the lower and upper tails of the SIR distribution.

The lower tail of the SIR distribution decays polynomially. Only the path loss exponent or the fading parameter determines the asymptotic order for ad hoc networks; only the fading parameter determines the asymptotic order for cellular networks. This indicates that we can use the SIR distribution of the PPP case to approximate the SIR distribution of non-Poisson cases in high-reliability regime by applying a horizontal shift which can be obtained using the mean interference-to-signal ratio (MISR) defined in [61]. For the tail of the SIR distribution, only cellular network models with singular path loss have tails decaying polynomially. In these cases, we can approximate the tail of the SIR distribution of non-Poisson networks using the corresponding Poisson result and the expected fading-to-interference ratio (EFIR) defined in [61]. For cellular networks with bounded path loss and ad hoc networks, we mainly investigated the Poisson case with Rayleigh fading and showed that the tail of the SIR distribution decays exponentially. Note that the exponential decay does not mean there is no approach to approximate the tail of the SIR distribution for non-Poisson cases. Using the same approximation method inside the exponential may be a potential approach, but it needs further analyses on the tail of the SIR distribution and justification.

Moreover, we investigated the impact of the nearest interferer on the asymptotic properties of the SIR distribution. If the nearest interferer is the only interferer in the networks, we proved that for the lower tail of the SIR distribution, expect for non-simple cellular networks with singular path loss law, the asymptotic properties remain the same as those

with all interferers, which means that the nearest interferer alone determines the decay order. In contrast, for the tail of the SIR distribution, the nearest interferer alone does not dominate the asymptotic trend and the tail decays polynomially, except for simple cellular networks with singular path loss.

CHAPTER 5

JOINT SPATIAL AND PROPAGATION MODELS

In this chapter, we consider the cellular networks with coverage-oriented BS deployments (as opposed to capacity-oriented BS deployments) and propose a new class of cellular models, where BSs are deployed to make all users at the cell edges achieve a minimum required signal power level from the serving BS. The equalized received signal power at the cell edges is the outcome of both the spatial structure of the BSs and the propagation model of the signals. We call such system models joint spatial and propagation (JSP) models.

5.1 Approach 1: Redefined Path Loss Model

5.1.1 System Model

We introduce a novel cellular downlink model, where all BSs are always transmitting with equal power P and are *well* deployed, which means that the signal power averaged over the fading from each BS at its *cell edge* is equal to a constant target received power $P_0 < P$, as is illustrated in Fig. 5.1. The cell edge is defined as the association boundary for mobile users, inside which at any location, the received signal power averaged over the fading from the BS in the cell is larger than the signal power from any other BS. We assume the frequency reuse factor is 1. Thus all other BSs act as interferers. All signals are assumed to experience path loss and independent (small-scale) Rayleigh fading with mean 1. Without loss of generality, in our model, we assume $P = 1$.

Due to the factors such as terrain contours, environment (urban or rural, vegetation and foliage), propagation medium, etc., which influence the path loss of a signal, the cell

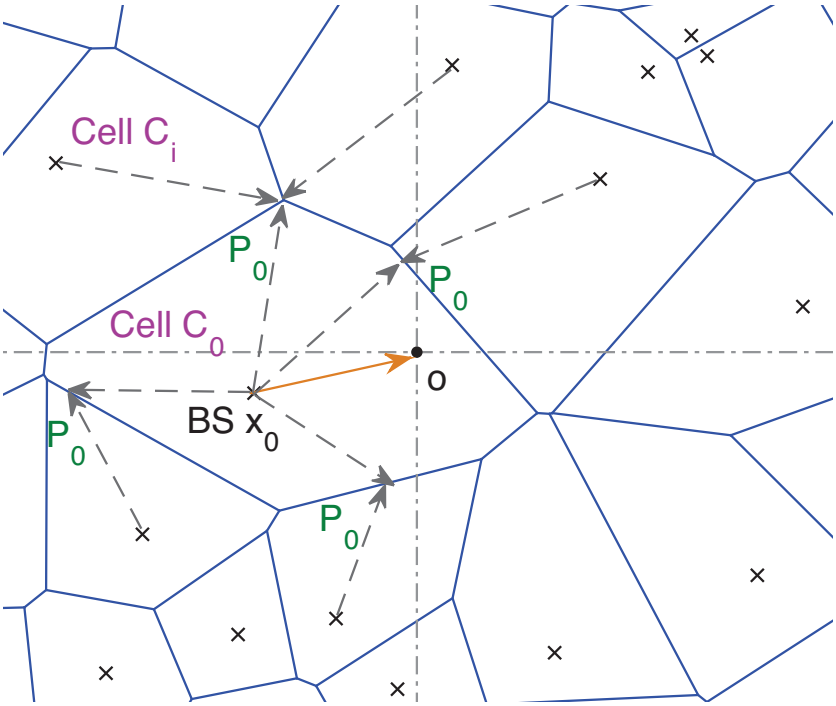

Figure 5.1. BSs (denoted by '×') and cell edges (e.g., the Voronoi tessellation). For any point on the cell edges, the received signal power averaged over the fading from any one of the closest two or three BSs is a constant P_0.

shape in real networks and in our model is not hexagonal but irregular. From a global perspective, the BSs appear to be deployed randomly and thus may be modeled as a homogenous Poisson point process (PPP) or some non-Poisson point process, such as the Ginibre process. In the rest of the chapter, we assume that the BSs follows a homogeneous PPP with intensity λ.

The path loss in our model is not modeled as the conventional one, i.e., a power law path loss model with a fixed path loss exponent. Instead, we consider the power law path loss model from x to the origin o as $\ell(x) = \|x\|^{-\alpha}$, where α is variable. The path loss exponent α is affected by the aforementioned factors and some other factors such as refraction, diffraction, reflection and absorption. Therefore, it is α that determines the shape of a cell. For simplicity, we assume in a cell C_i, the path loss exponent is a function of the direction ω from the BS, denoted by $\alpha_i(\omega)$. We call this path loss exponent *local path loss exponent*.

5.1.2 Poisson Networks and Voronoi Tessellations

The BS placement and the cell edges are a function of the propagation environment. Assuming that the resulting deployment is a PPP, we can *reverse engineer* the local path loss exponents α if the cell edges are known. We assume the cells correspond to the Poisson-Voronoi tessellation, which means that the serving BS of a mobile user is the one closest to the user. An illustration of our system model is shown in Fig. 5.1. Given a specific deployment of BSs on the plane, the cell edges are known from the Voronoi tessellation, and $\alpha_i(\omega)$ in each cell C_i can then be calculated.

In this subsection, we mainly analyze the *coverage probability*, defined as the CCDF of the signal-to-interference-plus-noise ratio (SINR), i.e., $P_{\mathrm{c}}(\theta) \triangleq \mathbb{P}(\mathrm{SINR} > \theta)$. We consider a typical user at the origin o, as is shown in Fig. 5.1, and denote the cell that contains o as C_0 and its size as S_0.

The interference to the typical user is the accumulated signal power from all BSs other

than the serving BS. Analyzing the interference is difficult for two reasons:

1. In the Poisson-Voronoi tessellation, conditioned on the Voronoi cell C_0 containing o, the locations of the interfering BSs in the adjacent Voronoi cells are determined, which means the received signal power is correlated with the interference. But such correlation is not necessarily difficult to deal with since we know we can handle it with the standard path loss model. It is only together with the dependent propagation model that this becomes difficult. To tackle the problem, in the rest of this chapter, we approximate irregular cell shapes as disks[1] of the same cell size and we make assumptions that the serving BS at x_0 is still the closest BS to the origin (regardless of the shape of the cell in the approximation we have made—"disk") and the interfering BSs follow a PPP with intensity λ outside the disk $b(o, \|x_0\|)$.

2. In the Poisson-Voronoi tessellation, it is hard to analyze the path loss that the interfering signal from an interfering BS experiences. The path loss depends on the path the signal traverses, and the local path loss exponents vary from cell to cell and also depend on the direction, which makes an exact calculation of the path loss intractable. To simplify the analysis, we assume that all interfering signals experience a path loss with a fixed path loss exponent $\bar{\alpha}$.

5.1.2.1 Cell Shape: Irregular Shape and Disk

Consider the Voronoi cell C_i and assume the BS of C_i is at the origin, as is shown in Fig. 5.2. B_i is disk. We make some comparisons between the actual shape of C_i and the disk B_i with the same size, in terms of the distribution of the desired signal power averaged over the fading and the distribution of the distance from a user to the BS.

For a mobile user at x in C_i, the received signal power averaged over the fading, denoted as $P_r(x)$, is expressed as $P_r(x) = \|x\|^{-\alpha_i(\angle x)}$, which depends on the distance to the origin $\|x\|$ and the corresponding local path loss exponent $\alpha_i(\angle x)$, where $\angle x$ the angle from the serving BS to x.

For a mobile user who is uniformly distributed in the cell, the cumulative distribution function (CDF) of the desired signal power $\hat{P}_r$ averaged over the fading is denoted by $F_{\hat{P}_r}(y) = \mathbb{P}(\hat{P}_r < y)$, where $y \geq P_0$. In the rest of this subsection, we compare the CCDF

[1] In [67], it has been proved that asymptotically, large cells are indeed disks. So the disk assumption makes sense at least when cell size is large. In Section 5.1.3, we will show by simulations that the approximation is good.

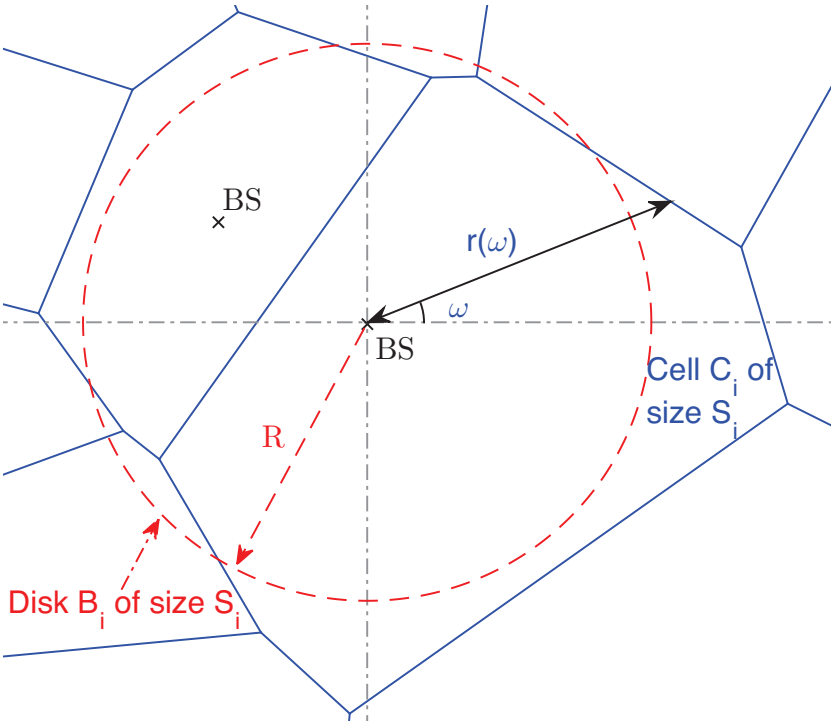

Figure 5.2. The Voronoi cell C_i of size $S_i = S$ and its corresponding disk B_i of the same size. $r(\omega)$ is the distance from the BS to its cell edge with angle ω. $R = \sqrt{\frac{S}{\pi}}$ is the radius of B_i.

of the desired signal power averaged over the fading in the Voronoi cell C_i of size $S_i = S > 0$ with that in B_i.

As is illustrated in Fig. 5.2, denote by $r(\omega)$ the distance from the BS to its Voronoi cell edge with angle ω. It follows that $S = \frac{1}{2}\int_0^{2\pi} (r(\omega)^2)dw$. Since $r(\omega)^{-\alpha_i(\omega)} = P_0$, we have $\alpha_i(\omega) = -\frac{\ln P_0}{\ln r(\omega)}$. We have $\alpha_i(\omega) < 0$ if $r(\omega) < 1$, and $\alpha_i(\omega) > 0$ if $r(\omega) > 1$. Therefore, for $1 \geq y \geq P_0$,

$$\begin{aligned} F^c_{P_r}(y) &= \mathbb{P}(P_r > y) = \mathbb{E}_{x\in C_i}[\mathbf{1}(\|x\|^{-\alpha_i(\angle x)} > y)] \\ &= \frac{1}{S}\int_0^{2\pi}\int_0^{y^{-\frac{1}{\alpha_i(\omega)}}} \mathbf{1}(r(\omega) > 1) z dz dw \\ &= \frac{1}{2S}\int_0^{2\pi} y^{-\frac{2}{\alpha_i(\omega)}} \mathbf{1}(r(\omega) > 1) dw \\ &= \frac{1}{2S}\int_0^{2\pi} (r(\omega)^2)^{\frac{\ln y}{\ln P_0}} \mathbf{1}(r(\omega) > 1) dw. \end{aligned} \tag{5.1}$$

In disk B_i of size S with radius $R = \sqrt{\frac{S}{\pi}}$, to meet the assumption of equal power at the cell edge, the local path loss exponent α is the same everywhere in B_i, and we have $R^{-\alpha} = P_0$. So, $\alpha = -\frac{2\ln P_0}{\ln S - \ln \pi}$.

For $S > \pi$, we have $\alpha > 0$ and $R > 1$. The CCDF of the desired signal power $\tilde{P}_r$ averaged over the fading in B_i, denoted as $F^c_{\tilde{P}_r}$, is

$$\begin{aligned} F^c_{\tilde{P}_r}(y) &= \mathbb{P}(\tilde{P}_r > y) = \mathbb{E}_{x\in b(o,R)}[\mathbf{1}(\|x\|^{-\alpha} > y)] \\ &= \frac{1}{S}\int_0^{2\pi}\int_0^{y^{-\frac{1}{\alpha}}} z dz dw \\ &= \frac{1}{S}\pi y^{-\frac{2}{\alpha}} = \frac{\pi}{S}\left(\frac{S}{\pi}\right)^{\frac{\ln y}{\ln P_0}}. \end{aligned} \tag{5.2}$$

Since $1 \geq y \geq P_0$, $H(x) = x^{\frac{\ln y}{\ln P_0}}$ is a concave function for $x > 0$. By Jensen's inequality,

we have

$$
\begin{aligned}
F^c_{\hat{P}_r}(y) &= \frac{\pi}{S}\frac{1}{2\pi}\int_0^{2\pi} (r(\omega)^2)^{\frac{\ln y}{\ln P_0}} \mathbf{1}(r(\omega) > 1) dw \\
&\leq \frac{\pi}{S}\frac{1}{2\pi}\int_0^{2\pi} (r(\omega)^2)^{\frac{\ln y}{\ln P_0}} dw \\
&\leq \frac{\pi}{S}\left(\frac{1}{2\pi}\int_0^{2\pi} (r(\omega)^2) dw\right)^{\frac{\ln y}{\ln P_0}} \\
&= \frac{\pi}{S}\left(\frac{S}{\pi}\right)^{\frac{\ln y}{\ln P_0}} = F^c_{\tilde{P}_r}(y). \qquad (5.3)
\end{aligned}
$$

According to (5.3), $\tilde{P}_r$ in B_i stochastically dominates $\hat{P}_r$ in C_i. In the rest of the chapter, we approximate the cell shape with a disk of the same size. In doing so, for cell size $S > \pi$, the CCDF of the desired signal power averaged over the fading becomes larger and thus, the average received signal power P_r over the whole cell $\frac{1}{|C_i|}\int_{x\in C_i} P_r(x)dx$ becomes larger.

For $S < \pi$, we have $\alpha < 0$, $R < 1$ and $F^c_{\tilde{P}_r}(y) = \mathbb{E}_{x\in b(o,R)}[\mathbf{1}(\|x\|^{-\alpha} > y)] = 0$. Thus, $F^c_{\hat{P}_r}(y) \geq F^c_{\tilde{P}_r}(y)$. $\hat{P}_r$ in C_i stochastically dominates $\tilde{P}_r$ in B_i. When the intensity of the PPP becomes small, the case of $S < \pi$ can be ignored.

As to the distribution of the distance from a user to the BS, for a user who is uniformly distributed in C_i, denote the CDF of the distance from it to the BS $\hat{d}$ as $F_{\hat{d}}$. For a user who is uniformly distributed in the disk B_i with the same size as C_i, denote the CDF of the distance from it to the BS $\tilde{d}$ as $F_{\tilde{d}}$. It is obvious that $F_{\tilde{d}}(x) \geq F_{\hat{d}}(x)$, for all $x \geq 0$. $\tilde{d}$ in B_i stochastically dominates $\hat{d}$ in C_i. Therefore, with the approximation, the mean distance from a user to the BS becomes smaller.

5.1.2.2 Coverage Analysis

As is mentioned in Section 5.1.2.1, we assume all Voronoi cells can be treated as disks. In [58], it has been derived that the *normalized* probability density function (PDF) of the

Voronoi cell sizes in the plane can be approximated as

$$f_{\bar{S}}(x) = \frac{c^c}{\Gamma(c)} x^{c-1} \exp(-cx), \tag{5.4}$$

where $c = \frac{7}{2}$ and $\bar{S} = \lambda S$ is the normalized cell size. (The mean of Voronoi cell size S for any stationary point process with intensity λ is $\frac{1}{\lambda}$.) Thus, the Voronoi cell size S for a PPP with intensity λ follows the gamma distribution with parameters c and $\frac{1}{\lambda c}$, denoted as gamma$(c, \frac{1}{\lambda c})$, and the PDF of S is

$$f_S(x) = \frac{(\lambda c)^c}{\Gamma(c)} x^{c-1} \exp(-\lambda c x). \tag{5.5}$$

For the typical user at o with serving cell size S_0, conditioned on S_0, the serving BS is uniformly distributed on the disk B_0 of size S_0, and thus the CDF of the distance d from the BS to the origin is $\hat{F}_d(x) = \frac{\pi}{S_0} x^2$, for $0 \le x \le \sqrt{\frac{S_0}{\pi}}$. Therefore, conditioning on the serving cell size S_0 and the serving BS at x_0, which is subject to $S_0 > \pi x_0^2$, we have the desired received power at the origin o

$$P_r = h_0 \|x_0\|^{-\alpha_0}, \tag{5.6}$$

where h_0 is the fading parameter satisfying $h_0 \sim \text{Exp}(1)$ and $\alpha_0 = -\frac{2 \ln P_0}{\ln S_0 - \ln \pi}$. The interference can be expressed as

$$I_{x_0} = \sum_{x \in \Phi \setminus b(o, \|x_0\|)} h_x \|x\|^{-\bar{\alpha}}, \tag{5.7}$$

where $\{h_x\}$ are the i.i.d. fading parameters that follow Exp(1) and are independent of h_0. Assume the thermal noise is additive and constant with power W. This gives the SINR expression

$$\text{SINR} = \frac{h_0 \|x_0\|^{-\alpha_0}}{\sum_{x \in \Phi \setminus b(o, \|x_0\|)} h_x \|x\|^{-\bar{\alpha}} + W}. \tag{5.8}$$

In this subsection, for the interfering signal, we assume the fixed path loss exponent $\bar{\alpha}$ is the average of the local path loss exponent (under the disk approximation) over the plane, which is given as

$$\bar{\alpha} = \frac{\int_0^\infty \alpha_x x f_S(x) dx}{\int_0^\infty x f_S(x) dx}, \tag{5.9}$$

where $\alpha_x \triangleq -\frac{2 \ln P_0}{\ln x - \ln \pi}$. However, by the properties of the logarithmic integral function, we have $\int_0^\pi \alpha_x dx = -\infty$ and $\int_\pi^\zeta \alpha_x dx = +\infty$ for any $\pi < \zeta < \infty$. To avoid considering the singularity of α_x, we choose a constant $\tau_0 > \pi$ and define $\bar{\alpha}$ as

$$\begin{aligned} \bar{\alpha} &= \frac{\int_{\tau_0}^\infty \alpha_x x f_S(x) dx + \int_0^{\tau_0} \alpha_{\tau_0} x f_S(x) dx}{\int_0^\infty x f_S(x) dx} \\ &= \int_0^\infty \frac{-2 \ln P_0}{\ln(\max\{x, \tau_0\}) - \ln \pi} \frac{(\lambda c)^{c+1}}{\Gamma(c+1)} x^c \exp(-\lambda c x) dx, \end{aligned} \tag{5.10}$$

where $\alpha_{\tau_0} \triangleq -\frac{2 \ln P_0}{\ln \tau_0 - \ln \pi}$. In the rest of the chapter, we set $\tau_0 = 4$. The coverage probability is given in the following theorem.

Theorem 5.1. *In the JSP model consisting of disk-shaped cells whose sizes follow gamma*$(c, \frac{1}{\lambda c})$*, for the approach of redefined path loss model, the coverage probability is*

$$P_{\mathrm{c}}(\theta) = \int_0^\infty \frac{2\pi}{\upsilon} \int_0^{\sqrt{\frac{\upsilon}{\pi}}} \exp\Bigg(- y^{\alpha_\upsilon} \theta W - 2\pi\lambda \int_y^\infty \Big(1 - \frac{1}{1 + y^{\alpha_\upsilon} \theta z^{-\bar{\alpha}}}\Big) z dz \Bigg) y dy f_{S_0}(\upsilon) d\upsilon, \tag{5.11}$$

where $\alpha_x \triangleq -\frac{2 \ln P_0}{\ln x - \ln \pi}$, $f_{S_0}(x) = \frac{(\lambda c)^{c+1}}{\Gamma(c+1)} x^c \exp(-\lambda c x)$ *and* $\bar{\alpha}$ *is expressed in* (5.10)*.*

Proof. Let us first derive the CDF $F_{S_0}(x)$ of the size S_0 of the cell that contains o. Since the probability of o falling into a cell with size smaller than x is equal to the area ratio of

all cells with size smaller than x to the entire plane, we have

$$F_{S_0}(x) = \mathbb{P}(S_0 < x) = \frac{\int_0^x z\frac{(\lambda c)^c}{\Gamma(c)} z^{c-1}\exp(-\lambda c z)dz}{\int_0^\infty z\frac{(\lambda c)^c}{\Gamma(c)} z^{c-1}\exp(-\lambda c z)dz}$$
$$= \lambda\int_0^x \frac{(\lambda c)^c}{\Gamma(c)} z^c \exp(-\lambda c z)dz. \tag{5.12}$$

(5.12) is shown in a more general context in [68]. The PDF of S_0 is thus $f_{S_0}(x) = \frac{(\lambda c)^{c+1}}{\Gamma(c+1)} x^c \exp(-\lambda c x)$. So, $S_0 \sim \text{gamma}(c+1, \frac{1}{\lambda c})$.

The coverage probability can be expressed as

$$P_{\text{c}}(\theta) = \mathbb{P}(\text{SINR} > \theta)$$
$$= \int_0^\infty \mathbb{P}(\text{SINR} > \theta \mid S_0 = v) f_{S_0}(v)dv. \tag{5.13}$$

Conditioning on $S_0 = v$, we have the coverage probability in the following form.

$$\mathbb{P}(\text{SINR} > \theta \mid S_0 = v) = \mathbb{E}_{x_0}\mathbb{P}\left(\frac{h_0\|x_0\|^{-\alpha_v}}{I_{x_0}+W} > \theta \mid x_0\right)$$
$$= \mathbb{E}_{x_0}\mathbb{E}_{I_{x_0}}\big(\exp(-\|x_0\|^{\alpha_v}\theta(I_{x_0}+W))\big)$$
$$= \int_0^{\sqrt{\frac{v}{\pi}}} \exp(-y^{\alpha_v}\theta W)\mathbb{E}_{I_y}\big(\exp(-y^{\alpha_v}\theta I_y)\big)\hat{f}_d(y)dy, \tag{5.14}$$

where $\hat{f}_d(y) = \frac{2\pi}{S_0}y$, for $0 \le y \le \sqrt{\frac{S_0}{\pi}}$ is the PDF of the distance d from the serving BS to the origin, $\alpha_x \triangleq -\frac{2\ln P_0}{\ln x - \ln \pi}$ and $I_y = \sum_{x\in\Phi\setminus b(o,y)} h_x\|x\|^{-\bar{\alpha}}$. Since the Laplace transform of I_y is

$$\mathcal{L}_{I_y}(s) = \mathbb{E}_{I_y}(\exp(-sI_y))$$
$$= \mathbb{E}\bigg(\exp\Big(-s\sum_{x\in\Phi\setminus b(o,y)} h_x\|x\|^{-\bar{\alpha}}\Big)\bigg)$$
$$= \exp\bigg(-2\pi\lambda\int_y^\infty \Big(1-\frac{1}{1+sz^{-\bar{\alpha}}}\Big)zdz\bigg), \tag{5.15}$$

combining (5.14) and (5.15) yields that

$$\begin{aligned}
&\mathbb{P}(\text{SINR} > \theta \mid S_0 = v) \\
&= \frac{2\pi}{v} \int_0^{\sqrt{\frac{v}{\pi}}} \exp\Big(- y^{\alpha_v} \theta W \\
&\quad - 2\pi\lambda \int_y^{\infty} \Big(1 - \frac{1}{1 + y^{\alpha_v} \theta z^{-\bar{\alpha}}}\Big) z dz \Big) y dy. \qquad (5.16)
\end{aligned}$$

Combining (5.13) and (5.16), we obtain (5.11). □

5.1.3 Simulations

We have analyzed the JSP model in Poisson networks by approximating irregular cell shapes as disks. In this subsection, we first investigate whether such approximation has good accuracy by comparing the approximation results with the simulation results of the JSP model with irregular cell shapes. Then, the distribution of the local path loss exponent is investigated. Finally, we make a comparison between our JSP model and the *conventional* models, where the path loss exponent is a constant and the desired received signal power averaged over the fading at cell edges is not a constant [8, 59].

As is discussed in Section 5.1.2.1, for any user at x in the Voronoi cell C_i in the JSP model with irregular cell shapes, the local path loss exponent $\alpha_i(\angle x)$ for the desired received signal is determined by the angle from the serving BS to x and the cell shape, i.e. $\alpha_i(\angle x) = -\frac{\ln P_0}{\ln r(\angle x)}$. For all interfering signals from other BSs, we assume the path loss exponent is constant and given in (5.10).

The simulations are performed on a 4000×4000 square. We take, unless otherwise specified, the intensity of the PPP $\lambda = 3.5 \times 10^{-5}$, which is reasonable if the distance unit is meter, since it is close to the density of BSs in one typical urban region in the UK (see [49] for details). We set $P_0 = 1 \times 10^{-8}$ unless otherwise specified. If the power unit is Watt, we have $P = 30$ dBm and $P_0 = -50$ dBm, hence the signal power decay is reasonable. By (5.10) with $\tau_0 = 4$, we have $\bar{\alpha} \approx 4.0$. In simulations, we only consider the

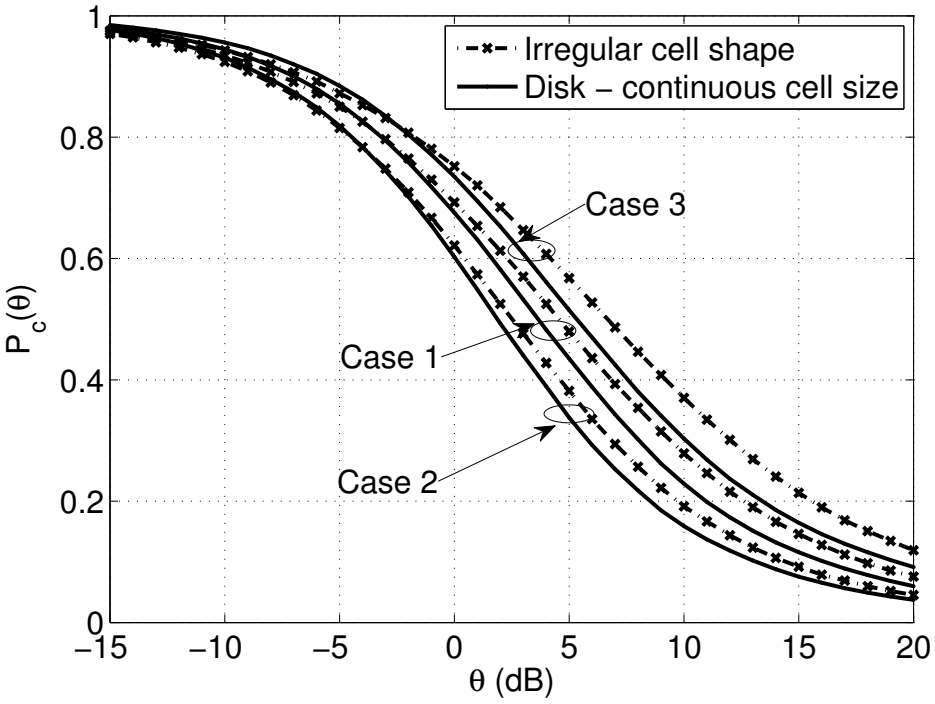

Figure 5.3. The coverage probability $P_{\rm c}(\theta)$ vs. θ for the JSP model with irregular cell shapes and disk approximation of the cell shape in three parameter setting cases. Case 1: $\lambda = 3.5 \times 10^{-5}, P_0 = 1 \times 10^{-8}, \bar{\alpha} = 4.0$; Case 2: $\lambda = 3.5 \times 10^{-5}, P_0 = 1 \times 10^{-7}, \bar{\alpha} = 3.5$; Case 3: $\lambda = 1 \times 10^{-4}, P_0 = 1 \times 10^{-8}, \bar{\alpha} = 4.5$.

interference-limited networks, i.e., the noise power is assumed to be 0.

5.1.3.1 Cell Shape: Irregular Shape vs. Disk

Fig. 5.3 compares the coverage probability for the JSP model with irregular cell shapes and disk approximation of the cell shape given different values of (λ, P_0), where $\bar{\alpha}$ is given in (5.10). The disk approximation of the cell shape is quite accurate, especially in the high-reliability regime, i.e., when θ is small, for all values of (λ, P_0) that we choose. Consider the parameter setting Case 1 with $(\lambda, P_0) = (3.5 \times 10^{-5}, 1 \times 10^{-8})$ as a reference. Case 3 with $(\lambda, P_0) = (1 \times 10^{-4}, 1 \times 10^{-8})$ has better coverage probability, while Case 2 with $(\lambda, P_0) = (3.5 \times 10^{-5}, 1 \times 10^{-7})$ has worse coverage probability. One dominating reason

is the difference of $\bar{\alpha}$. For example, compared to Case 1, Case 2 has a larger P_0 and a larger desired received signal power averaged over the fading. Case 2 should have a better coverage than Case 1, if the interference levels (indicated by $\bar{\alpha}$) were the same. But in fact, the interference in Case 2 is much higher and Case 2 has a worse coverage, as is shown in Fig. 5.3, which implies that $\bar{\alpha}$ is a dominating factor.

5.1.3.2 Distribution of the Local Path Loss Exponent

In Fig. 5.4, the empirical PDF of the local path loss exponent for the desired received signal the JSP model with irregular cell shapes is drawn. We choose the known probability distributions—the gamma distribution and the inverse gamma distribution and use the maximum likelihood estimation (MLE) method to approximate the empirical PDF. For the gamma distribution, the PDF is expressed as $f_{\text{gamma}}(x) = x^{k-1}\exp(-x/a)/(a^k\Gamma(k))$, the mean is ka and the variance is ka^2. For the inverse gamma distribution, the PDF is expressed as $f_{\text{igamma}}(x) = a^{\kappa-1}x^{-\kappa-1}\exp(-a/x)/\Gamma(\kappa)$, the mean is $a/(\kappa-1)$ and the variance is $a^2/((\kappa-1)^2(\kappa-2))$. Fig. 5.4 shows that both fits provide good matches with the inverse gamma distribution fit slightly better than the gamma distribution fit. We observe that most empirical local path loss exponents falls in the range $[3.5, 4.5]$; outside the range, according to the fitting results, the PDF decays fast.

5.1.3.3 JSP Model and Conventional Model

Since the JSP model is brand new, it is crucial to compare our model with the conventional model to see how different our model performs. We use the simulation result of the JSP model with irregular shapes to do the comparison, not the approximation result (i.e., the JSP model with disk approximation of the cell), although our approximation provides accurate coverage probability in the high-reliability regime. Consider the JSP model with irregular cell shapes ($\lambda = 3.5 \times 10^{-5}$, $P_0 = 1 \times 10^{-8}$ and by (5.10), $\bar{\alpha} = 4.0$). We assume a path loss exponent $\alpha = 4$ and the same intensity $\lambda = 3.5 \times 10^{-5}$ for the conventional

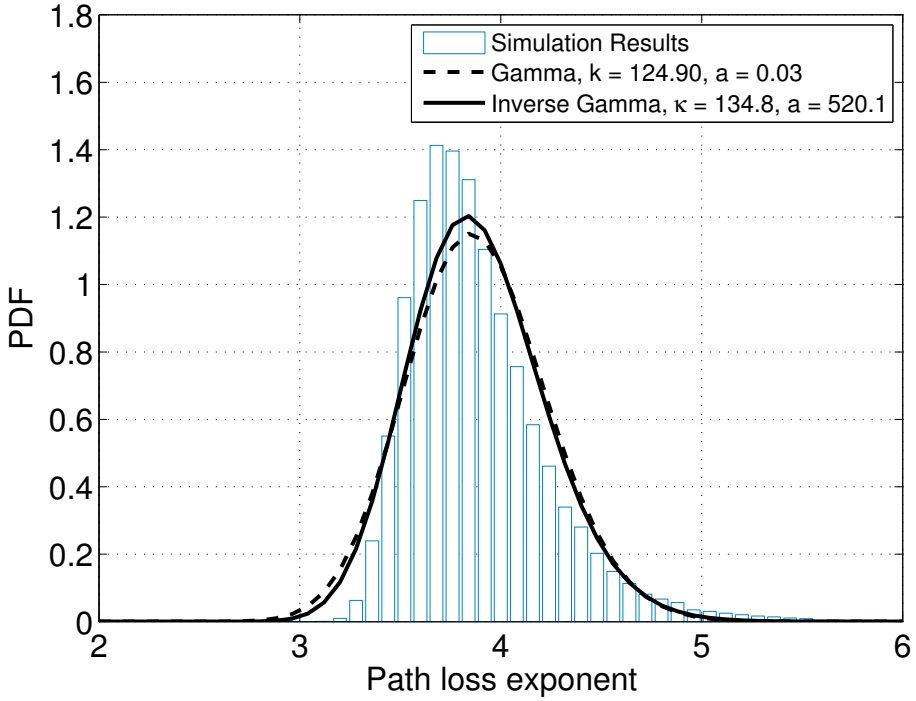

Figure 5.4. Empirical PDF of the local path loss exponent for the desired received signal and the fits of the gamma distribution and the inverse gamma distribution ($\lambda = 3.5 \times 10^{-5}$, $P_0 = 1 \times 10^{-8}$ and $\bar{\alpha} = 4.0$). The average of the empirical local path loss exponents is 3.89.

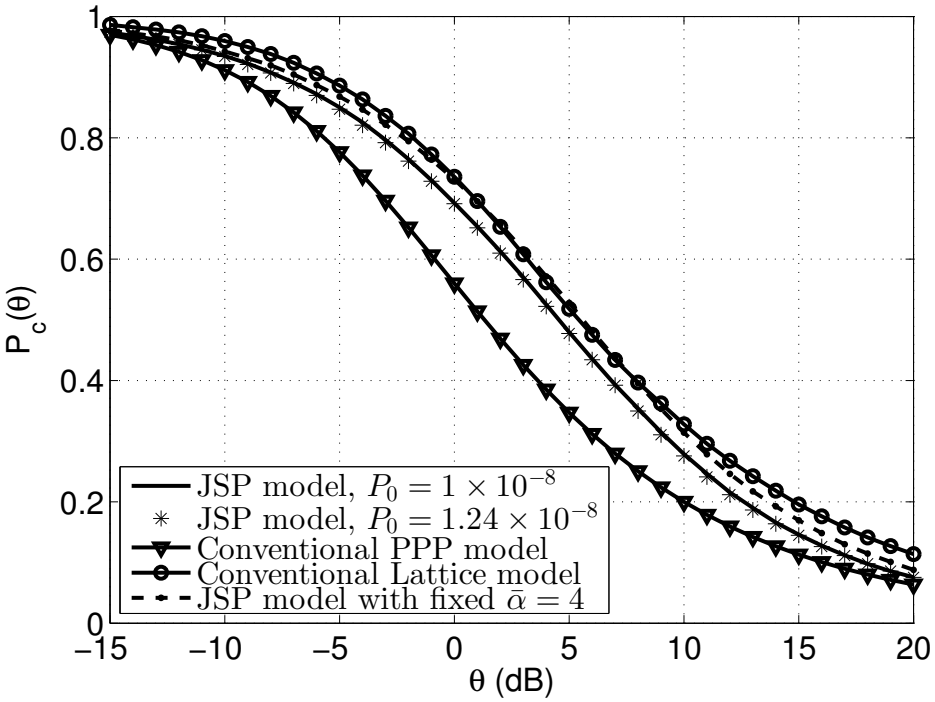

Figure 5.5. Comparison between the JSP models with irregular cell shapes $((P_0, \lambda, \bar{\alpha}) = (1 \times 10^{-8}, 3.5 \times 10^{-5}, 4.0), (1.24 \times 10^{-8}, 3.5 \times 10^{-5}, 3.95))$ and conventional models—the conventional PPP model and the conventional triangular lattice model ($\lambda = 3.5 \times 10^{-5}$ and $\alpha = 4.0$). For the JSP model with fixed $\bar{\alpha} = 4$ (the dashed line), $P_0 = 1.24 \times 10^{-8}$, $\lambda = 3.5 \times 10^{-5}$ and $\bar{\alpha}$ is not given in (5.10), but is a constant 4.

model. Fig. 5.5 compares the JSP model with irregular cell shapes and two conventional models—the conventional PPP model and the conventional triangular lattice model. Note that in the conventional PPP model [8], $P_{\rm c}(\theta) = (1 + \sqrt{\theta}\arctan(\sqrt{\theta}))^{-1}$. It has been shown that in conventional models, the coverage curve of a general point process is quite accurately approximated by a horizontal shift (gain) of the curve of the PPP [59, 60]. The triangular lattice has the largest gain of 3.4 dB.

We observe that the coverage probability of the JSP model lies between that of the two conventional models and is close to that of the conventional triangular lattice model. The actual network perceived by the typical user is approximately a conventional triangular lattice network. The small gap (roughly 1 dB horizontal difference) between the JSP model and the conventional lattice model mainly results from the fact that the received signal powers averaged over the fading at the cell edges are not equal for the two models. If we approximate the hexagonal cell shape as a disk, we can obtain the received power at cell edges, which is 1.24×10^{-8} and is larger than 1×10^{-8}.

Consider the JSP model with $\lambda = 3.5 \times 10^{-5}$ and $P_0 = 1.24 \times 10^{-8}$. By (5.10), $\bar{\alpha} = 3.95$. We observe in Fig. 5.5 that this JSP model has the same performance as the JSP model with $\lambda = 3.5 \times 10^{-5}$ and $P_0 = 1 \times 10^{-8}$. There is a roughly 1 dB horizontal gap between the JSP model and the conventional lattice model. It is mainly because the interference level in the JSP model is higher than that in the conventional lattice model, since $\bar{\alpha} < 4.0$.

To investigate how much impact the path loss exponent $\bar{\alpha}$ for the interference has on the coverage probability in the JSP model, we here assume $\bar{\alpha}$ is not given in (5.10), but is a constant 4.0 for the JSP model with $\lambda = 3.5 \times 10^{-5}$ and $P_0 = 1.24 \times 10^{-8}$. As is shown in Fig. 5.5, the new case nearly overlaps with that of the conventional lattice model. Therefore, the difference in $\bar{\alpha}$ is the main reason of the 1 dB gap between the JSP model and the conventional lattice model.

5.2 Approach 2: Redefined Shadowing Model

In recent years, the cell size in cellular systems is becoming smaller and smaller, and thus the signal propagation environment with respect to the path loss and the shadowing in a single cell is becoming more and more homogeneous. In this approach, we assume the path loss model are the conventional power-law model with constant exponent α among all cells, but each cell has a "shadowing" parameter, which can be treated as a power attenuation factor. Here, we assume that all cells are disks as in Section 5.1.2.2. Therefore, the "shadowing" parameter is a constant within each cell but varies among cells with different sizes. Similar assumption can be found in [69], where an indoor correlated shadowing model was proposed and the shadowing effect is the same within a room but different among different rooms. In our model, a large cell indicates less severe shadowing, and thus its shadowing parameter is large. For small cells, their shadowing parameter are small.

In this section, we suppose the path loss model is $\ell(x) = \|x\|^{-\alpha}$ with $\alpha > 2$, the BS transmit power is 1 and the desired received power at the cell edge is P_0. For each cell C_i with size S_i, it has a shadowing parameter K_i. The radius of the cell C_i is denoted as R_i. We have $K_i R_i^{-\alpha} = P_0$ and $\pi R_i^2 = S_i$, and thus,

$$K_i = P_0 \left(\frac{S_i}{\pi}\right)^{1/\delta}, \tag{5.17}$$

where $\delta \triangleq 2/\alpha$.

Statistically, among all cells, the shadowing parameter K is a random variable.

5.2.1 Distribution of the Shadowing Parameter

We use the same notations as in Section 5.1.2.1. Define $Y \triangleq \frac{P_0^\delta}{\pi} S$. Since $S \sim$ gamma$(c, \frac{1}{\lambda c})$, where $c = \frac{7}{2}$, we have $Y \sim$ gamma$(c, \frac{P_0^\delta}{\pi \lambda c})$.

It can be shown that if $X \sim$ gamma$(k, \bar{\theta})$, then $Z \triangleq X^q$ for $q > 0$ follows a generalized

gamma distribution with parameters $p = 1/q$, $d = k/q$, and $a = \bar{\theta}^q$. The PDF of Z is

$$f_Z(x) = \frac{(p/a^d)x^{d-1}e^{-(x/a)^p}}{\Gamma(d/p)}. \tag{5.18}$$

Since $K = \left(\frac{P_0^\delta}{\pi}S\right)^{1/\delta}$, the PDF of K can be derived as

$$f_K(x) = \frac{\delta x^{\delta k-1}e^{-x^\delta\bar{\theta}^{-1}}}{\bar{\theta}^k\Gamma(k)}, \tag{5.19}$$

where $k = c$, and $\bar{\theta} = \frac{P_0^\delta}{\pi\lambda c}$. K follows a generalized gamma distribution with parameters $p = \delta$, $d = c\delta$, and $a = \left(\frac{P_0^\delta}{\pi\lambda c}\right)^{\frac{1}{\delta}}$. The mean of K is $\mathbb{E}[K] = a\frac{\Gamma((d+1)/p)}{\Gamma(d/p)} = \left(\frac{P_0^\delta}{\pi\lambda c}\right)^{\frac{1}{\delta}}\frac{\Gamma((c\delta+1)/\delta)}{\Gamma(c)}$. The variance of K is

$$\begin{aligned}
\mathrm{Var}(K) &= a^2\left(\frac{\Gamma\left((d+2)/p\right)}{\Gamma\left(d/p\right)} - \left(\frac{\Gamma\left((d+1)/p\right)}{\Gamma\left(d/p\right)}\right)^2\right) \\
&= P_0^2\left(\frac{1}{\pi\lambda c}\right)^{\frac{2}{\delta}}\left(\frac{\Gamma\left((c\delta+2)/\delta\right)}{\Gamma\left(c\right)} - \left(\frac{\Gamma\left((c\delta+1)/\delta\right)}{\Gamma\left(c\right)}\right)^2\right) \\
&= (\mathbb{E}[K])^2\left(\frac{\Gamma\left((c\delta+1)/\delta\right)}{\Gamma(c)}\right)^{-2}\left(\frac{\Gamma\left((c\delta+2)/\delta\right)}{\Gamma\left(c\right)} - \left(\frac{\Gamma\left((c\delta+1)/\delta\right)}{\Gamma\left(c\right)}\right)^2\right).
\end{aligned} \tag{5.20}$$

The mean and variance of K are functions of P_0, λ and δ. It is different from the conventional shadowing model where the shadowing parameter is independent of δ. Given the mean of K, by (5.20), $\mathrm{Var}(K)$ only depends on δ (or equivalently, α). In Fig. 5.6, we show $\mathrm{Var}(K)$ as a function of α, for $\mathbb{E}[K] = 1$. We observe that when $\alpha = 4$, $\mathrm{Var}(K) = 1.27$ and as α increases, $\mathrm{Var}(K)$ grows exponentially.

In the literature, log-normal shadowing is usually assumed. Suppose K_{LN} is the log-normal shadowing random variable with parameter μ and σ. The PDF of K_{LN} is $f_{K_{\mathrm{LN}}}(x) = \frac{1}{x\sigma\sqrt{2\pi}}e^{-\frac{(\ln x-\mu)^2}{2\sigma^2}}$, and the mean and the variance of K_{LN} are, respectively, $e^{\mu+\sigma^2/2}$ and $(e^{\sigma^2}-1)e^{2\mu+\sigma^2}$. Letting $\mathbb{E}[K_{\mathrm{LN}}] = \mathbb{E}[K] = 1$ and $\mathrm{Var}(K_{\mathrm{LN}}) = \mathrm{Var}(K)$, we have $\mu = -\frac{\log(\mathrm{Var}(K)+1)}{2}$, $\sigma = \sqrt{\log(\mathrm{Var}(K)+1)}$. In Fig. 5.7, we compare the distributions of

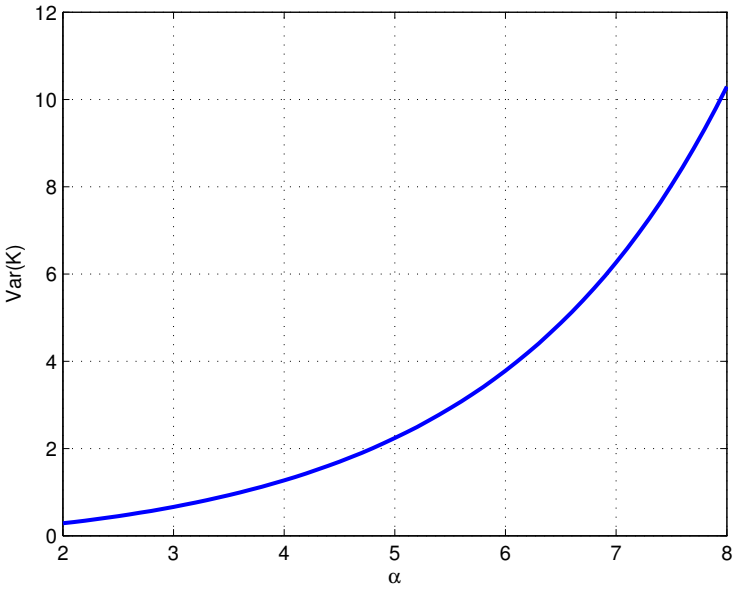

Figure 5.6. The variance of K vs. α for $\mathbb{E}[K] = 1$.

$\log(K_{\text{LN}})$ and $\log(K)$ given $\mathbb{E}[K_{\text{LN}}] = \mathbb{E}[K] = 1$ and $\text{Var}(K_{\text{LN}}) = \text{Var}(K)$, for $\alpha \in \{2.5, 4\}$. $\log(K_{\text{LN}})$ follows a normal distribution and we can easily obtain the PDF of $\log(K)$ is $f_{\log(K)}(x) = \frac{(p/a^d)e^{xd-(e^x/a)^p}}{\Gamma(d/p)}$, where $p = \delta$, $d = c\delta$, and $a = \left(\frac{P_0^\delta}{\pi\lambda c}\right)^{\frac{1}{\delta}}$. As is observed from Fig. 5.7, when α is small, the PDFs of $\log(K_{\text{LN}})$ and $\log(K)$ have similar shapes.

5.2.2 Coverage Analysis

Similar to the approach of the redefined path loss model, to simplify the analysis, we assume the shadowing parameter for all interfering signals are a constant $\bar{K} = \mathbb{E}[K]$. So, conditioned on the serving cell size S_0 and the serving BS at x_0, the SINR expression is

$$\text{SINR} = \frac{h_0 K_0 \|x_0\|^{-\alpha}}{\sum_{x\in\Phi\setminus b(o,\|x_0\|)} h_x \bar{K} \|x\|^{-\alpha} + W}, \tag{5.21}$$

where $K_0 = P_0(S_0/\pi)^{1/\delta}$.

The coverage probability is given in the following theorem.

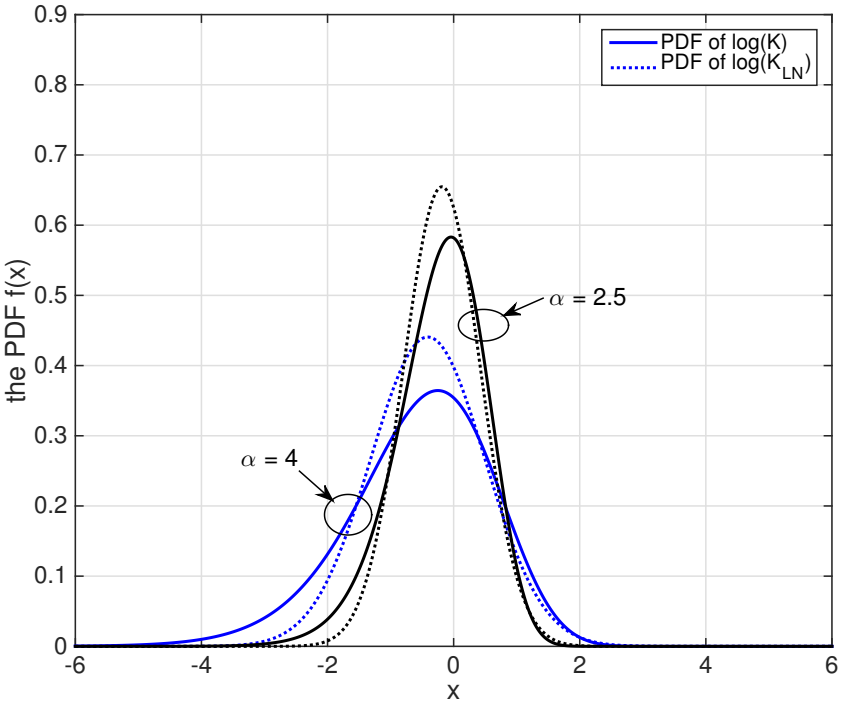

Figure 5.7. Comparison of the distributions of K and K_{LN} if K and K_{LN} have the same mean 1 and the same variance.

Theorem 5.2. *In the JSP model consisting of disk-shaped cells whose sizes follow a gamma*$(c, \frac{1}{\lambda c})$ *distribution, for the approach of redefined shadowing model, the coverage probability is*

$$P_{\mathrm{c}}(\theta) = \int_0^\infty \frac{2\pi}{\upsilon} \int_0^{\sqrt{\frac{\upsilon}{\pi}}} \exp\left(- \left(\frac{P_0^{2/\alpha}}{\pi} v \right)^{-\alpha/2} y^\alpha \theta W \right.$$
$$\left. - 2\pi\lambda \int_y^\infty \left(1 - \frac{1}{1 + \pi^{\alpha/2} \left(P_0^{2/\alpha} v \right)^{-\alpha/2} y^\alpha \theta \bar{K} z^{-\alpha}} \right) z dz \right) y dy f_{S_0}(\upsilon) d\upsilon, \quad (5.22)$$

where W *is the noise power,* $\bar{K} = \left(\frac{P_0^\delta}{\pi\lambda c} \right)^{\frac{1}{\delta}} \frac{\Gamma((c\delta+1)/\delta)}{\Gamma(c)}$ *and* $f_{S_0}(x) = \frac{(\lambda c)^{c+1}}{\Gamma(c+1)} x^c \exp(-\lambda c x)$. *For the case with no noise, the coverage probability is*

$$P_{\mathrm{c}}(\theta) = \int_0^\infty \frac{2\pi}{\upsilon} \int_0^{\sqrt{\frac{\upsilon}{\pi}}} \exp\left(- 2\pi\lambda \int_y^\infty \left(1 - \frac{1}{1 + \pi^{\alpha/2} \left(P_0^{2/\alpha} v \right)^{-\alpha/2} y^\alpha \theta \bar{K} z^{-\alpha}} \right) z \mathrm{d}z \right) y \mathrm{d}y f_{S_0}(\upsilon) \mathrm{d}\upsilon. \quad (5.23)$$

Proof. Similar to the proof of Theorem 5.1, we can obtain the result (5.22). □

5.2.3 Numerical Results

We consider the three parameter settings same as in Section 5.1.3. They are, respectively, Case 1 with $(\lambda, P_0, \alpha) = (3.5 \times 10^{-5}, 1 \times 10^{-8}, 4.0)$, Case 2 with $(\lambda, P_0, \alpha) = (3.5 \times 10^{-5}, 1 \times 10^{-7}, 3.5)$ and Case 3 with $(\lambda, P_0, \alpha) = (1 \times 10^{-4}, 1 \times 10^{-8}, 4.5)$. (Note that the values of α are exactly the values of $\bar{\alpha}$ in Section 5.1.3.) Also, we set $W = 0$. We compare our numerical results of (5.23) with those of (5.11) in Fig. 5.8. We observe that the approach of the redefined shadowing model has a similar SIR performance to the approach of the redefined path loss model. This indicates that the coverage probability of the JSP model with redefined shadowing model lies between that of the conventional PPP and triangular lattice models and is close to that of the conventional triangular lattice

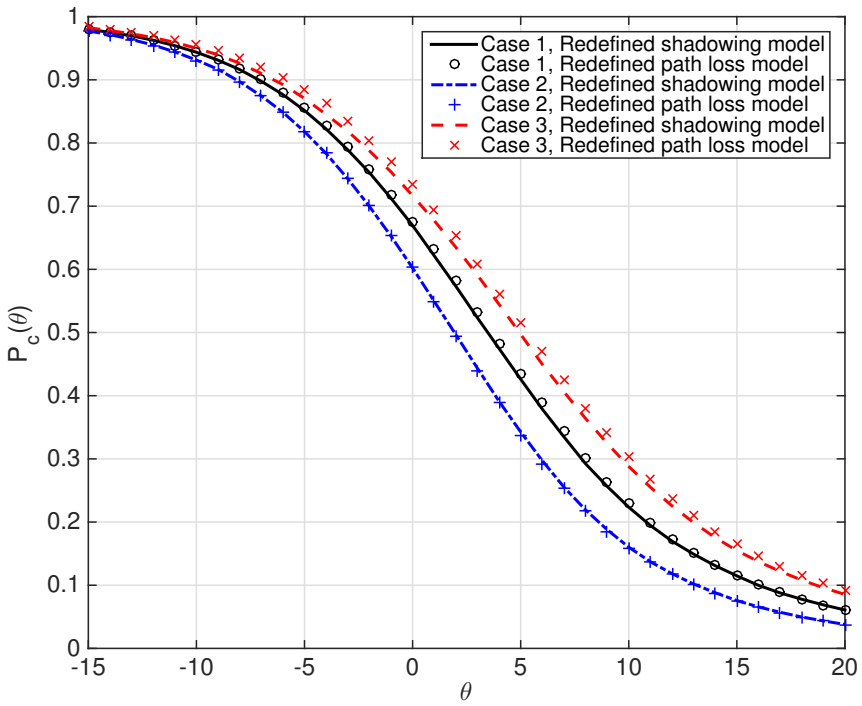

Figure 5.8. The comparison of the numerical results of the SIR distribution between the JSP model with redefined path loss model and the JSP model with redefined shadowing model, for three parameter setting cases.

model, similar to the JSP model with redefined path loss model.

5.3 Summary

In this chapter, we argue that for coverage-oriented deployments, a new class of models is needed—the joint spatial and propagation models, where BSs are deployed to make all users at cell edges achieve a minimum target signal power level from the serving BS. In other words, the BSs are deployed "optimally" given the surrounding signal propagation conditions. We proposed two instances of such a JSP model, within one of which, the target signal power on the cell edges is achieved using a variable path loss exponent. Then, for networks where the BSs form a homogeneous PPP, we obtained the expressions of the

coverage probability by approximating the irregular Voronoi cell shapes as disks of the same cell size. Simulation results showed that the approximation is quite accurate. For the second instance, we use a redefined shadowing model to make the target signal power on the cell edges achieved. Numerical results of the coverage probability show that the second instance has quite similar SIR performance to the first instance.

It is insightful to contrast our results with those in [66], where it is proved that with increasing shadowing variance, the received powers at the origin for all motion invariant point processes and lattices converge weakly to those of a PPP, which means that the actual network is perceived by a typical user as an equivalent Poisson point process distributed network, provided shadowing is strong enough.

Our results show that the JSP model exhibits a coverage performance that is very similar to that of a triangular lattice. Hence we come to the opposite conclusion of [5], which stated that *wireless networks appear Poissonian due to strong shadowing*. Here we have demonstrated that *Poisson networks appear like lattices due to dependence between propagation and BS placement*. This shows that even though BSs may geographically form a PPP, the resulting performance is not as bad as previously assumed if the dependence between cell sizes and propagation conditions is accounted for.

CHAPTER 6

CONCLUDING REMARKS

6.1 Summary

In this dissertation, we mainly analyzed the SINR distributions and interference peoperties in cellular networks in several aspects. From spatial stochastic model fitting to the real base station location date set collected from the UK official website to deriving the theoretical expressions of the SINR distributions, from discovering the fantastic asymptotic property of the lower tail of the SINR distribution in the cellular networks models with general simple point processes to analyzing the asymptotic properties of both the lower and upper tail of the SIR distribution in cellular networks with both simple and non-simple point processes (and even in ad hoc networks, although not quite related with the main work of this dissertation), and from evaluating the SINR distributions in conventional cellular networks, where independent randomness in the positions of the base stations and the propagation conditions is assumed, to proposing the novel joint spatial and propagation models and analyzing the SINR distributions, we provide a comprehensive yet relatively complete (asymptotics) study on the SINR distributions in cellular networks using stochastic geometry.

6.2 Conclusions

We discussed four main topics about the SINR distributions in cellular networks in detail from Chapter 2 to Chapter 5, which are concluded as follows.

- Actual BS deployments can be accurately modeled using some repulsive point processes in stochastic geometry. e.g., the SP, the PHCP and the perturbed triangular lattice. We proposed a general procedure for point process fitting and applied it to publicly available base station data. By observations from simulations, we found that the CCDFs of the SIR distributions of different point sets or point processes have similar shape, and thus we introduced a new metric on the regularity of a point set or a point process, called deployment gain.

- The SIR distribution of arbitrary m.i. processes can be accurately approximated by applying a horizontal shift—ADG to the SIR distribution of the PPP with the same intensity. We proved that given a m.i. point process with general fading assumptions, the lower tail of the CCDF of the SIR decays polynomially. The order of the decay is merely determined by the fading.

- The asymptotic behavior of the SIR distribution is comprehensively investigated for a variety of scenarios in cellular networks where BSs follow general simple or non-simple point processes. We analyzed both the lower and upper tails of the SIR distribution. For all scenarios, the lower tail of the SIR distribution decays polynomially and only the fading parameter determines the asymptotic order. For the upper tail of the SIR distribution, only cellular network models with singular path loss have tails decaying polynomially; in contrast, in cellular network models with bounded path loss, the tails decay exponentially.

- The dependence between propagation and BS deployment should be taken into account. We argued that for coverage-oriented deployments, a new class of models is needed—the joint spatial and propagation models, where BSs are deployed to make all users at cell edges achieve a minimum target signal power level from the serving BS. We proposed two instances of such JSP models, derived the expressions of the SINR distributions and found that the JSP models have the coverage performance that is very similar to that of a triangular lattice.

APPENDIX A

PROOFS

A.1 Proof of Lemma 3.4

Proof. We first prove that $\forall n \in \mathbb{N}$, there exists a positive $K_0 < \infty$, s.t. $\mathbb{E}(I(\Phi_o^\zeta)^n) \leq K_0 \mathbb{E}(\hat{I}(\Phi^\zeta)^n)$. Let $\zeta \in \mathbb{R}^2$ and $\|\zeta\| = y$. According to Def. 3.3, for $y > y_0$, $\mathbb{P}(I(\Phi_o^\zeta) > z) \leq \mathbb{P}(\hat{I}(\Phi^\zeta) > z)$, $\forall z \geq 0$, hence $\mathbb{E}(I(\Phi_o^\zeta)^n) \leq \mathbb{E}(\hat{I}(\Phi^\zeta)^n)$. For $y \leq y_0$, we have

$$\begin{aligned}\mathbb{E}(\hat{I}(\Phi^\zeta)^n) &\geq \mathbb{E}(\hat{I}(\Phi^\zeta)^n \mid \Phi^\zeta(b(o,y))=0))\mathbb{P}(\Phi^\zeta(b(o,y))=0) \\ &\overset{(a)}{\geq} \mathbb{E}(I(\Phi_o^\zeta)^n)\mathbb{P}(\Phi^{\zeta'}(b(o,y_0)) = 0), \end{aligned} \tag{A.1}$$

where $\zeta' \in \mathbb{R}^2$, $\|\zeta'\| = y_0$, and (a) holds since Φ is motion-invariant, $y_0 \geq y$ and thus $\mathbb{P}(\Phi^{\zeta'}(b(o,y_0)) = 0) \leq \mathbb{P}(\Phi^\zeta(b(o,y)) = 0)$. The second condition in Def. 3.3 implies that for all $y > 0$, $\forall \zeta \in \mathbb{R}^2$ with $\|\zeta\| = y$, $\mathbb{P}(\Phi^\zeta(b(o,y)) = 0) \neq 0$. So, we have $\mathbb{P}(\Phi^{\zeta'}(b(o,y_0)) = 0) \neq 0$, letting $K_0 = \max\{1, 1/\mathbb{P}(\Phi^{\zeta'}(b(o,y_0)) = 0)\}$, we have

$$\mathbb{E}(I(\Phi_o^\zeta)^n) \leq K_0 \mathbb{E}(\hat{I}(\Phi^\zeta)^n). \tag{A.2}$$

Second, we prove that all moments of $I(\Phi_o^\zeta)$ are bounded. For $n = 1$, by the third

condition in Def. 3.3, we have

$$\begin{aligned}\mathbb{E}(I(\Phi_o^\zeta)) \leq K_0\mathbb{E}(\hat{I}(\Phi^\zeta)) &= K_0\mathbb{E}_h\mathbb{E}^{!\zeta}\bigg(\sum_{x\in\Phi\bigcap B_{\zeta/2}} h_x\ell(x)\bigg)\\ &= K_0\mathbb{E}^{!\zeta}\bigg(\sum_{x\in\Phi\bigcap B_{\zeta/2}} \mathbb{E}(h_x)\ell(x)\bigg)\\ &\overset{(a)}{=} K_0\frac{\mathbb{E}(h)}{\lambda}\int_{B_{\zeta/2}}\ell(x)\rho^{(2)}(x-\zeta)dx, \end{aligned} \tag{A.3}$$

where $\mathbb{E}^{!\zeta}(\cdot)$ is the expectation with respect to the reduced Palm distribution $P^{!\zeta}$, which is the conditional expectation conditioned on $\zeta\in\Phi$ but excluding ζ. (a) follows from the Campbell-Mecke theorem.

For $n\geq 2$, we have

$$\begin{aligned}\mathbb{E}(I(\Phi_o^\zeta)^n) &\leq K_0\mathbb{E}_h\mathbb{E}^{!\zeta}\bigg(\sum_{x\in\Phi\bigcap B_{\zeta/2}} h_x\ell(x)\bigg)^n\\ &\overset{(a)}{=} K_0\mathbb{E}_h\mathbb{E}^{!\zeta}\bigg[\sum_{x\in\Phi\bigcap B_{\zeta/2}}\big(h_x\ell(x)\big)^n\bigg] + K_0\sum_{k_1+k_2=n,k_1\geq k_2>0}\binom{n}{k_1,k_2}\\ &\quad\cdot\mathbb{E}_h\mathbb{E}^{!\zeta}\bigg[\sum_{x_1,x_2\in\Phi\bigcap B_{\zeta/2}}^{\neq}\big(h_{x_1}\ell(x_1)\big)^{k_1}\big(h_{x_2}\ell(x_2)\big)^{k_2}\bigg]+\cdots\\ &\quad+K_0\sum_{\sum_{j=1}^n k_j=n,k_n\geq\cdots\geq k_1>0}\binom{n}{k_1,...,k_n}\mathbb{E}_h\mathbb{E}^{!\zeta}\bigg[\sum_{x_1,...,x_n\in\Phi\bigcap B_{\zeta/2}}^{\neq}\prod_{j=1}^n\big(h_{x_j}\ell(x_j)\big)^{k_j}\bigg]\\ &\overset{(b)}{=} K_0\frac{\mathbb{E}(h^n)}{\lambda}\int_{B_{\zeta/2}}(\ell(x))^n\rho^{(2)}(x-\zeta)dx+\frac{K_0}{\lambda}\sum_{J=2}^n\sum_{\sum_{j=1}^J k_j=n,k_J\geq\cdots\geq k_1>0}\binom{n}{k_1,...,k_J}\\ &\quad\cdot\bigg(\prod_{j=1}^J\mathbb{E}(h^{k_j})\bigg)\int_{B_{\zeta/2}}\cdots\int_{B_{\zeta/2}}\prod_{j=1}^J(\ell(x_j))^{k_j}\rho^{(J+1)}(x_1-\zeta,...,x_J-\zeta)dx_1...dx_J, \end{aligned} \tag{A.4}$$

where (a) follows by the multinomial theorem and (b) follows by the Campbell-Mecke theorem.

We discuss the cases of the non-singular and singular path loss models, separately.

For $\ell(x) = (1 + \|x\|^{\alpha})^{-1}$, when $n = 1$, since by Def. 3.3, there exists $q_2 < \infty$, such that $\rho^{(2)}(x) < q_2$ for $x \in \mathbb{R}^2$, it yields that $\int_{B_{\zeta/2}} \ell(x)\rho^{(2)}(x)dx \leq \int_{\mathbb{R}^2} \ell(x)\rho^{(2)}(x)dx < \infty$ and thus by (A.3), there exists $c_1 \in \mathbb{R}^+$, such that $\mathbb{E}(I(\Phi_o^{\zeta})) < c_1$. Similarly, when $n > 1$, by (A.4), there exists $c_n \in \mathbb{R}^+$, such that $\mathbb{E}(I(\Phi_o^{\zeta})^n) < c_n$, where c_n does not depend on ζ.

For $\ell(x) = \|x\|^{-\alpha}$, when $n = 1$, we have that $\int_{B_{\zeta/2}} \ell(x)\rho^{(2)}(x)dx \leq q_2 \int_{B_{\zeta/2}} \|x\|^{-\alpha}dx = \frac{2\pi q_2}{(\alpha-2)2^{2-\alpha}}\|\zeta\|^{2-\alpha} \leq \frac{2\pi q_2}{(\alpha-2)2^{2-\alpha}} \max\{1, \|\zeta\|^{2-\alpha}\}$, and hence by (A.3), there exists $c_1 \in \mathbb{R}^+$, such that $\mathbb{E}(I(\Phi_o^{\zeta})) < c_1 \max\{1, \|\zeta\|^{2-\alpha}\}$. When $n > 1$, for $k_j \in \{1, 2, ..., n\}$, $\int_{B_{\zeta/2}} (\ell(x))^{k_j}dx = \int_{B_{\zeta/2}} \|x\|^{-\alpha k_j}dx = \frac{2\pi}{(\alpha k_j - 2)2^{2-\alpha k_j}}\|\zeta\|^{2-\alpha k_j}$, and therefore $\int_{B_{\zeta/2}} \cdots \int_{B_{\zeta/2}} \prod_{j=1}^{J} (\ell(x_j))^{k_j} dx_1 ... dx_J = (\prod_{j=1}^{J} (\frac{2\pi}{(\alpha k_j - 2)2^{2-\alpha k_j}}))\|\zeta\|^{2J-\alpha n}$. Further, we have $\|\zeta\|^{2J-\alpha n} \leq \max\{1, \|\zeta\|^{2-\alpha n}\}$. Hence, by (A.4), there exists $c_n \in \mathbb{R}^+$, such that $\mathbb{E}(I(\Phi_o^{\zeta})^n) < c_n \max\{1, \|\zeta\|^{2-\alpha n}\}$.

□

A.2 Proof of Theorem 3.5

Proof. We first consider the case when the noise power $W = 0$. Since Φ is m.i., we can assume $\zeta = (y, 0)$. Let $\hat{\ell}(x) = 1/\ell(x)$. The coverage probability is

$$\begin{aligned} P_{\mathrm{c}}(\theta) &= \mathbb{E}_{\xi}[\mathbb{P}(\mathrm{SINR} > \theta \mid \xi)] \\ &= \int_0^{\infty} \mathbb{P}(h_{\zeta} > \theta\hat{\ell}(\zeta)I(\Phi_o^{\zeta}))f_{\xi}(y)dy \\ &= \int_0^{\infty} \mathbb{E}_{I(\Phi_o^{\zeta})}[F_h^{\mathrm{c}}(\theta\hat{\ell}(\zeta)I(\Phi_o^{\zeta}))]f_{\xi}(y)dy, \end{aligned} \tag{A.5}$$

Thus,

$$\lim_{\theta\to 0} \frac{1 - P_{\mathrm{c}}(\theta)}{\theta^m} = \lim_{\theta\to 0} \int_0^{\infty} \mathbb{E}_{I(\Phi_o^{\zeta})}\left[\frac{F_h(\theta\hat{\ell}(\zeta)I(\Phi_o^{\zeta}))}{\theta^m}\right] f_{\xi}(y)dy. \tag{A.6}$$

Assume $G(t) \triangleq F_h(t)/t^m$, for $t > 0$, and $G(0) = \lim_{t\to 0} F_h(t)/t^m = a$. $\forall \epsilon > 0$, there exists $\tau > 0$, such that for all $t \in (0, \tau)$, $|G(t) - a| < \epsilon$. So, $G(t) < a + \epsilon$ for $t \in (0, \tau)$. For $t \geq \tau$, $G(t) = F_h(t)/t^m < \tau^{-m}$. Letting $A = \max\{a + \epsilon, \tau^{-m}\}$, we have $G(t) < A$, for all

$t \geq 0$.

In the following, we discuss the cases of $\ell(x) = (1 + \|x\|^{\alpha})^{-1}$ and $\ell(x) = \|x\|^{-\alpha}$, separately.

For $\ell(x) = (1 + \|x\|^{\alpha})^{-1}$, by Lemma 3.4, we have that $\forall n \in \mathbb{N}$, $\exists c_n \in \mathbb{R}^+$, such that $\mathbb{E}(I(\Phi_o^{\zeta})^n) < c_n$. It follows that

$$H(y) \triangleq \mathbb{E}_{I(\Phi_o^{\zeta})}\left[\frac{F_h(\theta\hat{\ell}(\zeta)I(\Phi_o^{\zeta}))}{\theta^m}\right] < \mathbb{E}_{I(\Phi_o^{\zeta})}\left[A(\hat{\ell}(\zeta)I(\Phi_o^{\zeta}))^m\right] < Ac_m\hat{\ell}(y)^m < +\infty, \quad \text{(A.7)}$$

and thus, by the fourth condition in Def. 3.3,

$$\int_0^{\infty} H(y)f_{\xi}(y)dy < Ac_m\mathbb{E}_{\xi}\big(\hat{\ell}(\xi)^m\big) < +\infty. \quad \text{(A.8)}$$

For $\ell(x) = \|x\|^{-\alpha}$, by Lemma 3.4, we have that $\forall n \in \mathbb{N}$, $\exists d_n \in \mathbb{R}^+$, such that $\mathbb{E}(I(\Phi_o^{\zeta})^n) < d_n \max\{1, \|\zeta\|^{2-\alpha n}\}$. Therefore, $H(y) < Ay^{\alpha m}d_m \max\{1, y^{2-\alpha m}\} < +\infty$, and $\int_0^{\infty} H(y)f_{\xi}(y)dy < Ad_m\mathbb{E}_{\xi}\big(\xi^{\alpha m}\max\{1, \xi^{2-\alpha m}\}\big) \leq Ad_m\big(\mathbb{E}_{\xi}(\xi^{\alpha m}) + \mathbb{E}_{\xi}(\xi^2)\big) < +\infty$.

Assume $\{\theta_n\}$ is any sequence that converges to 0. Consider $\ell(x) = (1 + \|x\|^{\alpha})^{-1}$. Define $\tilde{f}(z) \triangleq a(\hat{\ell}(\zeta)z)^m f_{I(\Phi_o^{\zeta})}(z)$, and $\tilde{f}_n(z) \triangleq \frac{F_h(\theta_n\hat{\ell}(\zeta)z)}{\theta_n^m} f_{I(\Phi_o^{\zeta})}(z)$, where $f_{I(\Phi_o^{\zeta})}(z)$ is the PDF of $I(\Phi_o^{\zeta})$. $\{\tilde{f}_n\}$ is a sequence of functions and $\tilde{f}_n \to \tilde{f}$, as $n \to \infty$. Let $g(z) \triangleq A(\hat{\ell}(\zeta)z)^m f_{I(\Phi_o^{\zeta})}(z)$. We have that $\tilde{f}_n \leq g$, for all n, and (A.7) indicates $g(z)$ is integrable. By the Dominated Convergence Theorem, we have $\int_0^{\infty} \tilde{f}(z)dz = \lim_{n\to\infty} \int_0^{\infty} \tilde{f}_n(z)dz$. Similarly, define $\hat{f}(y) \triangleq \mathbb{E}_{I(\Phi_o^{\zeta})}\big[a(\hat{\ell}(\zeta)I(\Phi_o^{\zeta}))^m\big] f_{\xi}(y)$, $\hat{f}_n(y) \triangleq \mathbb{E}_{I(\Phi_o^{\zeta})}\big[\frac{F_h(\theta_n\hat{\ell}(\zeta)I(\Phi_o^{\zeta}))}{\theta_n^m}\big] f_{\xi}(y)$ and $\hat{g}(z) \triangleq Ac_m\hat{\ell}(y)^m f_{\xi}(y)$. By the Dominated Convergence Theorem, we have $\int_0^{\infty} \hat{f}(y)dy = \lim_{n\to\infty} \int_0^{\infty} \hat{f}_n(y)dy$. By the same reasoning, the Dominated Convergence Theorem can also be applied twice for the case $\ell(x) = \|x\|^{-\alpha}$. Thus, for both cases of $\ell(x)$, we obtain

that

$$\lim_{\theta\to 0}\frac{1-P_{\mathrm{c}}(\theta)}{\theta^m} = \int_0^\infty \mathbb{E}_{I(\Phi_o^\zeta)}\left[\lim_{\theta\to 0}\frac{F_h(\theta\hat{\ell}(\zeta)I(\Phi_o^\zeta))}{\theta^m}\right] f_\xi(y)dy$$
$$= \int_0^\infty \mathbb{E}_{I(\Phi_o^\zeta)}\left[a(\hat{\ell}(\zeta)I(\Phi_o^\zeta))^m\right] f_\xi(y)dy. \tag{A.9}$$

Note that by (A.8), (A.9) is finite.

Next, we consider the case when $W > 0$. In (A.6), we only need to replace $I(\Phi_o^\zeta)$ with $(I(\Phi_o^\zeta) + W)$ in the expectation $\mathbb{E}_{I(\Phi_o^\zeta)}(\cdot)$ and the expectation becomes

$$H(y) = \mathbb{E}_{I(\Phi_o^\zeta)}\left[\frac{F_h(\theta\hat{\ell}(\zeta)(I(\Phi_o^\zeta)+W))}{\theta^m}\right]$$
$$< \mathbb{E}_{I(\Phi_o^\zeta)}\left[A\hat{\ell}(\zeta)^m(I(\Phi_o^\zeta)+W)^m\right]. \tag{A.10}$$

By expanding $(I(\Phi_o^\zeta)+W)^m$, we observe that the right-hand side of (A.10) is finite. Analogous to the case when $W = 0$, we can prove that Theorem 3.5 also holds for $W > 0$. □

A.3 Proof of Corollary 3.7

Proof. Consider the worst case, $F_h^{\mathrm{c}}(x) \sim \exp(-ax)$, $x \to \infty$. First, we will show that the Laplace transform of $I(\Phi_o^\zeta)$, denoted by $\mathcal{L}_{I(\Phi_o^\zeta)}(s)$, converges for $s > \tau_0$, where $\tau_0 < 0$. Since $\mathcal{L}_{I(\Phi_o^\zeta)}(s)$ always converges for $s \geq 0$, we only consider the case $s < 0$. To prove the property, we need to derive an upper bound of $\mathcal{L}_{I(\Phi_o^\zeta)}(s)$ that only depends on the Φ^ζ. Similar to the proof of Lemma 3.4, we can prove the proposition that $\forall s < 0$, there exists

a positive $K < \infty$, s.t. $\mathbb{E}_{I(\Phi_o^\zeta)}(\exp(-sI(\Phi_o^\zeta))) \leq K\mathbb{E}_{\hat{I}(\Phi^\zeta)}(\exp(-s\hat{I}(\Phi^\zeta)))$. Thus, we have

$$\begin{aligned}
\mathcal{L}_{I(\Phi_o^\zeta)}(s) &= \mathbb{E}_{I(\Phi_o^\zeta)}(\exp(-sI(\Phi_o^\zeta))) \\
&\leq K\mathbb{E}_{\Phi^\zeta,\{h_x\}}\Big(\prod_{x\in\Phi^\zeta\bigcap B_{\zeta/2}\setminus\{\zeta\}}\exp(-sh_x\ell(x))\Big) \\
&= K\mathbb{E}^{!\zeta}\Big(\prod_{x\in\Phi\bigcap B_{\zeta/2}}\mathbb{E}_h\big(\exp(-sh\ell(x))\big)\Big) \\
&= K\mathbb{E}^{!\zeta}\Big(\prod_{x\in\Phi\bigcap B_{\zeta/2}}\mathcal{L}_h(s\ell(x))\Big), \qquad \text{(A.11)}
\end{aligned}$$

where $\mathcal{L}_h(s)$ denotes the Laplace transform of h.

Let $k(s,x) \triangleq \mathcal{L}_h(s\ell(x))$. We have that $\mathcal{L}_{\hat{I}(\Phi^\zeta)}(s) = \mathbb{E}^{!\zeta}\big(\prod_{x\in\Phi\bigcap B_{\zeta/2}}k(s,x)\big)$ is finite if and only if

$$\eta(s) = \mathbb{E}^{!\zeta}\Big(\sum_{x\in\Phi\bigcap B_{\zeta/2}}|\log k(s,x)|\Big) < \infty.$$

Now we show that τ_0 is strictly less than 0. We have

$$\begin{aligned}
\eta(s) &= \mathbb{E}^{!\zeta}\Big(\sum_{x\in\Phi\bigcap B_{\zeta/2}}|\log k(s,x)|\Big) \\
&\overset{(a)}{=} \frac{1}{\lambda}\int_{B_{\zeta/2}}\big|\log k(s,x)\big|\rho^{(2)}(x-\zeta)dx, \qquad \text{(A.12)}
\end{aligned}$$

where (a) follows from the Campbell-Mecke theorem.

Since $F_h^c(x) \sim \exp(-ax)$ for large x, without loss of generality, we assume for some large H_0, the PDF of h is $f_\xi(x) = a\exp(-ax)$ for $x > H_0$. So,

$$\begin{aligned}
k(s,x) &= \int_0^\infty \exp(-sy\ell(x))dF_h(y) \\
&= \int_0^{H_0}\exp(-sy\ell(x))dF_h(y) + \int_{H_0}^\infty a\exp\big(-y(a+s\ell(x))\big)dy. \qquad \text{(A.13)}
\end{aligned}$$

Since $x \in \Phi\bigcap B_{\zeta/2}$, by the Dominated Convergence Theorem, $k(s,x)$ is bounded for all x and $s > -a\ell(\|\zeta\|/2)^{-1}$. Also, for $s \in (-a\ell(\|\zeta\|/2)^{-1}, 0)$, we have $k(s,x) > 1$ and

$\log(k(s,x)) \leq k(s,x)-1$. To show $\eta(s)<\infty$ for $s \in (-a\ell(\|\zeta\|/2)^{-1}, 0)$, we need to prove $\int_{B(o,\omega)^c}(k(s,x)-1)\rho^{(2)}(x)dx<\infty$, for large ω. Since for large $\|x\|$, we have $\rho^{(2)}(x-\zeta)\to\lambda^2$, where λ is the intensity of Φ, we choose ω large enough such that $\rho^{(2)}(x)$ is approximately λ^2 for all $\|x\|>\omega$. So we only need to show that $\int_{B(o,\omega)^c}(k(s,x)-1)dx<\infty$. We have

$$\begin{aligned}&\int_{B(o,\omega)^c}(k(s,x)-1)dx\\ &=\int_{B(o,\omega)^c}\int_0^{H_0}(\exp(-sy\ell(x))-1)dF_h(y)dx+\int_{B(o,\omega)^c}\int_{H_0}^{\infty}(\exp(-sy\ell(x))-1)dF_h(y)dx.\end{aligned}$$

For large ω,

$$\int_{B(o,\omega)^c}\int_0^{H_0}(\exp(-sy\ell(x))-1)dF_h(y)dx=\int_{B(o,\omega)^c}\int_0^{H_0}(-sy\ell(x))dF_h(y)dx<\infty,$$

and

$$\begin{aligned}&\int_{B(o,\omega)^c}\int_{H_0}^{\infty}(\exp(-sy\ell(x))-1)dF_h(y)dx\\ &=\exp(-aH_0)\int_{B(o,\omega)^c}\left(\frac{-s}{a\ell(x)+s}+\frac{a\ell(x)(\exp(-sH_0\ell(x))-1)}{a\ell(x)+s}\right)dx<\infty.\end{aligned}$$

Thus, $\eta(s)<\infty$ and $\mathcal{L}_{I(\Phi_o^\zeta)}(s)<\infty$. Since $I(\Phi_o^\zeta)$ is nonnegative, according the region of convergence (ROC) for Laplace transforms, there exists $\tau<-a\ell(\|\zeta\|/2)^{-1}$, such that $\mathcal{L}_{I(\Phi_o^\zeta)}(s)$ converges for $s<\tau$ and diverges for $s>\tau$. τ is called the abscissa of convergence. By Theorem 3 in [55], it follows that the interference has an exponential tail. Therefore, if the fading has at most an exponential tail, the interference tail is bounded by an exponential. □

A.4 Proof of Lemma 3.8

Proof. Since $\tilde{h}$ and $\hat{h}$ are independent, we have

$$F_h(t) = \mathbb{P}(\tilde{h}\hat{h} \le t) = \int_0^\infty \mathbb{P}(\tilde{h} \le \frac{t}{u} \mid \hat{h} = u) f_{\hat{h}}(u) du = \int_0^\infty F_{\tilde{h}}\Big(\frac{t}{u}\Big) f_{\hat{h}}(u) du$$
$$= \int_0^\infty \frac{1}{\sqrt{\pi}\Gamma(m)} \Big(\int_0^{\frac{mt}{u}} w^{m-1} \exp(-w) dw \Big) \frac{V_\sigma}{u} \exp(-V_\sigma^2 (\log u)^2) du, \tag{A.14}$$

where $V_\sigma \triangleq \frac{10}{\sigma\sqrt{2}\log 10}$.

To prove the first property, we have

$$\lim_{t\to 0} \frac{F_h(t)}{t^m} = \lim_{t\to 0} \frac{F_h'(t)}{m t^{m-1}} = \lim_{t\to 0} \int_0^\infty \frac{V_\sigma m^{m-1}}{\sqrt{\pi}\Gamma(m) u^{m+1}} \exp\Big(-\frac{mt}{u}\Big) \exp(-V_\sigma^2 (\log u)^2) du$$
$$\le \int_0^\infty \frac{V_\sigma m^{m-1}}{\sqrt{\pi}\Gamma(m) u^{m+1}} \exp(-V_\sigma^2 (\log u)^2) du. \tag{A.15}$$

Since as $u \to 0$, $\exp(-V_\sigma^2 (\log u)^2) = o(u^n)$ for any $n \in \mathbb{N}$, (A.15) is bounded. Thus we can apply the Dominated Convergence Theorem and have that

$$\lim_{t\to 0} \frac{F_h(t)}{t^m} = \int_0^\infty \frac{V_\sigma m^{m-1}}{\sqrt{\pi}\Gamma(m) u^{m+1}} \exp(-V_\sigma^2 (\log u)^2) du = \frac{m^{m-1}}{\Gamma(m)} \exp\Big(\frac{m^2}{4V_\sigma^2}\Big) < \infty,$$

which is the first property.

For the second property, on the one hand, for any $n \in \mathbb{N}$,

$$\lim_{t\to\infty} \frac{1 - F_h(t)}{t^{-n}} = \lim_{t\to\infty} \frac{F_h'(t)}{n t^{-n-1}} = \lim_{t\to\infty} \int_0^\infty \frac{V_\sigma m^m t^{n+m}}{\sqrt{\pi}\Gamma(m) u^{m+1} n} \exp\Big(-\frac{mt}{u}\Big) \exp(-V_\sigma^2 (\log u)^2) du.$$

Assume $H(t) = t^{n+m} \exp\big(-\frac{mt}{u}\big)$. Since $H'(t) = t^{n+m-1}\big(n+m-\frac{mt}{u}\big) \exp\big(-\frac{mt}{u}\big)$, when $t = \frac{u(n+m)}{m}$, $H(t)$ achieves its maximum value and $\max_{t>0} H(t) = \big(\frac{u(n+m)}{m}\big)^{n+m} \exp(-(n+m))$. Thus,

$$\lim_{t\to\infty} \frac{1 - F_h(t)}{t^{-n}} \le \int_0^\infty \frac{V_\sigma u^{n-1}}{\sqrt{\pi}\Gamma(m) n} \frac{(n+m)^{n+m}}{m^n} \exp(-(n+m)) \exp(-V_\sigma^2 (\log u)^2) du < \infty.$$

Applying the Dominated Convergence Theorem, we obtain $\lim_{t\to\infty} \frac{1-F_h(t)}{t^{-n}} = 0$ and thus $F_h^{\mathrm{c}}(t) = o(t^{-n})$, as $t \to \infty$, for any $n \in \mathbb{N}$.

On the other hand, for any $a > 0$,

$$\begin{aligned}\lim_{t\to\infty} \frac{1-F_h(t)}{\exp(-at)} &= \lim_{t\to\infty} \frac{F_h'(t)}{a\exp(-at)} \\ &= \lim_{t\to\infty} \int_0^\infty \frac{V_\sigma m^m}{\sqrt{\pi}\Gamma(m)u^{m+1}a} t^{m-1} \exp\left(\left(a - \frac{m}{u}\right)t\right) \exp(-V_\sigma^2(\log u)^2)du.\end{aligned} \tag{A.16}$$

For any $a > 0$, there exists $\hat{K} > 0$, such that for $u > \hat{K}$, $\exp(mt/u) < \exp(at/3)$. Hence, $\lim_{t\to\infty} \frac{1-F_h(t)}{\exp(-at)} = \infty$, for any $a > 0$. Thus, $-\log F_h^{\mathrm{c}}(t) = o(t)$, $t \to \infty$. □

A.5 Proof of Lemma 3.10

Proof. Conditions 1 and 2 in Def. 3.3 hold for all the three point processes obviously. For Conditions 3 and 4, we treat the three point processes separately.

For the PPP, Condition 3 holds, because the points in Φ are independent; Condition 4 holds, because $\mathbb{P}(\xi > x) = \mathbb{P}(\Phi(b(o,x)) = 0) = \exp(-\lambda\pi x^2)$.

For the MCP, we first prove that Condition 3 holds. For $y > r_{\mathrm{c}}$, the interference $I(\Phi_o^\zeta)$ consists of two parts. One is the interference from the clusters with center points inside the region $B(o, y + r_{\mathrm{c}}) \setminus b(o, y - r_{\mathrm{c}})$, denoted by I_1, and the other part is the interference from the clusters with center points in $B(o, y + r_{\mathrm{c}})^{\mathrm{c}}$, denoted by I_2. I_1 and I_2 are independent. Similarly, $\hat{I}(\Phi^\zeta)$ consists of $\hat{I}_1$ and $\hat{I}_2$, where $\hat{I}_1$ is from the clusters with center points inside $B(o, y + r_{\mathrm{c}}) \setminus b(o, y/2)$ and $\hat{I}_2$ is from the clusters with center points in $B(o, y + r_{\mathrm{c}})^{\mathrm{c}}$.

Since the parent points are independent, I_2 and $\hat{I}_2$ have the same distribution. For $y \gg r_{\mathrm{c}}$, we can easily prove that $\hat{I}_1$ stochastically dominates I_1. As $\mathbb{P}(I(\Phi_o^\zeta) > z) = \mathbb{P}(I_1 + I_2 > z) = \mathbb{E}_{I_2}[\mathbb{P}(I_1 > z - I_2 \mid I_2)]$, we have $\mathbb{P}(I(\Phi_o^\zeta) > z) \le \mathbb{P}(\hat{I}(\Phi^\zeta) > z)$ for all $z \ge 0$.

Then we prove Condition 4 holds for the MCP. For large y, let $\mathcal{S}$ be the set of the

parent points that are in $B(o, y - r_{\rm c})$, i.e., $\mathcal{S} = \{x \in \Phi_{\rm p} : x \in B(o, y - r_{\rm c})\}$ and $\tilde{\Phi}_x$ be the daughter process for the cluster centered at $x \in \Phi_{\rm p}$. We have

$$\begin{aligned}\mathbb{P}(\xi > y) &= \mathbb{P}(\Phi(B(o, y)) = 0) \overset{(a)}{\leq} \mathbb{P}(\tilde{\Phi}_x(B(x, r_{\rm c})) = 0, \text{ for all } x \in \mathcal{S}) \\ &= \sum_{k=0}^{\infty} \frac{(\lambda_{\rm p}\pi(y - r_{\rm c})^2)^k \exp(-\lambda_{\rm p}\pi(y - r_{\rm c})^2)}{k!} \exp(-\bar{c})^k \\ &= \exp\big(-(1 - \exp(-\bar{c}))\lambda_{\rm p}\pi(y - r_{\rm c})^2\big), \end{aligned} \tag{A.17}$$

where (a) follows since $\Phi(B(o, y)) = 0$ implies $\Phi(B(x, r_{\rm c})) = 0$, for all $x \in \mathcal{S}$. As $\mathbb{E}(\xi^n) = -\int z^n d\mathbb{P}(\xi > z)$, performing integration by parts, it follows that $\mathbb{E}(\xi^n)$ is bounded.

For the MHP, to prove Condition 3, we consider Φ_o^{ζ} and Φ^{ζ} in term of the base PPP $\Phi_{\rm b}$. Conditioned on $\Phi_{\rm b} \bigcap (B(o, y + 2r_{\rm h}) \setminus B(o, y + r_{\rm h}))$, the interference from the region $B(o, y + 2r_{\rm h})^{\rm c}$ in Φ^{ζ} and that in Φ_o^{ζ} are i.i.d.. So we only need to consider the region $B(o, y+2r_{\rm h})$ for large y. As $y \to \infty$, $\mathbb{E}[\Phi^{\zeta}(B(o, y) \setminus B(o, y/2))] = \Theta(y^2)$, and $\mathbb{E}[\Phi_o^{\zeta}(B(o, y + 2r_{\rm h}) \setminus B(o, y))] = \Theta(y)$.[1] It can be proved that the portion of $\hat{I}(\Phi^{\zeta})$ that comes from the retained points in $B(o, y + 2r_{\rm h}) \setminus B(o, y/2)$ stochastically dominates the portion of $I(\Phi_o^{\zeta})$ that comes from the retained points in $B(o, y + 2r_{\rm h}) \setminus B(o, y)$. Hence, Condition 3 holds.

To prove that Condition 4 holds for the MHP, we use the CCDF of ξ expressed in the form (15.1.5) in [56]:

$$F_{\xi}^{\rm c}(x) = \sum_{k=0}^{\infty} \frac{(-1)^k}{k!} \int_{B(o,x)} \cdots \int_{B(o,x)} \rho^{(k)}(y_1, \ldots, y_k) dy_1 \cdots dy_k \tag{A.18}$$

$$= \sum_{k=0}^{\infty} \frac{(-1)^k}{k!} \alpha^{(k)}[B(o, x)^{\bigotimes_k}], \tag{A.19}$$

where $B(o, x)^{\bigotimes_k}$ is the Cartesian product of k balls and $\alpha^{(k)}$ is the kth-order factorial

[1] $f(x) = \Theta(g(x))$, if both $f(x)/g(x)$ and $g(x)/f(x)$ remain bounded as $x \to \infty$.

moment measure. For the MHP, the nth moment density satisfies

$$\rho^{(n)}(z_1,\ldots,z_n)=\lambda^n,\quad \text{for } (z_1,\ldots,z_n)\in S_n(x), \tag{A.20}$$

where $S_n(x)\triangleq\{(z_1,\ldots,z_n)\in B(o,x)^{\otimes_n}:\|z_i-z_j\|>2r_{\mathrm{h}},\forall i\neq j\}$. The complementary set of $S_n(x)$ with respect to $B(o,x)^{\otimes_n}$ is $S_n^{\mathrm{c}}(x)=B(o,x)^{\otimes_n}\setminus S_n(x)=\{(z_1,\ldots,z_n)\in B(o,x)^{\otimes_n}:\exists i\neq j,\text{ s.t. }\|z_i-z_j\|\leq 2r_{\mathrm{h}}\}$. The Lebesgue measure of $S_n^{\mathrm{c}}(x)$ satisfies $\nu(S_n^{\mathrm{c}}(x))=O(x^{2n-1})$. So, as $x\to\infty$, $\int_{S_n^{\mathrm{c}}(x)}\rho^{(n)}(y_1,\ldots,y_n)dy_1\cdots dy_n\to 0$. Since (A.18) can be rewritten as

$$F_\xi^{\mathrm{c}}(x)=\sum_{k=0}^{\infty}\frac{(-1)^k}{k!}\bigg(\int_{S_k(x)}\rho^{(k)}(y_1,\ldots,y_k)dy_1\cdots dy_k+\int_{S_k^{\mathrm{c}}(x)}\rho^{(k)}(y_1,\ldots,y_k)dy_1\cdots dy_k\bigg),$$

it follows that as $x\to\infty$,

$$\begin{aligned}F_\xi^{\mathrm{c}}(x)&\sim\sum_{k=0}^{\infty}\frac{(-1)^k}{k!}\bigg(\int_{S_k(x)}\rho^{(k)}(y_1,\ldots,y_k)dy_1\cdots dy_k+\int_{S_k^{\mathrm{c}}(x)}\lambda^k dy_1\cdots dy_k\bigg)\\&=\sum_{k=0}^{\infty}\frac{(-1)^k}{k!}(\lambda\pi x^2)^k=\exp(-\lambda\pi x^2).\end{aligned}$$

Therefore, $\mathbb{E}(\xi^n)$ is bounded for all n and Condition 4 holds.

□

A.6 Proof of Theorem 4.3

Proof. Using the same method in the proof of Theorem 5.6 in [42], we can prove that

$$\mathbb{P}(\tilde{I}\geq y)\sim\frac{\pi\lambda}{2}\mathbb{E}[(h_a+h_b)^\delta]y^{-\delta},\quad y\to\infty. \tag{A.21}$$

The success probability can be rewritten as

$$\begin{aligned}
P_{\mathrm{s}}(\theta) &= 1 - \mathbb{P}\left(\tilde{I} > h_0 b^{-\alpha}\theta^{-1} - h_1 b^{-\alpha}\right) \\
&= 1 - \mathbb{E}_{h_0,h_1}\left[\mathbb{P}\left(\tilde{I} > h_0 b^{-\alpha}\theta^{-1} - h_1 b^{-\alpha}\right)\mathbf{1}(h_0 b^{-\alpha}\theta^{-1} \geq h_1 b^{-\alpha}) \mid h_0, h_1\right] \\
&\quad - \mathbb{E}_{h_0,h_1}\left[\mathbb{P}\left(\tilde{I} > h_0 b^{-\alpha}\theta^{-1} - h_1 b^{-\alpha}\right)\mathbf{1}(h_0 b^{-\alpha}\theta^{-1} < h_1 b^{-\alpha}) \mid h_0, h_1\right] \\
&= 1 - \mathbb{E}_{h_0,h_1}\left[\mathbb{P}\left(\tilde{I} > h_0 b^{-\alpha}\theta^{-1} - h_1 b^{-\alpha}\right)\mathbf{1}(h_0\theta^{-1} \geq h_1) \mid h_0, h_1\right] - \mathbb{P}\left(h_0\theta^{-1} < h_1\right).
\end{aligned} \tag{A.22}$$

Thus,

$$\begin{aligned}
\lim_{\theta\to 0}\frac{1-P_{\mathrm{s}}(\theta)}{\theta^{\delta}} &= \lim_{\theta\to 0}\frac{\mathbb{E}_{h_0,h_1}\left[\mathbb{P}\left(\tilde{I} > h_0 b^{-\alpha}\theta^{-1} - h_1 b^{-\alpha}\right)\mathbf{1}(h_0\theta^{-1} \geq h_1) \mid h_0, h_1\right] + \mathbb{P}\left(h_0\theta^{-1} < h_1\right)}{\theta^{\delta}} \\
&= \lim_{\theta\to 0}\frac{\mathbb{E}_{h_0,h_1}\left[\mathbb{P}\left(\tilde{I} > h_0 b^{-\alpha}\theta^{-1} - h_1 b^{-\alpha}\right)\mathbf{1}(h_0\theta^{-1} \geq h_1) \mid h_0, h_1\right]}{\theta^{\delta}} \\
&\overset{(a)}{=} \mathbb{E}_{h_0,h_1}\left[\lim_{\theta\to 0}\frac{\mathbb{P}\left(\tilde{I} > h_0 b^{-\alpha}\theta^{-1} - h_1 b^{-\alpha}\right)\mathbf{1}(h_0\theta^{-1} \geq h_1)}{\theta^{\delta}} \mid h_0, h_1\right] \\
&\overset{(b)}{=} \mathbb{E}_{h_0,h_1}\left[\lim_{\theta\to 0}\frac{\pi\lambda b^2\mathbb{E}[(h_a+h_b)^{\delta}]}{2}\frac{\left(h_0\theta^{-1}-h_1\right)^{-\delta}\mathbf{1}(h_0\theta^{-1} \geq h_1)}{\theta^{\delta}} \mid h_0, h_1\right] \\
&= \frac{\pi\lambda b^2\mathbb{E}[(h_a+h_b)^{\delta}]}{2}\mathbb{E}_{h_0,h_1}\left[\lim_{\theta\to 0}\left(h_0-h_1\theta\right)^{-\delta}\mathbf{1}(h_0 \geq h_1\theta) \mid h_0, h_1\right] \\
&= \frac{\pi\lambda b^2}{2}\mathbb{E}[(h_a+h_b)^{\delta}]\mathbb{E}[h^{-\delta}],
\end{aligned} \tag{A.23}$$

where (a) follows from the Dominated Convergence Theorem and (b) follows from (A.21).

□

A.7 Proof of Theorem 4.6

Proof. The SIR distribution can be expressed as

$$\begin{aligned} P_{\mathrm{s}}(\theta) &= \mathbb{P}\left(\frac{h_0 R^{-\alpha}}{h_1 R^{-\alpha} + \tilde{I}} > \theta\right) \\ &= \mathbb{P}\left(h_0 > \theta(h_1 + R^{\alpha}\tilde{I})\right) \\ &= \mathbb{E}\left[\bar{F}_h\left(\theta(h_1 + R^{\alpha}\tilde{I})\right)\right]. \end{aligned} \tag{A.24}$$

So,

$$\begin{aligned} &\lim_{\theta\to\infty} \frac{P_{\mathrm{s}}(\theta)}{\theta^{-(m+\delta)}} = \lim_{\theta\to\infty} \frac{\mathbb{E}\left[\bar{F}_h\left(\theta\left(h_1 + R^{\alpha}\tilde{I}\right)\right)\right]}{\theta^{-(m+\delta)}} = \lim_{\theta\to\infty} \frac{\frac{\partial}{\partial\theta}\mathbb{E}\left[\bar{F}_h\left(\theta\left(h_1 + R^{\alpha}\tilde{I}\right)\right)\right]}{-(m+\delta)\theta^{-(m+\delta+1)}} \\ &= \lim_{\theta\to\infty} \mathbb{E}\left[\frac{\frac{\partial}{\partial\theta}F_h\left(\theta\left(h_1 + R^{\alpha}\tilde{I}\right)\right)}{(m+\delta)\theta^{-(m+\delta+1)}}\right] \\ &= \frac{1}{(m+\delta)\Gamma(m)} \lim_{\theta\to\infty} \mathbb{E}\left[\theta^{2m+\delta} m^m \left(h_1 + R^{\alpha}\tilde{I}\right)^m e^{-\theta m\left(h_1 + R^{\alpha}\tilde{I}\right)}\right] \\ &= \frac{m^m}{(m+\delta)\Gamma(m)} \lim_{\theta\to\infty} \mathbb{E}\left[\theta^{2m+\delta}\left(\sum_{i=0}^{m}\binom{m}{i} h_1^i \left(R^{\alpha}\tilde{I}\right)^{m-i}\right) e^{-\theta m\left(h_1 + R^{\alpha}\tilde{I}\right)}\right] \\ &= \frac{m^m}{(m+\delta)\Gamma(m)} \sum_{i=0}^{m}\binom{m}{i} \lim_{\theta\to\infty} \mathbb{E}\left[\left(\theta^{m+i} h_1^i e^{-\theta m h_1}\right)\left(\theta^{m-i+\delta}\left(R^{\alpha}\tilde{I}\right)^{m-i} e^{-\theta m R^{\alpha}\tilde{I}}\right)\right] \\ &= \frac{m^m}{(m+\delta)\Gamma(m)} \sum_{i=0}^{m}\binom{m}{i} \lim_{\theta\to\infty} \mathbb{E}\left[\theta^{m+i} h_1^i e^{-\theta m h_1}\right] \mathbb{E}\left[\theta^{m-i+\delta}\left(R^{\alpha}\tilde{I}\right)^{m-i} e^{-\theta m R^{\alpha}\tilde{I}}\right] \end{aligned} \tag{A.25}$$

where F_h and $\bar{F}_h$ are respectively the CCDF and the CDF of h.

In the following, we evaluate $\lim_{\theta\to\infty} \mathbb{E}\left[\theta^{m+i} h_1^i e^{-\theta m h_1}\right]$ and $\lim_{\theta\to\infty} \mathbb{E}\left[\theta^{m-i+\delta}\left(R^{\alpha}\tilde{I}\right)^{m-i} e^{-\theta m R^{\alpha}\tilde{I}}\right]$, separately.

For $\lim_{\theta\to\infty}\mathbb{E}\left[\theta^{m+i}h_1^i e^{-\theta m h_1}\right]$, we have

$$\begin{aligned}\lim_{\theta\to\infty}\mathbb{E}\left[\theta^{m+i}h_1^i e^{-\theta m h_1}\right] &= \lim_{\theta\to\infty}\int_0^\infty \frac{m^m}{\Gamma(m)}\left(\theta^{m+i}x^i e^{-\theta m x}\right)x^{m-1}e^{-mx}\mathrm{d}x \\ &= \lim_{\theta\to\infty}\frac{\Gamma(m+i)}{m^i\Gamma(m)}\left(\frac{\theta}{1+\theta}\right)^{m+i}\int_0^\infty \frac{(m\,(1+\theta))^{m+i}}{\Gamma(m+i)}x^{m+i-1}e^{-m(1+\theta)x}\mathrm{d}x \\ &= \lim_{\theta\to\infty}\frac{\Gamma(m+i)}{m^i\Gamma(m)}\left(\frac{\theta}{1+\theta}\right)^{m+i} \\ &= \frac{\Gamma(m+i)}{m^i\Gamma(m)}. \end{aligned} \tag{A.26}$$

For $\lim_{\theta\to\infty}\mathbb{E}\left[\theta^{m-i+\delta}\left(R^\alpha\tilde{I}\right)^{m-i}e^{-\theta m R^\alpha\tilde{I}}\right]$, we discuss the cases when $i<m$ and when $i=m$, separately.

When $i<m$, let $g_i\sim\text{gamma}(m-i,1)$, and we have

$$\begin{aligned}\lim_{\theta\to\infty}\mathbb{E}\left[\theta^{m-i+\delta}\left(R^\alpha\tilde{I}\right)^{m-i}e^{-\theta m R^\alpha\tilde{I}}\right] &= \lim_{\theta\to\infty}\frac{\delta\Gamma(m-i)}{m^{m-i}}\frac{\frac{\partial}{\partial\theta}\mathbb{E}\left[1-\int_0^{\theta m R^\alpha\tilde{I}}\frac{1}{\Gamma(m-i)}x^{m-i-1}e^{-x}\mathrm{d}x\right]}{\frac{\partial}{\partial\theta}\theta^{-\delta}} \\ &\overset{(a)}{=} \lim_{\theta\to\infty}\frac{\delta\Gamma(m-i)}{m^{m-i}}\frac{\mathbb{E}\left[1-\int_0^{\theta m R^\alpha\tilde{I}}\frac{1}{\Gamma(m-i)}x^{m-i-1}e^{-x}\mathrm{d}x\right]}{\theta^{-\delta}} \\ &= \lim_{\theta\to\infty}\frac{\delta\Gamma(m-i)}{m^{m-i}}\frac{\mathbb{E}\left[\bar{F}_{g_i}(\theta m R^\alpha\tilde{I})\right]}{\theta^{-\delta}}, \end{aligned} \tag{A.27}$$

where (a) follows by applying the L'Hospital's rule reversely and $\bar{F}_{g_i}$ is the CCDF of g_i.

Using the same method in the proof of Theorem 4 in [61], we have

$$
\begin{aligned}
&\lim_{\theta\to\infty}\frac{\mathbb{E}\left[\bar{F}_{g_i}\left(\theta m R^{\alpha}\tilde{I}\right)\right]}{\theta^{-\delta}}\\
&=\lim_{\theta\to\infty}\theta^{\delta}\sum_{x\in\Phi_{\mathrm{s}}}\bar{F}_{g_i}\left(\theta m\|x\|^{\alpha}\left(\sum_{y\in\Phi_{\mathrm{s}}\setminus\{x\}}\left(\left(h_{y,1}+h_{y,2}\right)\|y\|^{-\alpha}\right)\right)\right)\mathbf{1}(\Phi(b(o,\|x\|)=0))\\
&\overset{(b)}{=}\lim_{\theta\to\infty}\frac{\theta^{\delta}\lambda}{2}\int_{\mathbb{R}^2}\mathbb{E}_o^{!}\left[\bar{F}_{g_i}\left(\theta m\|x\|^{\alpha}\left(\sum_{y\in\Phi_x}\left(\left(h_{y,1}+h_{y,2}\right)\|y\|^{-\alpha}\right)\right)\right)\mathbf{1}\left(b(o,\|x\|)\text{ empty}\right)\right]\mathrm{d}x\\
&\overset{(c)}{=}\lim_{\theta\to\infty}\frac{\lambda}{2}\int_{\mathbb{R}^2}\mathbb{E}_o^{!}\left[\bar{F}_{g_i}\left(m\|x\|^{\alpha}\left(\sum_{y\in\Phi_{x\theta^{-\delta/2}}}\left(\left(h_{y,1}+h_{y,2}\right)\|y\|^{-\alpha}\right)\right)\right)\mathbf{1}\left(b(o,\|x\|\theta^{-\delta/2})\text{ empty}\right)\right]\mathrm{d}x\\
&\overset{(d)}{=}\frac{\lambda}{2}\int_{\mathbb{R}^2}\mathbb{E}_o^{!}\left[\bar{F}_{g_i}\left(m\|x\|^{\alpha}I_{\infty}\right)\right]\mathrm{d}x\\
&\overset{(e)}{=}\frac{\lambda}{2}m^{-\delta}\mathbb{E}_o^{!}\left[I_{\infty}^{-\delta}\right]\int_{\mathbb{R}^2}\bar{F}_{g_i}\left(\|x\|^{\alpha}\right)\mathrm{d}x\\
&=\frac{\lambda}{2}m^{-\delta}\mathbb{E}_o^{!}\left[I_{\infty}^{-\delta}\right]\pi\delta\int_0^{\infty}r^{\delta-1}\bar{F}_{g_i}\left(r\right)\mathrm{d}r\\
&=\frac{\lambda}{2}\pi m^{-\delta}\mathbb{E}_o^{!}\left[I_{\infty}^{-\delta}\right]\mathbb{E}[g_i^{\delta}]\\
&=\frac{\lambda\pi m^{-\delta}\Gamma(m-i+\delta)}{2\Gamma(m-i)}\mathbb{E}_o^{!}\left[I_{\infty}^{-\delta}\right],
\end{aligned}
\tag{A.28}
$$

where (b) follows from the Campbell-Mecke theorem, $\Phi_x \triangleq \{y\in\Phi : y+x\}$ is a translated version of Φ, (c) follows by using the substitution $x\theta^{\delta/2}\to x$, (d) follows by the Dominated Convergence Theorem and the fact that $\theta^{-\delta/2}\to 0$ and thus $\mathbf{1}\left(b(o,\|x\|\theta^{-\delta/2})\text{ empty}\right)\to 1$, (e) follows by using the substitution $x\left(mI_{\infty}\right)^{\delta/2}\to x$. So, by substituting (A.28) into (A.27), it yields that

$$
\lim_{\theta\to\infty}\mathbb{E}\left[\theta^{m-i+\delta}\left(R^{\alpha}\tilde{I}\right)^{m-i}e^{-\theta m R^{\alpha}\tilde{I}}\right]=\frac{\delta\lambda\pi\Gamma(m-i)}{2m^{m-i+\delta}}\mathbb{E}_o^{!}\left[I_{\infty}^{-\delta}\right]\mathbb{E}[g_i^{\delta}].
\tag{A.29}
$$

When $i = m$, let $g_m \sim \exp(1)$, and we have

$$\begin{aligned}\lim_{\theta\to\infty} \mathbb{E}\left[\theta^{m-i+\delta}\left(R^\alpha \tilde{I}\right)^{m-i} e^{-\theta m R^\alpha \tilde{I}}\right] &= \lim_{\theta\to\infty} \mathbb{E}\left[\theta^\delta e^{-\theta m R^\alpha \tilde{I}}\right] \\ &= \lim_{\theta\to\infty} \theta^\delta \mathbb{E}\left[\bar{F}_{g_m}\left(\theta m R^\alpha \tilde{I}\right)\right] \\ &\overset{(a)}{=} \frac{\lambda}{2}\pi m^{-\delta}\mathbb{E}_o^!\left[I_\infty^{-\delta}\right]\mathbb{E}[g_m^\delta] \\ &= \frac{\lambda}{2}\pi m^{-\delta}\Gamma(1+\delta)\mathbb{E}_o^!\left[I_\infty^{-\delta}\right], \qquad \text{(A.30)}\end{aligned}$$

where (a) follows from (A.28).

Substituting (A.26), (A.29) and (A.30) into (A.25), we obtain (4.28). □

BIBLIOGRAPHY

1. V. P. Mhatre and C. P. Rosenberg, "Impact of Network Load on Forward Link Inter-Cell Interference in Cellular Data Networks," *IEEE Transactions on Wireless Communications*, Vol. 5, No. 12, pp. 3651-3661, Dec. 2006.

2. P. Charoen and T. Ohtsuki, "Codebook Based Interference Mitigation with Base Station Cooperation in Multi-Cell Cellular Network," *IEEE Vehicular Technology Conference 2011*, pp. 1-5, Sep. 2011

3. F. G. Nocetti, I. Stojmenovic, and J. Zhang, "Addressing and routing in hexagonal networks with applications for tracking mobile users and connection rerouting in cellular networks," *IEEE Transactions on Parallel and Distributed Systems*, Vol. 13, No. 9, pp. 963-971, Sep. 2002.

4. M. Haenggi, J. G. Andrews, F. Baccelli, O. Dousse, and M. Franceschetti, "Stochastic Geometry and Random Graphs for the Analysis and Design of Wireless Networks," *IEEE Journal on Selected Areas in Communications*, Vol. 27, No. 7, pp. 1029-1046, Sep. 2009.

5. M. Haenggi, *Stochastic Geometry for Wireless Networks*, Cambridge University Press, 2012.

6. F. Baccelli and B. Blaszczyszyn, *Stochastic Geometry and Wireless Networks*, NOW: Foundations and Trends in Networking, 2010.

7. D. Stoyan, W. Kendall, and J. Mecke, *Stochastic Geometry and Its Applications, 2nd edition*, John Wiley and Sons, 1995.

8. J. G. Andrews, F. Baccelli, and R. K. Ganti, "A Tractable Approach to Coverage and Rate in Cellular Networks," *IEEE Transactions on Communications*, Vol. 59, No. 11, pp. 3122-3124, Nov. 2011.

9. H. S. Dhillon, R. K. Ganti, F. Baccelli, and J. G. Andrews, "Modeling and Analysis of K-Tier Downlink Heterogeneous Cellular Networks," *IEEE Journal on Selected Areas in Communications*, Vol. 30, No. 3, pp. 550-560, Apr. 2012.

10. T. T. Vu, L. Decreusefond, and P. Martins, "An analytical model for evaluating outage and handover probability of cellular wireless networks," *15th International Symposium on Wireless Personal Multimedia Communications (WPMC'12)*, pp. 643-647, Sep. 2012.

11. D. Cao, S. Zhou, and Z. Niu, "Optimal Base Station Density for Energy-Efficient Heterogeneous Cellular Networks," *IEEE ICC'12*, pp. 4379-4383, 2012.

12. N. Deng, S. Zhang, W. Zhou, and J. Zhu, "A stochastic geometry approach to energy efficiency in relay-assisted cellular networks," *IEEE GLOBECOM'12*, pp. 3484-3489, 2012.

13. C.-H. Lee and M. Haenggi, "Interference and Outage in Poisson Cognitive Networks," *IEEE Transactions on Wireless Communications*, Vol. 11, No. 4, pp. 1392-1401, Apr. 2012.

14. X. Liu and M. Haenggi, "Towards Quasi-Regular Sensor Networks: Topology Control Algorithms for Improved Energy Efficiency," *IEEE Transactions on Parallel and Distributed Systems*, Vol. 17, No. 9, pp. 975-986, Sep. 2006.

15. A. Busson, G. Chelius, and J. M. Gorce, "Interference Modeling in CSMA Multi-Hop Wireless Networks," *Tech. Rep. 6624, INRIA*, Feb. 2009.

16. A. Busson and G. Chelius, "Point Processes for Interference Modeling in CSMA/CA Ad Hoc Networks," *Sixth ACM International Symposium on Performance Evaluation of Wireless Ad Hoc, Sensor, and Ubiquitous Networks (PE-WASUN09)*, pp. 33-40, Oct. 2009.

17. M. Haenggi, "Mean Interference in Hard-Core Wireless Networks," *IEEE Communications Letters*, Vol. 15, No. 8, pp. 792-794, Aug. 2011.

18. H. Q. Nguyen, F. Baccelli, and D. Kofman, "A Stochastic Geometry Analysis of Dense IEEE 802.11 Networks," *IEEE INFOCOM'07*, pp. 1199-1207, 2007.

19. C. Geyer, "Likelihood inference for spatial point processes", in *Current Trends in Stochastic Geometry and Applications*, ed. by O. E. Barndorff-Nielsen, W. S. Kendall, and M. N. M. Lieshout, London: Chapman and Hall, pp. 141-172, 1999.

20. J. Riihijarvi and P. Mahonen, "A spatial statistics approach to characterizing and modeling the structure of cognitive wireless networks," *Ad Hoc Networks*, Vol. 10, No. 5, pp. 858-869, 2012.

21. P. Mitran and C. Rosenberg, "On fractional frequency reuse in imperfect cellular grids," *IEEE Wireless Communications and Networking Conference (WCNC) 2012*, pp. 2967-2972, Apr. 2012.

22. A. Baddeley and R. Turner, "Practical Maximum Pseudolikelihood for Spatial Point Patterns," *Australian and New Zealand Journal of Statistics*, Vol. 42, No. 3, pp. 283-322, 2000.

23. P. J. Diggle and R. J. Gratton, "Monte Carlo Methods of Inference for Implicit Statistical Models", *Journal of the Royal Statistical Society. Series B (Methodological)*, Vol. 46, No. 2, pp. 193-227, 1984.

24. A. Baddeley, *Analysing Spatial Point Patterns in R*, Version 3, CSIRO, 2008.

25. The R Project for Statistical Computing, `http://www.r-project.org` [Accessed March 2014].

26. A. Baddeley and G. Nair, "Fast approximation of the intensity of Gibbs point processes," *Electronic Journal of Statistics*, Vol. 6, pp. 1155-1169, 2012.

27. R. M. Corless, G. H. Gonnet, D. E. G. Hare, D. J. Jeffrey, and D. E. Knuth, "On the Lambert W function," *Advances in Computational Mathematics*, Vol. 5, No. 4, pp. 329-359, 1996.

28. A. Baddeley and R. Turner. "spatstat: An R Package for Analyzing Spatial Point Patterns," *Journal of Statistical Software*, Vol. 12, Iss. 6, pp. 1-42, Jan. 2005.

29. K. K. Berthelsen and J. Moller, "A Primer on Perfect Simulation for Spatial Point Processes," *Bulletin of the Brazilian Mathematical Society*, Vol. 33, No. 3, pp. 351-367, 2002.

30. J. S. Ferenc and Z. Neda, "On the size distribution of Poisson Voronoi cells," *Physica A: Statistical Mechanics and its Applications*, Vol. 385, Iss. 2, pp. 518-526, Nov. 2007.

31. M. Tanemura, "Statistical Distributions of Poisson Voronoi Cells in Two and Three Dimensions," *Forma*, Vol. 18, No. 4, pp. 221-247, 2003.

32. S. Lin and D. J. Costello, *Error Control Coding*, 2nd ed., Englewood Cliffs, NJ: Prentice-Hall, 2004.

33. J. G. Andrews, R. K. Ganti, M. Haenggi, N. Jindal, and S. Weber, "A primer on spatial modeling and analysis in wireless networks," *IEEE Communications Magazine,* Vol. 48, No. 11, pp. 156-163, Nov. 2010.

34. T. D. Novlan, R. K. Ganti, A. Ghosh, and J. G. Andrews, "Analytical Evaluation of Fractional Frequency Reuse for OFDMA Cellular Networks," *IEEE Transactions on Wireless Communications,* Vol. 10, No. 12, pp. 4294-4305, Dec. 2011.

35. H. S. Dhillon, R. K. Ganti, F. Baccelli and J. G. Andrews, "Modeling and Analysis of K-Tier Downlink Heterogeneous Cellular Networks," *IEEE Journal on Selected Areas in Communications*, Vol. 30, No. 3, pp. 550-560, Apr. 2012.

36. W. C. Cheung, T. Q. S. Quek, and M. Kountouris, "Throughput Optimization, Spectrum Allocation, and Access Control in Two-Tier Femtocell Networks," *IEEE Journal on Selected Areas in Communications,* Vol. 30, No. 3, pp. 561-574, Apr. 2012.

37. Y. Zhong and W. Zhang, "Multi-Channel Hybrid Access Femtocells: A Stochastic Geometric Analysis," *IEEE Transactions on Communications,* Vol. 61, No. 7, pp. 3016-3026, Jul. 2013.

38. S. P. Weber, X. Yang, J. G. Andrews, and G. de Veciana, "Transmission capacity of wireless ad hoc networks with outage constraints," *IEEE Transactions on Information Theory,* Vol. 51, No. 12, pp. 4091-4102, Dec. 2005.

39. S. Bandyopadhyay and E. J. Coyle, "An energy efficient hierarchical clustering algorithm for wireless sensor networks," *Proc. IEEE INFOCOM 2003,* Vol. 3, pp. 1713-1723, Apr. 2003.

40. R. K. Ganti and M. Haenggi, "Interference and outage in clustered wireless ad hoc networks," *IEEE Transactions on Information Theory*, Vol. 55, No. 9, pp. 4067-4086, Sep. 2009.

41. H. ElSawy and E. Hossain, "A Modified Hard Core Point Process for Analysis of Random CSMA Wireless Networks in General Fading Environments," *IEEE Transactions on Communications,* Vol. 61, No. 4, pp. 1520-1534, Apr. 2013.

42. M. Haenggi and R. K. Ganti, "Interference in Large Wireless Networks," *Foundations and Trends in Networking*, Vol. 3, No. 2, pp. 127-248, 2008.

43. R. K. Ganti, J. G. Andrews, and M. Haenggi, "High-SIR Transmission Capacity of Wireless Networks with General Fading and Node Distribution," *IEEE Transactions on Information Theory*, Vol. 57, pp. 3100-3116, May 2011.

44. R. Giacomelli, R. K. Ganti, and M. Haenggi, "Outage Probability of General Ad Hoc Networks in the High-Reliability Regime," *IEEE/ACM Transactions on Networking*, Vol. 19, pp. 1151-1163, Aug. 2011.

45. R. K. Ganti and M. Haenggi, "Interference in Ad Hoc Networks with General Motion-Invariant Node Distributions," *in 2008 IEEE International Symposium on Information Theory (ISIT'08)*, (Toronto, Canada), Jul. 2008.

46. R. K. Ganti and J. G. Andrews, "A new method for computing the transmission capacity of non-Poisson wireless networks," *IEEE ISIT'10*, Jun. 2010.

47. N. Miyoshi and T. Shirai, "A cellular network model with Ginibre configurated base stations," *Advances in Applied Probability*, Vol. 46, No. 3, pp. 832-845, 2014.

48. N. Deng, W. Zhou, and M. Haenggi, "The Ginibre Point Process as a Model for Wireless Networks with Repulsion," *IEEE Transactions on Wireless Communications*, Vol. 14, No. 1, pp. 107-121, Jan. 2015.

49. A. Guo and M. Haenggi, "Spatial Stochastic Models and Metrics for the Structure of Base Stations in Cellular Networks," *IEEE Transactions on Wireless Communications*, Vol. 12, No. 11, pp. 5800-5812, Nov. 2013.

50. M. D. Renzo, A. Guidotti, and G. E. Corazza, "Average rate of down- link heterogeneous cellular networks over generalized fading channels: A stochastic geometry approach," *IEEE Transactions on Communications*, Vol. 61, No. 7, pp. 3050-3071, Jul. 2013.

51. F. Hansen and F. I. Meno, "Mobile fading-Rayleigh and lognormal superimposed," *IEEE Transactions on Vehicular Technology,* Vol. 26, No. 4, pp. 332-335, Nov. 1977.

52. A. M. D. Turkmani, "Probability of error for M-branch macroscopic selection diversity," *IEE Proceedings I Communications, Speech and Vision,* Vol. 139, No. 1, pp. 71-78, Feb. 1992.

53. B. Blaszczyszyn, M. K. Karray, and H. P. Keeler, "Using Poisson processes to model lattice cellular networks," in *Proc. IEEE INFOCOM,* Apr. 2013.

54. D. Xenakis, N. Passas, L. Merakos, and C. Verikoukis, "Energy-efficient and interference-aware handover decision for the LTE-Advanced femtocell network," *IEEE ICC'13*, Jun. 2013.

55. K. Nakagawa, "Application of Tauberian theorem to the exponential decay of the tail probability of a random variable," *IEEE Transactions on Information Theory*, Vol. 53, pp. 3239-3249, Sep. 2007.

56. D. J. Daley and D. Vere-Jones, *An Introduction to the Theory of Point Processes: Volume II: General Theory and Structure (Vol. 2)*, Springer, second edition, 2007.

57. S. Weber and J.G. Andrews, "A Stochastic geometry approach to Wideband Ad Hoc Networks with Channel Variations", *Workshop on Spatial Stochastic Models for Wireless Networks,* Apr. 2006.

58. J.-S. Ferenc and Z. Neda, "On the size distribution of Poisson-Voronoi cells," *Physica A-Statistical Mechanics And Its Applications*, Vol. 385, No. 2, pp. 518-526, 2007.

59. A. Guo and M. Haenggi, "Asymptotic Deployment Gain: A Simple Approach to Characterize the SINR Distribution in General Cellular Networks," *IEEE Transactions on Communications,* vol. 63, pp. 962-976, Mar. 2015.

60. M. Haenggi, "The Mean Interference-to-Signal Ratio and its Key Role in Cellular and Amorphous Networks," *IEEE Wireless Communications Letters,* vol. 3, pp. 597-600, Dec. 2014.

61. R. K. Ganti and M. Haenggi, "Asymptotics and Approximation of the SIR Distribution in General Cellular Networks," *IEEE Transactions on Wireless Communications,* vol. 15, no. 3, pp. 2130-2143, Mar. 2016.

62. R. K. Ganti, F. Baccelli, and J. G. Andrews, "Series Expansion for Interference in Wireless Networks," *IEEE Transactions on in Information Theory,* vol. 58, no. 4, pp. 2194-2205, Apr. 2012.

63. N. H. Bingham, C. M. Goldie, and J. L. Teugels, *Regular Variation.* Cambridge University Press, 1987.

64. R. Giacomelli, R. K. Ganti, and M. Haenggi, "Outage Probability of General Ad Hoc Networks in the High-Reliability Regime," *IEEE/ACM Transactions on Networking,* vol. 19, pp. 1151-1163, Aug. 2011.

65. G. Nigam, P. Minero, and M. Haenggi, "Coordinated Multipoint Joint Transmission in Heterogeneous Networks," *IEEE Transactions on Communications,* vol. 62, no. 11, pp. 4134-4146, Nov. 2014.

66. B. Blaszczyszyn, M. Karray, and H. Keeler, "Wireless networks appear Poissonian due to strong shadowing," *IEEE Transactions on Wireless Communications,* vol. 14, no. 8, pp. 4379-4390, Aug. 2015.

67. P. Calka and T. Schreiber, "Limit theorems for the typical Poisson-Voronoi cell and the Crofton cell with a large inradius," *The Annals of Probability,* vol. 33, no. 4, pp. 1625-1642, Jul. 2005.

68. J. Mecke, "On the relationship between the 0-cell and the typical cell of a stationary random tessellation," *Pattern Recognition,* vol. 32, no. 9, pp. 1645-1648, 1999.

69. X. Zhang, F. Baccelli, and R. W. Heath, "An indoor correlated shadowing model," *IEEE GLOBECOM'15*, Dec. 2012.

This document was prepared & typeset with pdfLaTeX*, and formatted with* NDdiss2$_\varepsilon$ *classfile (v3.2013[2013/04/16]) provided by Sameer Vijay and updated by Megan Patnott.*